AN INVESTIGATION OF SOIL PRESSURE BENEATH BUS STOPS IN THE CITY OF EDMONTON

P. J. Rivard.

T H E S I S

An Investigation of Soil Pressures, beneath Bus Stops,
in the city of Edmonton

Submitted as the Partial Fulfilment
of the Requirements for the Degree of
Master of Science

by

P. J. Rivard

Under the direction of

R. M. Hardy

University of Alberta
Edmonton, Alberta

April 8, 1950

A C K N O W L E D G M E N T

The author wishes to thank Dean R.M. Hardy and Mr. T. Blench for their helpful guidance and frequent assistance in this work.

INDEX

INTRODUCTION

In the city of Edmonton, since the Edmonton Transportation System has included the heavier types of trolly buses, there has been considerable deterioration of the road surface, particularly at the bus stops. This has shown up in the form of alligator cracks, heaving of the curbs, and in the formation of waves in the pavement.

The question then was:- "why are the buses causing the break-down at the bus stops first?" It was decided to measure stresses at the bus stops in an attempt to see whether increases in pressure due to braking and acceleration were causing the damage, or, whether the static load of the bus was enough to cause failure.

If the increased stresses were causing the disintegration, then some method must be found for measuring these stresses. Pressure cells were proposed since they could be placed within the soil mass and thus measure the actual stresses incurred.

GENERAL

CHOICE AND DESCRIPTION OF CELL

The Waterways Experiment Station has conducted an extensive investigation on most of the known types of pressure cells. They have found that data of particular significance was very scarce.

In nearly all cases, the failure of the installations to perform satisfactorily, was due to functional failure of the cells, or, to apparent lack of sufficiently conclusive data from the installation. The observed data were often illogical and inconsistent in trend. The information available did not indicate whether apparently erroneous results were due to:

(1) mechanical characteristics of the cells, or

(2) alteration of stress distribution by the method of placement or to the presence of the cells in the soil, or

(3) whether the cells actually indicated true soil pressure, and the failure was in the theory.

Consequently the Waterways Experiment Station did considerable research on the pressure cell known as the Waterways Experiment Station Cell. Since this was the most modern cell available, it was chosen for this investigation.

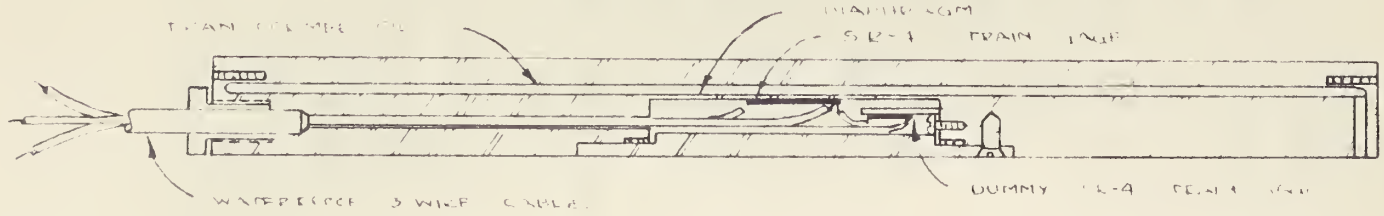

FIG - 1

CROSS-SECTION OF

U. S. WATERWAYS EXPERIMENT STATION PRESSURE CELL

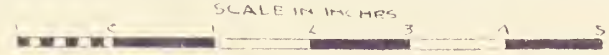

The Waterways Experiment Station Cell, as shown in figures 1 and 15, consists of a circular face plate welded at its perimeter to a thicker base plate and having a peripheral slot which forms a flexible joint between the two plates. A diaphragm is formed in the base plate by boring. The gage chamber thus formed is closed by a cover plate. A connector cable enters the gage chamber through a packing gland in the side of the base plate. The thin disc chamber between the face and base plates is filled with oil. Pressure applied to the face plate is averaged and transmitted by the oil to the diaphragm. Loading of the diaphragm produces radial and tangential strains in it which are maximum at the centre. The radial strain produced by the pressure is measured by an SR-4 electric resistance-wire strain gage. An inactive or "dummy" strain gage mounted in the gage chamber on a piece of unstressed metal provides temperature compensation. The two gages are connected through a three-conductor insulated cable to an SR-4 control box which includes the remaining elements of a special Wheatstone Bridge circuit. Alteration in the active gage resistance produced by the diaphragm strain and directly by the applied pressure is indicated by the control box.

PRESSURE CELL DESIGN

An investigation of the known and theoretical behavior of stresses in soils indicates that certain expected effects of pressure cell dimentions and rigidity must be considered.

A complete detailed theoretical and practical discussion will be found in references 1, and 2.

A pressure cell constructed of metal or similar rigid material, and necessarily constructed to obey Hookes' Law in its compressibility, could be expected to alter the stress distribution in soils which were only semi-elastic. It could be expected, in general, that the cell would produce a concentration of stress in its vicinity, in the same manner that a large stone would concentrate stresses in a sand or plastic soil mass. This concentration would be altered in both magnitude and direction by the size and shape of the cell. Since the cell usually reacts to stresses normal to one direction only, it will be more compressible in that direction and will probably present a much larger area to that direction than any other.

Theoretically a very thin, compressible plate would probably distort the stress pattern in the soil very little. Practically, this would suggest a cylindrical cell, thin in proportion to its diameter. Sizeable projections from the cell, such as those which

enclose the indicator mechanisms of some cells, could be expected, in soils, to increase stress distortion. The anamolous local stress variations, due to lack of complete homogeneity in the soil, also indicate the desirability of large, pressure-responsive area in a pressure cell.

The U.S. Waterways Experiment Station, after consideration of the above, conducted a series of tests on the Waterways Experiment Station Cell, the results of which follow:

(1) Effect of thickness of a cell within a sand mass. Pressures indicated by flat, cylindrical pressure cells placed within a loose sand mass vary negligibly with change of thickness, if the ratio of the cell diameter to its thickness remains greater than 5. The indicated pressures increase rapidly with decreasing diameter-thickness ratio below 5. If the diameter-thickness ratio is 5 or greater the indicated pressures are approximately 100 to 120% of the applied surface pressures.

(2) Effect of compressibility of a cell placed within a sand mass.

Pressures indicated by flat, cylindrical pressure cells placed within a sand mass will be essentially constant with changes in compressibility, provided the ratio of cell diameter to

deflection remains greater than 2000. The indicated pressures decrease rapidly with decreasing diameter deflection ratio below 2000. If the diameter deflection ratio is 2000 or greater, the indicated pressures are 120 to 150% of the applied surface pressure.

It will be noted that the above recommendations are for tests on Waterways Experiment Station Cells placed within a rigid pressure chamber and surrounded by Standard Ottawa sand compacted to a particular density.

The cell used was designed on the basis of these principals. The details of design may be found in Reference 1. A plan of the cell is found in figure 15.

RECORDING APPARATUS

The recording apparatus consisted of a Brush Two Channel Oscillograph, model number BL-202, and a Brush Strain Analyzer, model number BL-310.

The Two Channel Oscillograph was an instrument designed for the making of instantaneous, permanent chart records of a variety of electrical phenomena. The Brush Strain Analyzer contained a Wheatstone Bridge connected to a carrier supply. The bridge output, a modulated voltage if strain gage was subject to a dynamic measurement, was amplified and then demodulated. The strain frequency was fed into a d-c amplifier and then recorded by a Bruch direct-inking oscillograph as described above.

The pressure cell was connected to the Strain Analyzer and Oscillograph, thus giving an amplified record of the resistance changes which occurred in the SR-4 strain gage.

The recording apparatus used the first summer was an SR-4 Strain Indicator serial number D 43361. The Indicator was essentially a Wheatstone Bridge, the strain gage being one arm of the circuit. This instrument was used chiefly for static strain measurements. (See References 3 and 4)

TYPES OF BUSES

The types of buses encountered in this study were:

(1) Canadian Brill Trolly Coach, henceforth called a new bus. Dead weight 18,700 pounds, and

(2) American Pullman Trolly Coach, henceforth called an old bus. Dead weight 21,100 pounds, and

(3) American Brill Trolly Coach, henceforth called a middle bus. Dead weight 20,600 pounds.

The load distribution for all types of buses was 35% on front axle and 65% on the rear.

LOCATIONS

The locations of the testing areas were chosen at bus stops that had not been repaired.

One location, called the rigid pavement, had not deteriorated

and the profile consisted (see diagram) of

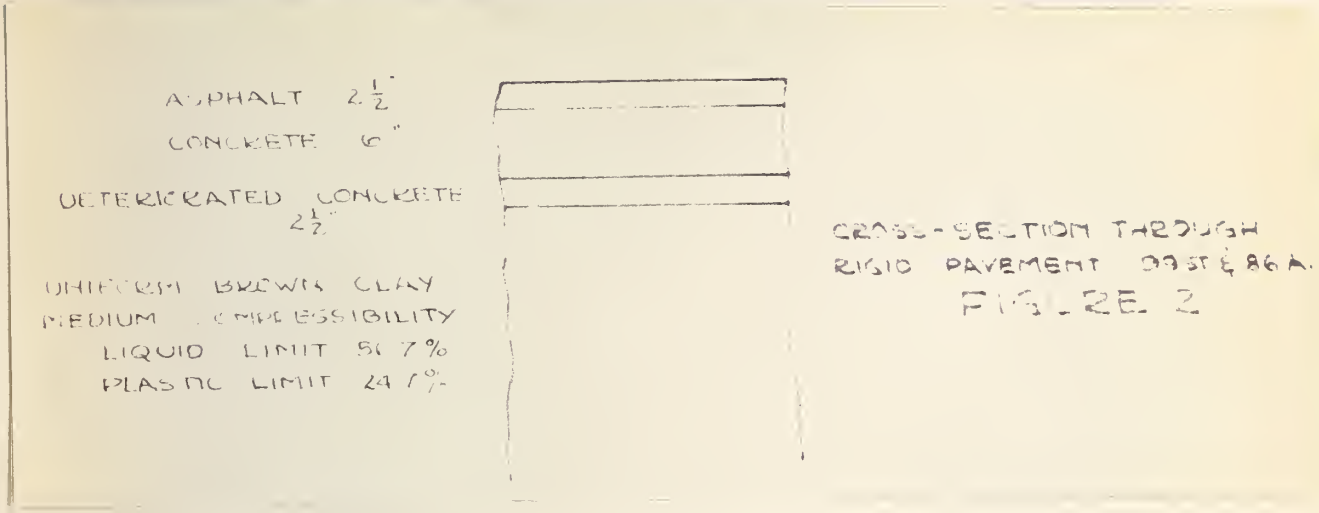

The other location, the flexible pavement, showed definite signs of deterioration and the profile consisted of

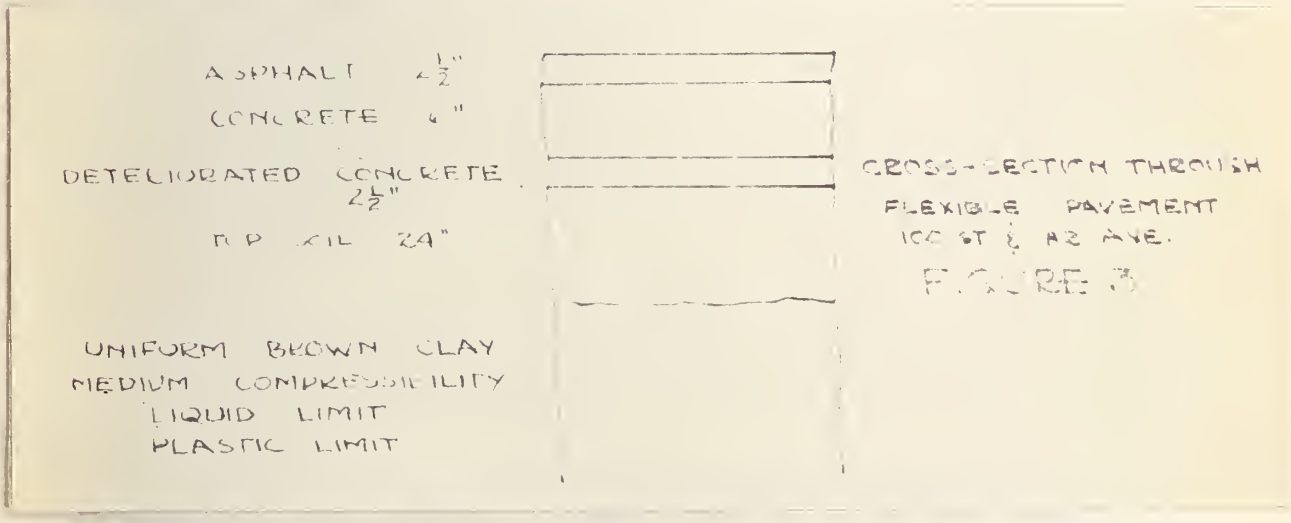

METHOD OF INSTALLATION

The pressure cell was installed by first digging a hole through the sidewalk. This hole was 3 x 5 ft. square and 6 ft. deep.

At a certain depth below the surface of the road another hole was dug. This second hole was just large enough to allow the cell

to be located. It was dug parallel to the surface of the pavements and perpendicular to the curb for a horizontal distance of 2½ ft. from the face of the curb.

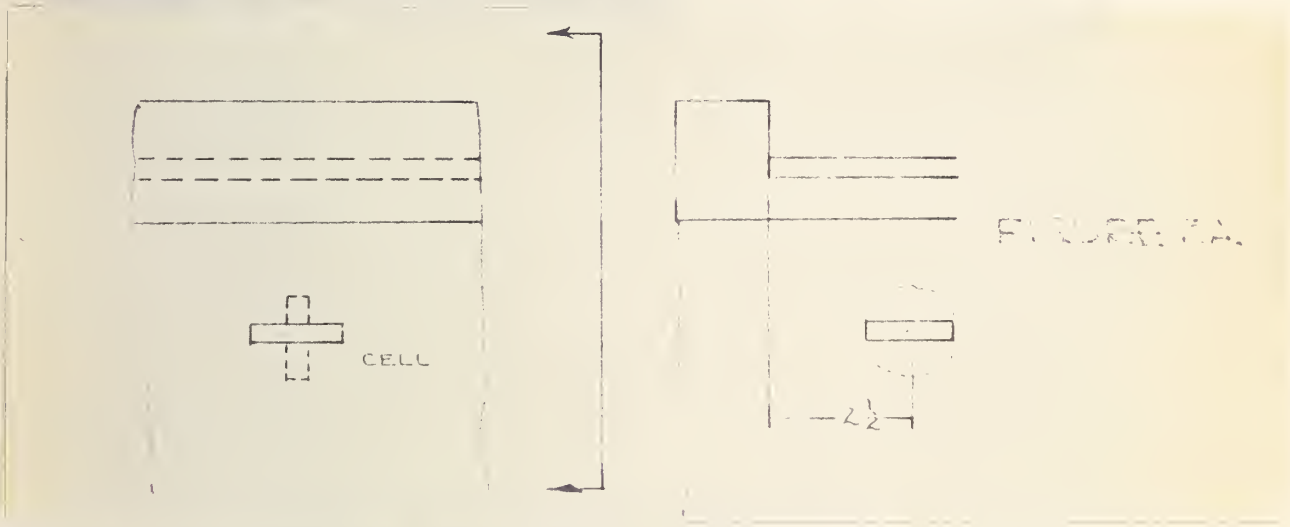

The opening for the cell was then rounded to fit the cell and checked to see that its floor was horizontal. The cell was placed in this slot with its pressure sensitive face up. The soil was then densely compacted around it.

Measurements were taken of horizontal distance under the road, depth, and location with regard to a reference point. The remainder of the slot was then backfilled and tamped until the replaced soil was as dense or denser than the surrounding soil. The larger hole was also backfilled.

The point directly above the centre of the cell was then located on the road surface and a grid of 6" squares marked. This grid was 3 ft. square. Along the curb, in both directions, one

foot intervals were marked for 12 ft. These markings thus facilitated the measuring of the location of the bus wheels with respect to the centre of the cell.

The vertical cell, and all other positions of the cells, were installed in the same manner as described for the horizontal cell.

METHOD OF TAKING READINGS

The Brush strain recording apparatus was connected to the pressure cell and allowed to warm up.

Bus drivers were then signalled as they travelled their routes and consequently pulled in towards the curb and ran over the pressure cell.

For buses that moved continually across the position of the cell the strain analyzer was switched on and allowed to record the pressures. The positions of the front and rear wheels with reference to the cell were noted and recorded on the chart paper. The load, or the number of people, on the bus were also recorded.

For stationary readings the strain analyzer was switched on and allowed to run continually while one man signalled the bus in and had it stop at 2 ft. intervals within the sphere of influence of the cell. A second man recorded the various positions of the wheel with respect to the cell, noted the type of bus and the load on it.

For braking effects the bus approached at high speeds and stopped over various positions as signalled by an experimentor. The location, load, and type of bus were recorded as above.

The following are typical examples of the types of data:

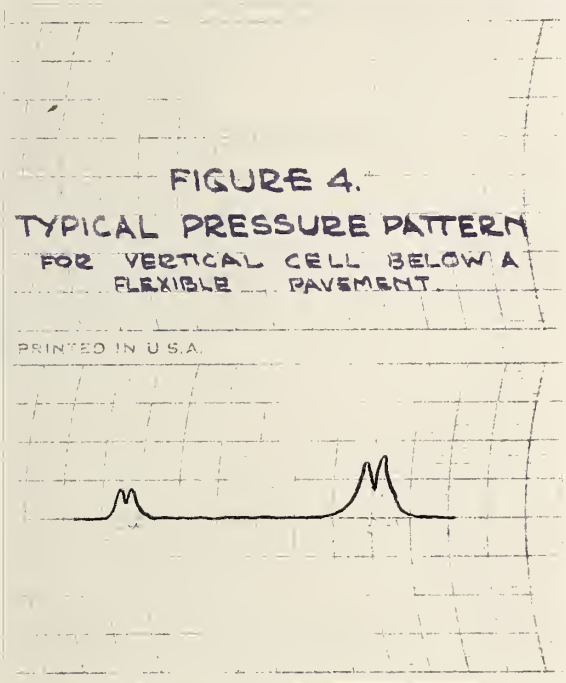

FIGURE 4.
TYPICAL PRESSURE PATTERN FOR VERTICAL CELL BELOW A FLEXIBLE PAVEMENT.

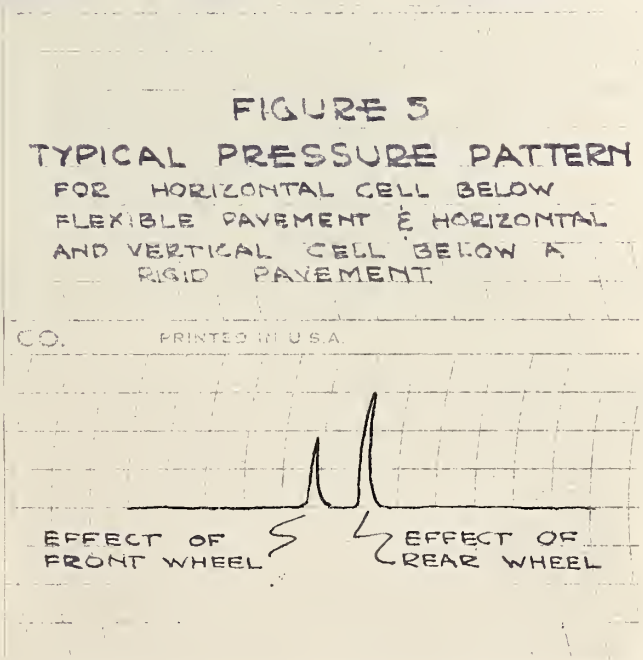

FIGURE 5
TYPICAL PRESSURE PATTERN FOR HORIZONTAL CELL BELOW FLEXIBLE PAVEMENT & HORIZONTAL AND VERTICAL CELL BELOW A RIGID PAVEMENT.

FIGURE 6

TYPICAL PRESSURE PATTERNS FOR HORIZONTAL CELL.
BELOW FLEXIBLE & RIGID PAVEMENTS

CHART NO. BL 909 THE BRU

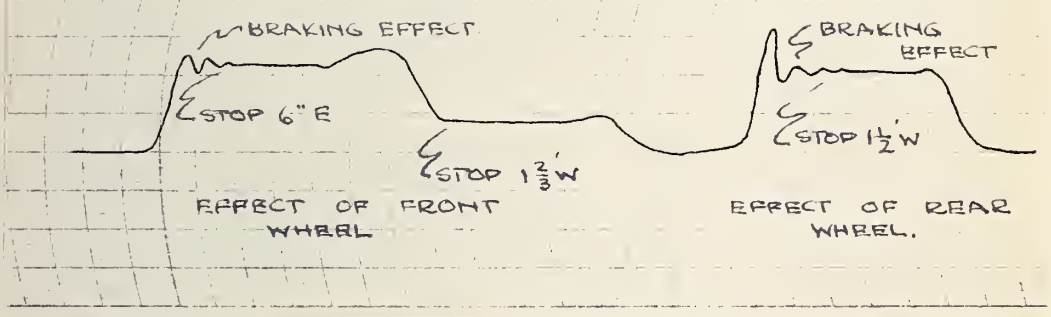

FIGURE 7.

TYPICAL PRESSURE PATTERNS FOR VERTICAL CELL
BELOW FLEXIBLE PAVEMENT.

CHART NO. BL 909 THE BR

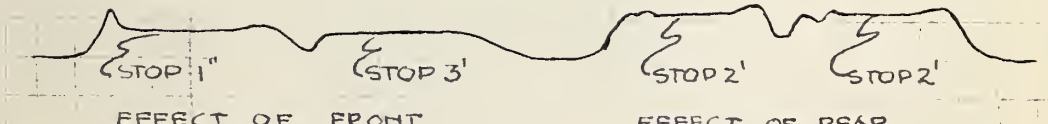

SUMMARY OF PROCEDURE

The pressure cell was designed as explained under pressure cell theory and design. A local machinist was employed to fabricate it. The machinist had considerable difficulty machining the membrane and the flexible rim. While the pressure cell was being constructed a soil survey was conducted at several locations along Jasper Avenue. The following field tests were run:

Field California Bearing Ratio tests

Cone Bearing tests

Density tests

and

Moisture Profiles

Undisturbed and disturbed samples were also taken and consolidation, triaxial compression, specific gravity, hydrometer and sieve analysis tests run.

After the cell was completed calibration tests were run in the hydraulic testing machine. It was very difficult to get calibration curves to check. This was attributed to instability of the strain gages, the connecting leads and the bedding of the cell. It was found that considerable care must be taken in placing the gages and that all connections must be well soldered and insulated. It was also found that the placement of rubber

mats both above and below the cells led to better calibration curves.

The cell was also placed within various types of soil, sand, clay and silt, in the laboratory and loading tests run. These tests did not indicate anything conclusive and were consequently discontinued.

The cell was then placed in the field at 117 Street and Jasper Avenue, as described under Method of Installation. The SR-4 strain indicator was used for recording. It was found that the SR-4 indicator could not be used with sufficient accuracy for dynamic loads because:

(1) the SR-4 strain gages were not sufficiently stable since they were not properly waterproofed, and

(2) the flexible membrane was too thick.

The following summer the membrane in the pressure cell was reduced in thickness, and a new strain recorder, the Brush Recorder as described under Apparatus, was used, giving the results that follow.

FIG- 8
PRESSURE CELLS

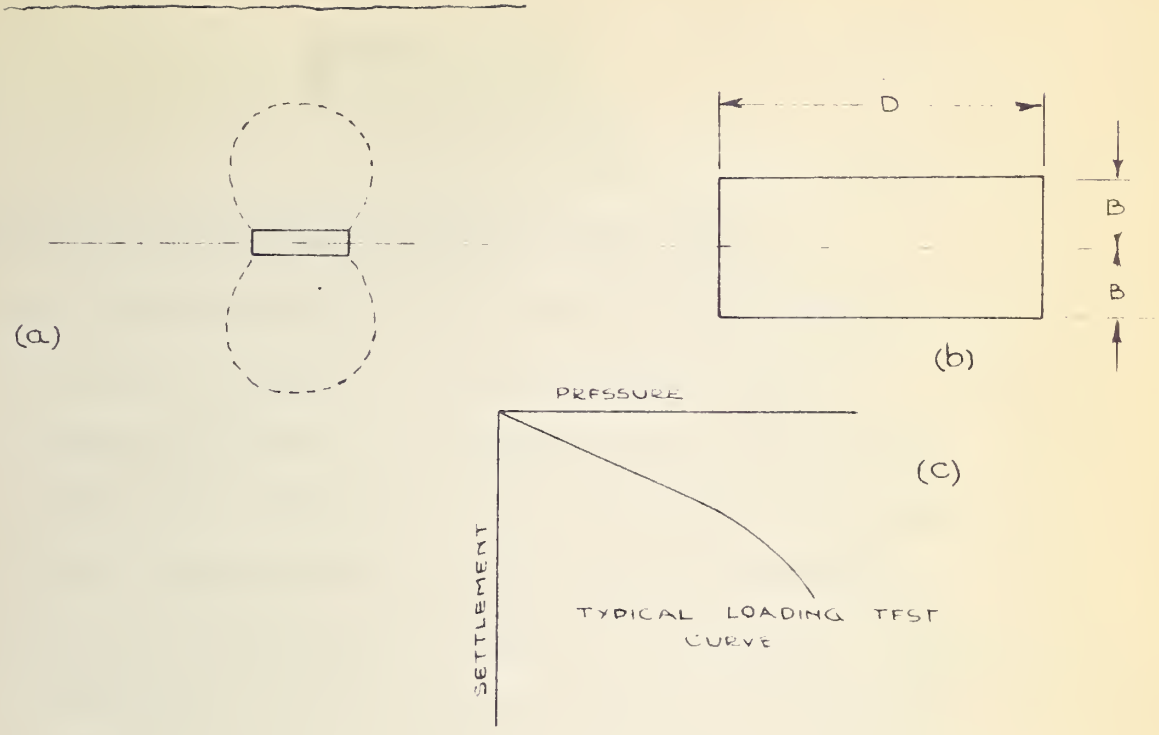

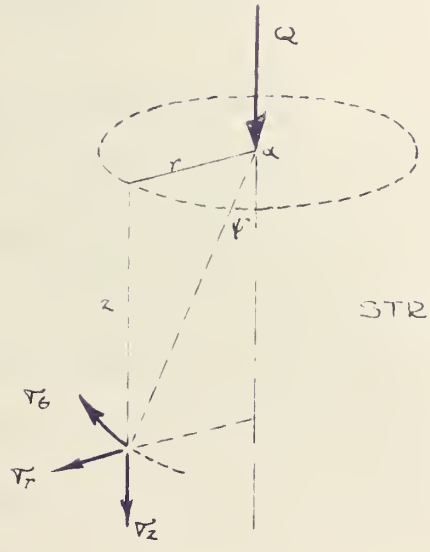

STRESS AT A POINT
FIG- 10

THEORY

THEORETICAL CONSIDERATIONS OF PRESSURE CELL ACTION

For an understanding of the problems associated with pressure cells the general nature of the strains and displacements in the soil surrounding the cell must be known; particularly, information must be available on the distribution of stresses around the cell and on the changes in stresses brought about by the presence of the cell. The revised stress condition at the cell which is caused by the presence of the cell gives rise to the important phenomenon known as "cell action."

To explain the mechanics of pressure cells D. W. Taylor has developed the following working hypothesis.

WORKING HYPOTHESIS FOR A RIGID CELL

A pressure cell is shown in Figure 8a embedded horizontally at depth Z in a mass which consists of dry soil with a level surface. The cell is shown to a larger scale and dimension notations are given in Figure 8b. The mass is assumed to be homogeneous except for irregularities introduced around the cell by the rigid nature of the cell. The unit weight of the soil is γ and at points not affected by the cell the initial

vertical pressure p at depth Z is equal to γz . The average vertical pressure on the cell will be designated by $p + pe$, where pe is the additional pressure introduced by the rigidity of the cell.

Let it now be assumed that a pressure Δp is added over the entire surface of the soil mass. At points not affected by the cell it causes at depth Z a pressure increase to $p + \Delta p$. The average pressure on the cell increases to $(p + pe) + (\Delta p + \Delta pe)$.

Let M designate the stress-strain modulus of the soil in the direction of the pressures under consideration which is here the vertical direction. The vertical compression $\Delta\rho$, caused by pressure Δp in a small element which is at some distance from the cell and which before the load increase was of thickness B, is expressed by

$$\Delta\rho = \frac{pB}{M} \qquad \ldots\ldots\ldots\ldots\ldots\ldots (1)$$

If the cell cannot compress it must cause, at both its top and bottom faces, an indentation into the soil of magnitude equal to $\Delta\rho$ of equation (1). The major portions of the compressions resulting from these indentations occur within the zones indicated by dotted lines in Figure 2a. The pressure required to cause the indentation is Δ pe. This indentation

and the corresponding compression in each of the zones affected by it closely resemble the settlement of a footing when subjected to a load and the compressions within the so-called "pressure bulb."

The one essential difference between the action of the cell, in compressing bulbs above and below it, and the action in a loading test on a deeply buried area, is that during the process of compression of the bulbs under pressure Δ pe there is a simultaneous compression all around under pressure Δ p.

Loading test plots in their initial stages are often straight-line relationships between pressure and settlement, as is shown in Figure 8c, and such a relationship will be assumed for this analysis. For materials which are of constant strength throughout the pressure bulb, the slope of this straight line is about proportional to the breadth of the loaded area. If the cell is deeply buried, or if pressure p is large compared to Δ p , an essentially constant strength exists throughout the bulbs above and below the cell and for either cohesive or cohesionless soil the indentation of either face of the cell or the compression of either bulb may be written

$$\Delta \rho = \frac{pe \cdot D}{N} \qquad \ldots\ldots\ldots\ldots\ldots (2)$$

The soil property obtained in loading tests and sometimes called the coefficient of subgrade reaction is analagous to N/D of this expression.

The two expressions for $\Delta\rho$ may be equated to give

$$\frac{\Delta\, pe}{\Delta\, p} = \frac{B}{D} \cdot \frac{N}{M} \qquad \text{.....(3)}$$

In the case under consideration the soil properties N and M both increase with increasing pressure, and there is the possibility that their ratio may, at least for limited loading ranges, be approximately constant. For the initial form of the working hypothesis it will be assumed that $\frac{N}{M}$ is a constant. If, in addition, pe is zero when p is zero, as would usually be the case, equation (3) may be written

$$\frac{pe}{p} = \frac{B}{D} \frac{N}{M} \qquad \text{.....(4)}$$

Pressure p may now be defined as the pressure which would exist at the cell location if the cell were not present; pe is the amount by which the cell reading exceeds p. The above expression indicates that a rigid cell in a given soil will register a pressure which is too large by an amount equal to a

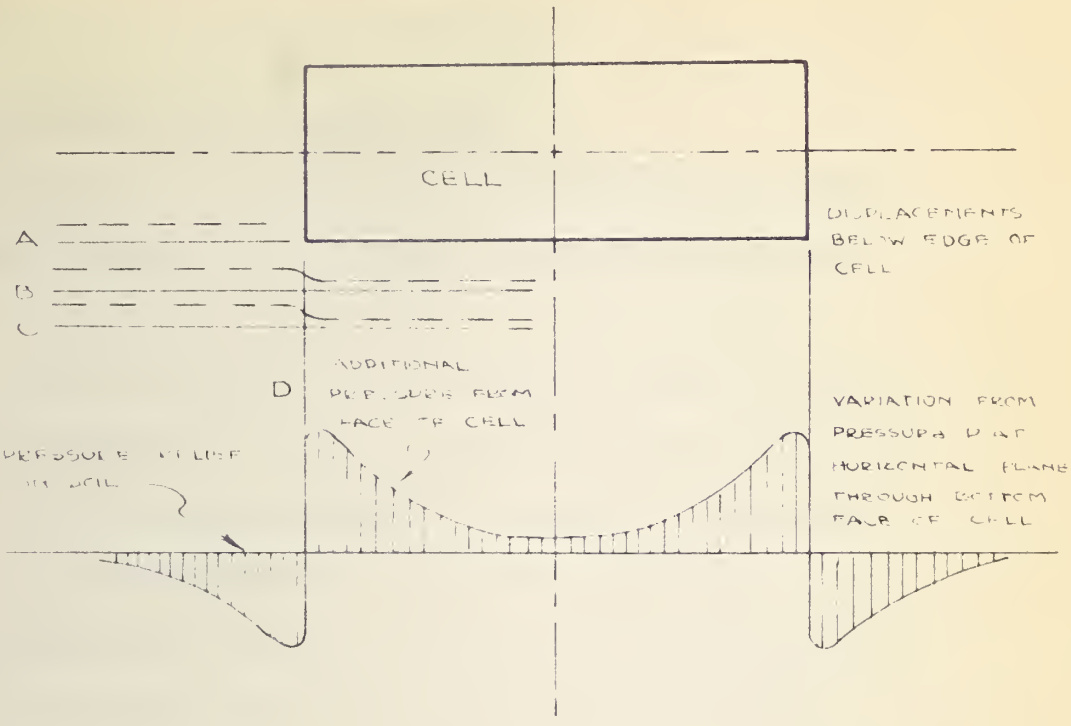

Fig. 9

PRESSURE DISTRIBUTION AT A RIGID CELL

constant times the thickness-diameter ratio.

PRESSURE DISTRIBUTION AT A RIGID CELL

A general idea of the pressure distribution on the faces of a pressure cell is of considerable help in understanding some of the details of cell action.

For the cell shown in Figure 9 above, the three horizontal lines through A, B and C represent three horizontal surfaces which existed within the soil before pressure was applied. The application of pressure has displaced the three surfaces to the positions shown by the dashed lines. A sharp dip occurs in the dashed lines near the vertical line which passes through the edge of the cell. It may be concluded that for this dip to exist there must be a much larger downward pressure at the right than there is at the left of the vertical line through D. This is shown graphically by the distribution curve in the lower part of the figure; the exact distribution of pressure depends on numerous factors, but the general pattern of pressure variation must be somewhat as shown above. The pressures in this figure are variations from the average pressure p. At the cell the pressures are greater than p by an average magnitude which

equals pe . At the same elevation, but outside the cell, the pressures are smaller than p .

THE WORKING HYPOTHESIS FOR A COMPRESSIBLE CELL

If the cell is compressed by the loading, the above derivation may easily be revised to allow for this compression. The cell compresses the bulb by an amount expressed in equation (2). This amount of compression, which previously was equal to the compression of the soil as expressed by equation (1), now becomes equal to the difference between this compression and the compression of the cell. If C is the amount of compression of the cell

$$\rho = \frac{pe\,D}{N} = \frac{p\,B}{M} - C$$

whence $$\frac{pe}{p} = \frac{B}{D} \cdot \frac{N}{M} - \frac{C}{D}\frac{N}{P} \quad \text{.....(5)}$$

If it is desired to obtain an expression in terms of the compressibility instead of the compression of the cell, the compression may be expressed

$$C = (p + pe)\frac{B}{MC} \quad , \text{.....(6)}$$

where p pe is the pressure on the cell and MC is the vertical

stress strain modulus of the cell.

Substituting this expression for C into equation (5) gives

$$\frac{pe}{p} = \frac{\frac{B}{D}\frac{N}{M} - \frac{B}{D}\frac{N}{MC}}{1 + \frac{B}{D}\frac{N}{MC}} \quad \text{.....(7)}$$

POCKET ACTION IN THE SOIL SURROUNDING A CELL

Unless the soil near a cell has the same compressibility as exists in the soil mass as a whole, the soil mass immediately surrounding a cell may be subject to phenomena which are in certain respects similar to cell action. When a pocket of soil surrounding the cell is of different compressibility from that of the soil mass as a whole, an action occurs which will be called "pocket action." Pocket action is an effect which occurs in addition to cell action and is an additional source of errors in the readings registered by pressure cells.

Assume that a rigid cell with ratio of half-thickness to diameter $\left(\frac{B}{D}\right)_C$ is imbedded at the centre of a cylindrical shaped soil pocket with a corresponding ratio of $\left(\frac{B}{D}\right)_P$ and this cylindrical pocket is in the centre of a large mass of soil.

This pocket is analagous to a compressible cell the average pressure being found by substitution in equation (7). This pressure varies over the cylindrical shaped soil pocket about

as shown by the curve in the lower portion of Figure 9, which in turn increases the pressure on the cell.

It is well known that the low compressibility of a dense pocket around a cell leads to an over-registration of the cell, whereas the high compressibility of a loose pocket may lead to an appreciable under-registration. The amount of over-registration which is possible in the case of a dense pocket is limited and is not large, but the amount of under-registration which is possible in the case of a loose pocket has no definite limit and may be of large magnitude. The above considerations tend to indicate that an effort toward greater density, even to the extent of deliberately making the pocket much denser than the surrounding soil, would have led to considerably better data. It is possible that this dense pocket need not be of the same soil as the surrounding mass.

COVER ACTION IN THE SOIL ABOVE A CELL

The presence of relatively compressible soil directly above the cell with a horizontal extent which is the same as the area of the cell leads to a condition of "cover action" which is a cause of under-registration of the cell. Cover action leads to a considerable and unlimited value of under-registration.

ACTION OF CELLS IN CLAY

The plastic characteristics of cohesive soils may be of considerable aid in reducing cell action, since over a period of time plastic flow near the cell may relieve arching and stress irregularities. There is no reason to believe that cell action, pocket action and cover action would be eliminated, but there is the possibility of their being considerably relieved due to plastic flow.

For a complete and detailed study of pressure cell theory see Reference 1.

STRESSES DUE TO A POINT LOAD ON A SEMI-INFINITE SOLID WITH A HORIZONTAL SURFACE.

If an external force acts on a very small area of the surface of a solid or on the walls of a little cavity in the interior of the solid it is called a point load, and the area which is acted upon by the force is called the point of application of the load. It represents the centre of the perturbation in the state of stress, caused by the load. The vertical component of an inclined point load acting on the horizontal surface of a semi-infinite solid produces a state of stress which has circular symmetry about a vertical line through the point of application. The state of stress due to the horizontal component is symmetrical with reference to a

vertical plane through the line of action of the horizontal component.

The simplest and by far the most important state of stress ensues if a vertical point load acts on the horizontal surface of a semi-infinite solid (Figure 10). Let

Q = the load,

r = the horizontal radial distance between an arbitrary point N below the surface and a vertical axis through the point a of application of Q,

ψ = the angle between the vector aN and the vertical axis through the point of application,

z = the vertical co-ordinate of point N, measured from the surface downward,

$\sigma_z, \sigma_r, \sigma_\theta$ = the vertical stress, the horizontal radial stress and the horizontal circumferential stress; all normal stresses,

τ_{rz} = shearing in the direction of r and , and

μ = Poissons ratio for the solid.

On account of the circular symmetry of the state of stress about the vertical axis through "a" the shearing stresses in

vertical radial planes are equal to zero. The intensity of the other stresses has been computed by means of a stress function which strictly satisfies the boundary conditions. The stresses are

$$\sigma_z = \frac{3Q}{2\pi z^2} \cos^5\psi \quad \text{.....(8)}$$

$$\sigma_r = \frac{Q}{2\pi z^2}\left[3\cos\psi^3 \sin^2\psi - (1-2\mu)\frac{\cos^2\psi}{1+\cos\psi}\right] \text{.....(9)}$$

$$\sigma_\theta = -(1-2\mu)\frac{Q}{2\pi z^2}\left[\cos^3\psi - \frac{\cos^2\psi}{1+\cos\psi}\right\} \text{.....(10)}$$

$$\tau_{rz} = \frac{3Q}{2\pi z^2} \cos^4\psi \sin\psi \text{.....(11)}$$

If one computes by means of the above equations the principal stresses produced by the point load Q, one finds that the direction of the largest principal stress at any point intersects the horizontal surface of the mass in the immediate vicinity of the point of application a of the load and that the two other

principal stresses σ_{II} and σ_{III} are very small. If μ 0.5 one obtains $\sigma_{II} = \sigma_{III} = 0$.

If r = horizontal radial distance and

R = true radial distance, then equations 8, 9 and 10 become

$$\sigma_z = \frac{3Q}{2\pi}\frac{z^3}{R^5} \qquad 12$$

$$\sigma_r = \frac{Q}{2\pi}\left\{(1-2\mu)\left[\frac{1}{r^2} - \frac{z}{r^2}(r^2+z^2)^{-\frac{1}{2}}\right] - 3r^2z(r^2+z^2)^{-\frac{5}{2}}\right\} \qquad 13$$

$$\sigma_\theta = \frac{Q}{2\pi}(1-2\mu)\left\{-\frac{1}{r^2} + \frac{z}{r^2}(r^2+z^2)^{-\frac{1}{2}} + z(r^2+z^2)^{-\frac{3}{2}}\right\} \qquad 14$$

and

$$\sigma_r = \frac{Q}{2\pi}\left\{(1-2\mu)\left[\frac{1}{r^2} - \frac{z}{r^2}\frac{1}{R}\right] - 3r^2z\frac{1}{R^5}\right\} \qquad 15$$

$$\sigma_\theta = \frac{Q}{2\pi}(1-2\mu)\left\{-\frac{1}{r^2} + \frac{z}{r^2}\frac{1}{R} + z\frac{1}{R^3}\right\} \qquad 16$$

where $x^2 + y^2 + z^2 = R^2$.

RESULTS

It was considered that the best method to analyze the data was as follows:

A. Investigate the stresses caused in the subsoil by the stationary loads and try to establish some form of relation between pressure and distance.

B. Using the results of the static cases to compare them with dynamic effects.

C. Consider if the stresses, caused by the loadings, are of a magnitude large enough to cause failure in the soil.

A. STRESSES CAUSED BY STATIONARY BUSES

1. Results for the Vertical Pressure below the flexible Pavement

To check any effects which might occur due to variation of weight and springing characteristics of the various types of buses noted under Equipment, the data for each type of bus were plotted individually.

(a) A Contour Relation

Values of vertical pressure were plotted on a plan view of the location as illustrated in Plate 1. The coordinates of the positions were plotted and the corresponding pressures recorded beside them. Similar plots were drawn for the front wheel of each type of

bus and for the various depths of cell below the flexible pavement.

It was hoped that these plots would tend to give a pressure contour diagram and thus aid in the determination of a stress relation. As can be seen there is only a slight indication towards this trend.

(b) Horizontal Radial Distance and Vertical Pressure

The horizontal radial distance, to the point of application of the load, was then measured on the plan view of the location. The corresponding pressure on the cell was noted against this. To facilitate plotting the vertical pressures, with corresponding horizontal radial distances, were grouped in 0.1 lbs. per sq. in. intervals. The grouped pressures and radial distances were averaged and plotted on numerical, semi-log, and log-log graph paper as illustrated in Plates 2, 3 and 4. Similar plots were made for the front wheels of new buses only and for the pressure cell at various depths below the flexible pavement. As can be seen, these plots do not indicate a simple relation between actual vertical pressure and horizontal radial distance.

(c) <u>True Radial Distance and Vertical Pressure</u>

A consideration of Boussinesque's equations at this point, see <u>Theory</u>, led the author to try plotting the true radial distance versus actual vertical pressure.

The true radial distance was the straight line joining the centre of the pressure cell to the point of application of the load. See diagram below.

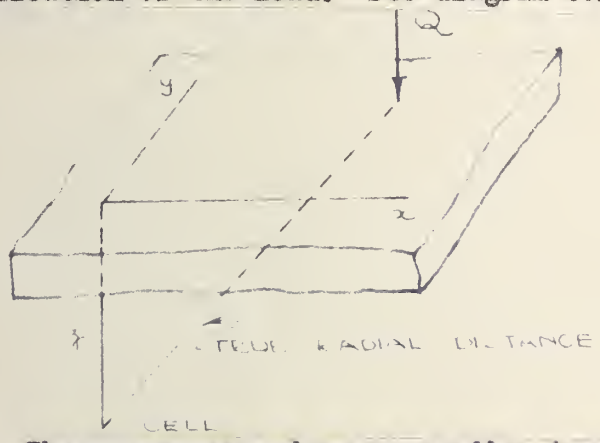

FIGURE 11

The pressures and corresponding true radial distances were again grouped and averaged as above. Plots of true radial distance and vertical pressure are illustrated in Plates 5, 6 and 7 for pressures caused by both old and new buses. Similar plots were made for the various depths of cell below the flexible pavement.

These plots do not indicate any significant difference in results due to effects that may have been contributed by the different type of buses. Henceforth, there was no

differentiation made between the results of old and new buses. Plate 7 shows a straight line relation between actual vertical pressure and true radial distance when plotted on log-log graph paper. The slope of this line is -4.7. Plates 8 and 9, which are plots for the same location at depths of 20 inches and 49 inches below the surface, show a similar straight line relation with slopes of -4.6 and -4.8 respectively. This would indicate that the vertical pressure is approximately proportional to the reciprocal of the true radial distance to the fifth power, as shown by Boussinesque theory.

Although the grouped and averaged pressures and true radial distances gave good results it was found that this type of averaging was not good statistical practice, particularly with numbers to a high power (see appendix). Consequently averaging results was discontinued and individual points were plotted.

(d) Corrected Radial Distance and Vertical Pressure

Further consideration brought forth the fact that the opposite front wheel also contributes to the total pressure. Since the pressure cell indicates the pressure contributed by both wheels, the true radial distance

must be adjusted as follows:

Let P = the total pressure, the pressure recorded by the pressure cell,

P_1 = the pressure contributed by the near wheel,

P_2 = the pressure contributed by the opposite or far wheel,

Rm = the corrected radial distance,

R_1 = the true radial distance to the near wheel,

R_2 = the true radial distance to the far wheel, and

a_1, a_2, a_3 = constants.

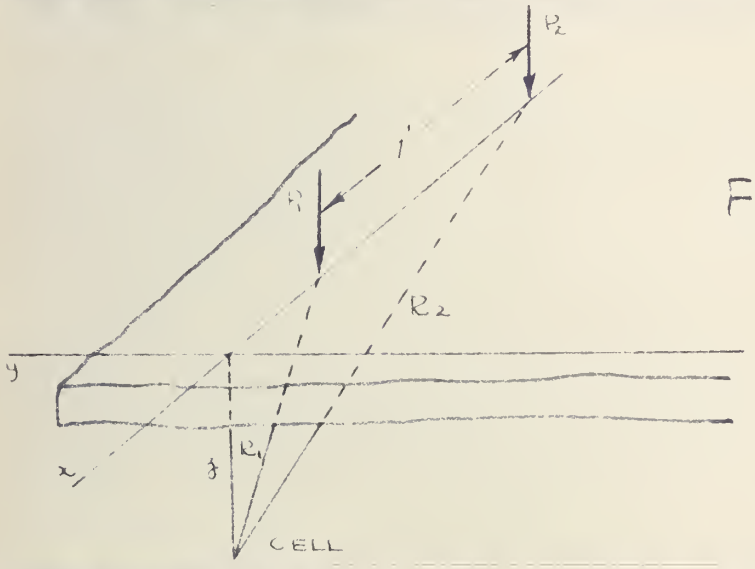

FIGURE 12

Assuming that the vertical pressure is proportional to the reciprocal of the true radial distance to the fifth power, and that the pressures contributed by the two wheels add, then we have:

$$P = P_1 + P_2$$

$$\frac{a_1}{Rm^5} = \frac{a_2}{R_1{}^5} + \frac{a_3}{R_2{}^5}$$

Assuming that $a_1 = a_2 = a_3$ we have

$$\frac{1}{Rm^5} = \frac{1}{R_1{}^5} + \frac{1}{R_2{}^5}$$

The true radial distances were then corrected according to the above formula.

Graphs of actual vertical pressure against corrected radial distance are shown in Plates 12, 13, 14 and 15. The plots are for the influence of both front and rear wheels and pressure cells 20", 31½", and 49" below the surface of the flexible pavement. Lines with a -5 slope were placed through the plotted points and as can be seen, fit very well. The constants for these curves are shown below:

CONSTANTS FOR FRONT WHEEL

Depth	Constant	Actual Constant
1.67 ft.	15.3	
2.62	18.1	
4.09	15.1	

CONSTANTS FOR REAR WHEEL

Depth	Constant	Actual Constant
1.67 ft.	27.5	
2.62	24.8	
4.09	24.3	

2. Results for the Vertical Pressure below the Rigid Pavement

(a) Corrected Radial Distance and Vertical Pressure

The corrected radial distance was computed for the rigid pavement, as shown under section 1 (d), and plotted against actual vertical pressure. Plates 16, 17, 18, 19 and 20 illustrate the above plots for the effect of both front and rear wheels and pressure cell at various depths below the rigid pavement. These graphs do not show the straight line relation as indicated by the relations for the flexible pavement. They do show that the lower portion of the curve tends to follow the reciprocal of the corrected radial distance to the fifth power relationship.

(b) Equivalent Depth

Since Boussinesque's equation holds for the flexible pavement it would be entirely reasonable to assume that the same relation would hold for the rigid pavement. The above assumption is somewhat verified by the relation

holding for the low pressures and corresponding large radial distances. If a constant was added to the depth, consequently increasing the radial distance, it was found that a plot of vertical pressure against the new radial distance, on log-log paper, showed:

(1) the top portion of the curve revolved considerably, and

(2) the bottom portion shifted slightly in the direction of increasing radial distance.

Thus it could be seen that the curves tended to straighten. It was therefore assumed that a given thickness of rigid concrete was equivalent to a depth of soil of much greater thickness. To find the depth of soil that would be equivalent to the thickness of concrete, the following method was used:

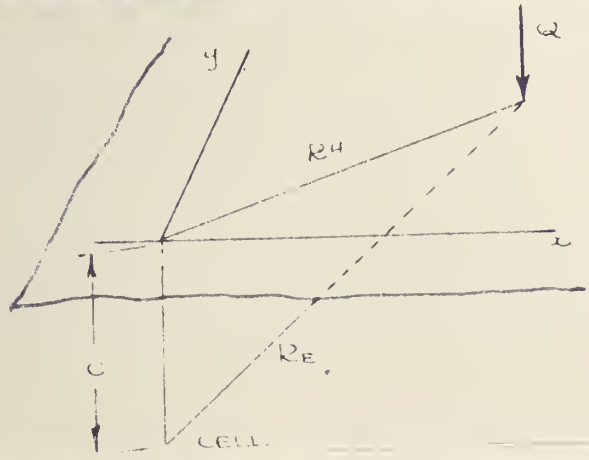

FIGURE 13

In the above diagram let

C = an assumed depth of soil greater than the actual depth to the cell. C equals the actual depth + the depth of soil equivalent to the

thickness of concrete,

RE = the equivalent true radial distance to the point of application of the load, and

RH = the horizontal radial distance to the point of application of the load.

Then

$$RE = \sqrt{RH^2 + C^2}$$

For each measured vertical pressure the equivalent radial distance to the cell was computed, with the above formula, and plotted on log-log paper. Several values of the constant C were chosen until the plots became straight; see Plates 21, 22, 23, 24 and 25. A best fit line of -5 slope was then placed through the points with the same C value. The deviation of each point from this line was then computed and squared. The average root mean square deviation was computed for each C value and plotted as shown in Plates 26, 27 and 28. The C value giving the minimum deviation was chosen as correct.

The above computations and plots were made for

the influence of both front and rear wheels on a pressure cell at depths of 15", 19" and 31" below the surface of the rigid pavement. The C values are shown below for the various depths and wheels.

FRONT		REAR
C VALUE	DEPTH	C VALUE
3.0 ft.	15"	3.5 ft.
3.5 ft.	19"	4.5 ft.
4.7 ft.	31"	5.0 ft.

The equivalent depth is computed by subtracting the actual depth from the C value. The equivalent ratio, the ratio of depth of soil equal to a depth of concrete, is also shown below.

DEPTH	EQUIVALENT DEPTH	EQUIVALENT RATIO		EQUIVALENT DEPTH	EQUIVALENT RATIO	
1.25 ft.	1.75 ft.	$\frac{1.75}{.835}$	2.1	2.25 ft.	$\frac{2.25}{.835}$	2.7
1.58 ft.	1.92 ft.	$\frac{1.92}{.835}$	2.3	2.92 ft.	$\frac{2.92}{.835}$	3.5
2.58 ft.	2.12 ft.	$\frac{2.12}{.835}$	2.25	2.42 ft.	$\frac{2.42}{.835}$	2.9

3. Results for Horizontal Pressure below a Flexible Pavement

(a) Corrected Radial Distance & Horizontal Pressure

Figure 4 illustrates the type of pressure pattern obtained for the horizontal pressure below the flexible pavement.

The corrected radial distance, as explained above in 1 (d), was computed and plotted against actual horizontal pressure on numerical and log-log paper as shown in plates 29 and 30. These curves indicate that the horizontal pressure tends to follow the Boussinesque relations.

(b) Influence & Contour Diagrams

If a set of axes are drawn as shown below, it will be seen

FIGURE 14.

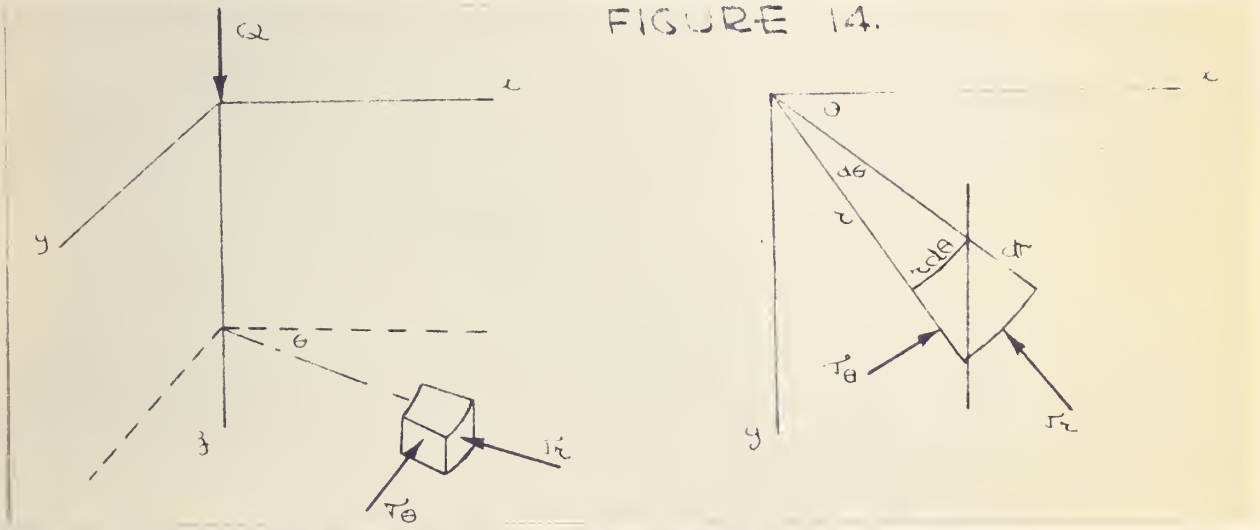

that the stresses σ_r and σ_θ may be resolved

into a stress parallel to the x axis, or the horizontal stress as measured by the pressure cell. The horizontal stress h is equal to

$$\sigma h = \sigma r \cos^2\theta + \sigma\theta \sin^2\theta$$

$$= \frac{Q}{2\pi}\left\{(1-2\mu)\left[\frac{1}{r^2} - \frac{z}{r^2}\frac{1}{R}\right] - 3r^2 z \frac{1}{R^5}\right\}\cos^2\theta \quad \ldots\ldots (17)$$

$$+\left\{\frac{Q}{2\pi}(1-2\mu)\left[-\frac{1}{r^2} + \frac{z}{r^2}\frac{1}{R} + z\frac{1}{R^5}\right]\right. \sin^2\theta$$

This relation, assuming $\mu = 0.4$ and $\frac{Q}{2\pi} = 1$, was used to compute an influence diagram for horizontal pressure when a unit load was moved along a line parallel to the x axis as shown in Figure 14.

Several different y distances were chosen and the influence diagrams plotted as illustrated in plate 31. A contour diagram with horizontal position plotted against theoretical pressures was drawn as shown in plate 32. The theoretical pressure was taken from this diagram using the actual locations of the wheel from the field data. The

theoretical horizontal pressure was plotted against actual horizontal pressure for the front wheels of buses as shown in plate 33. Since the rear wheels of the bus carry 2/3 the load on the bus, 2/3 of the actual horizontal pressure for the rear wheels was plotted against theoretical pressure in plate 34.

Both of these graphs have considerable scatter, but they indicate that the Boussinesque theory holds since the points tend to line on a straight line.

(c) Radial Distance versus Horizontal Pressure for $\mu = 0.5$ Case

If μ is assumed 0.5 then $(1-2\mu) = 0$ and consequently equation (17) reduces to

$$\sigma_h = \frac{Q}{2\pi}\left\{-3r^2 z \frac{1}{R^5}\right\} \cos^2\theta$$

From Figure 14 $\cos^2\theta = \frac{x^2}{r^2}$

Therefore

$$\sigma_h = -\frac{3Q}{2\pi} z \frac{x^2}{R^5}$$

Plate 35 shows actual horizontal pressure plotted against x^2 over corrected radial distance. This curve indicates a straight line relation and consequently indicates that Boussinesque's equations hold.

4. Results for Horizontal Pressure below a Rigid Pavement

(a) Influence Diagrams using C - Value

As can be seen from Figure 5 the horizontal pressure below a rigid foundation does not decrease when the point of application of the load is directly above the pressure cell. This seemed to indicate that the rigid pavement was equivalent to a greater thickness of soil as mentioned under results for vertical pressures. Consequently the theoretical horizontal pressure was computed using an average C value, found above, for finding the equivalent radial distance. Plate 36 is a plot showing theoretical pressure computed for the equivalent radial distance for various positions of the wheels. This graph indicates that the use of an equivalent depth does not eliminate the decrease in pressure when the point of application is directly above the cell.

(b) Influence and Contour Diagrams for Distributed Loads

The true radial distance was then used to compute influence diagrams for horizontal pressures on the pressure cell $18\frac{1}{2}$" below the rigid pavement. See plate 37. It was thought that the rigid pavement was tending to increase the area of application of pressure; therefore influence diagrams were computed for various areas of contact. To illustrate this point it was assumed that the pressure spread through the slab at 30 , 45 and according to Westergaard's theory. With a pavement .835 ft. thick and tire contact length of .6 ft., the load would spread over a diameter of 1.5 ft., 2.2 ft. and 0.6 ft. The influence diagrams for a distributed load, which were found by computing the area under the influence diagram for a point load, do not become parabolic when these load distributions are assumed.

(c) Radial Distance versus Horizontal Pressure for $\mu = 0.5$

If μ is assumed to be 0.5, as in the flexible

case, we find:

$$\sigma_h = -\frac{3}{2\pi} Q \frac{x^2}{R^5}$$

A plot of actual horizontal pressure versus theoretical pressure of the above expression shows a straight line relation in plate 38.

B. RESULTS OF DYNAMIC EFFECTS

1. Results of Moving and Braking Loads

(a) Results of Continually Moving Loads

The writer went through the original data and recorded the maximum pressure and wheel location of buses that passed over the pressure cell at various velocities without stopping or braking. These pressures were then plotted against horizontal radial distance, on graphs of static load versus horizontal radial distance. Plate 39 illustrates these plots which indicate that there is no significant difference between static and dynamic loading.

(b) Results of Braking Effects

As illustrated in Figure 6 it can be seen that braking effects are shown up clearly. The maximum pressure due to braking was compared to the static pressure recorded at the location where the bus had stopped. The ratio of braking pressure to static pressure was plotted against static pressure at both the rigid and flexible locations for all positions of the cell, as shown in plates 40 and 41. There was no trend to indicate that any particular position of the cell measured an appreciable increase in braking pressure compared to any other position. The frequency of repetition of braking ratio was also shown on the graphs.

(c) Effect of Braking on a Pressure Bulb

It was considered that this braking effect was in the form of a shock wave and that there may be a large increase in the diameter of the pressure bulb. Consequently, a pressure bulb was plotted, as shown in plate 42, for the vertical pressure below the flexible pavement. On this plot the increase in pressure due to braking, at the 0.1 $\frac{\text{tons}}{\text{in}^2}$

pressure, was plotted. This showed very little increase in diameter of the pressure bulb.

C. RESULTS OF SHEARING STRESSES

The principal stresses induced in a homogeneous semi infinite mass when under the influence of a point load occur in the general direction of the radial and at right angles to the radial. The maximum principal stress occurs directly below the point of application of the load and in the direction of the radial. Directly below the point of application of the load the stresses σr and $\sigma\theta$ are equal and are the minimum principal stresses.

Consequently the vertical pressure is the major principal stress and the horizontal pressure is the minor principal stress. Plate 43 shows Mohrs circles for the actual horizontal and vertical pressures measure below the rigid and flexible pavements.

Assuming that Boussinesque's theory applies, then the maximum and minimum principal stress occur directly below the load and are;

$$\sigma_1 = \sigma_z = \frac{3Q}{2\pi z^2}$$

$$\sigma_{II} = \sigma_{III} = \sigma_r, \sigma_\theta = -\frac{Q(1-2\mu)}{4\pi z^2}$$

If load = Q and $\mu = .4$ we have the following stresses:

z	$\sigma_1 = \frac{3Q}{2\pi z^2}$		$\sigma_{II} = -\frac{Q(1-2\ )}{4\pi z^2}$
0	∞	-	∞
1	.477Q	-	.0159Q
2	.119Q	-	.0040Q
3	.053Q	-	.0018Q
4	.0298Q	-	.0010Q
5	.0191Q	-	.0006Q

Mohrs Circles were plotted for the above stresses as shown in plate 44, and the maximum shearing stresses plotted against depth as shown in plate 45.

Plates 46, 47, 48 are plots of compressive strength versus moisture content for several locations on

Jasper Avenue which have similar soil types as the locations at which the cells were installed. Plate 49 indicates the variation of moisture content with depth for the Jasper Avenue locations.

DISCUSSION

1. Discussion of Vertical Pressure below a Flexible Pavement

It was noted in the results that the plots of grouped and averaged vertical pressure and true radial distance had slopes of -4.6, -4.7 and -4.8. Consequently, it was assumed that the vertical stress followed Boussinesque theory which indicated that the reciprocal of the true radial distance to the fifth power was proportional to the vertical pressure. In plates 12, 13, 14 and 15, which are plots of individual vertical pressures and corrected radial distance, it will be see n that a line of slope -5 fits the points very well.

The scatter of points are due to the error in measuring horizontal distance. Lines at one foot intervals were drawn on the road surface; consequently, the position was

accurate only to $\frac{1}{4}$ foot. At large horizontal distances and corresponding small vertical pressures, the pressure cell appeared to be rather insensitive. This is shown clearly in all plots.

The constants computed from the graphs check very well with one another and are approximately one half the values computed from theory. This assumes that the tire contact area could be considered as a point load and the load was equal to the tire pressure.

2. Discussion of Vertical Pressure below a Rigid Pavement

Plates 21, 22, 23, 24 and 25 show the use of a C-value in straightening the plots of vertical pressure versus radial distance. As stated in results, the assumption that the vertical pressure below a rigid pavement follows Boussinesque's theory, is justified by:

(1) having the Boussinesque relation verified for the vertical pressure below the flexible pavement, and

(2) having the lower portion of the plots of corrected radial distance versus vertical pressure follow the Boussinesque relation.

The equivalent ratio computed for various depths and both front and rear wheels has values lying between 2.0 and 3.5. Reference 5 states, "bituminous surfaces were

indicated by load test data to have a greater supporting capacity per unit of thickness than do granular bases. The ratio appears to vary from about 1.5 for those made with liquid asphalt and soft asphalt cement, etc., binders, to about 2.5 for well designed and constructed asphaltic concrete, penetration macadam, and sheet asphalt." This statement would indicate that the concept of equivalent depth is not erroneous.

3. Discussion of Horizontal Pressure below a Flexible Pavement

For the flexible pavement, plates 29 and 30 indicate that the horizontal pressure versus corrected radial distance tends to follow Boussinesque's relations.

The horizontal stress, equation (17), varies with the value of Poissons Ratio that is chosen for the soil. This then, may be the cause of the large scatter when actual horizontal pressure is plotted against theoretical pressure. The value of Poissons Ratio of 0.4 was chosen from reference 6. The above results, do however, show a straight line relation on numerical paper thus indicating that Boussinesque theory applies.

If Poissons Ratio is assumed equal to 0.5, then equation (17) reduces to:

$$\sigma h = -\frac{3Q}{2\pi} z \frac{x^2}{R^5}$$

Plate 35 is a plot of this equation, which also shows a straight line relation.

If a saturated soil is loaded and there is no possibility of drainage there would be no reduction in volume, that is, Poissons Ratio equals 0.5, since the water is incompressible. This may apply beneath a road surface, if the soil is saturated, and the load is applied over a short time interval, as in stopping at a bus stop.

The large scatter of points could be attributed to the shape and position of the pressure pattern or influence diagram. The theoretical pattern, as illustrated in plates 31 and 37, show very steep slopes to a maximum approximately 2.5 ft. from the centre of the cell. If, in the actual case, the influence diagram is shifted towards or away from the cell there will be large differences between actual and theoretical pressures, thus giving a very large scatter.

4. Discussion of the Horizontal Pressure below a Rigid Pavement

It will be noted that the horizontal pressure below a rigid pavement, as shown in Figure 5 , did not decrease when the point of application of the load was directly over the cell. It was hoped that the use of an equivalent depth, as in section 2 of results, would tend to make the theoretical pressure parabolic. This was not the case. Similarly, assuming a distributed load did not give the desired result. Consequently, it was assumed that some other factors were affecting the horizontal pressure below a rigid pavement.

If Poissons Ratio was assumed 0.5, plots of actual horizontal pressure versus theoretical pressure did indicate a straight line relation. Again, the effects of a saturated soil must be considered.

5. Discussion of Dynamic Effects

The plot of pressures due to dynamic, and static effects, as shown in plate 39, does not indicate a significant difference between pressure due to continually moving loads and static loads. The trend is to indicate that the continually moving loads do not give an appreciable increase

or decrease in pressure over the pressure caused by static loads.

The plots, plates 40 and 41, of the ratio of braking pressure to static pressure against static pressure did not indicate that any particular position of the cell measured an increase in braking pressure compared to any other position. Consequently, it was assumed that a large shearing stress was not developed due to braking.

The frequency of repetition of braking ratio was also shown on the above plots. Dr. McLeod reports, in Reference 5, that the deflection increases as the log of the number of repetitions of load. It is also indicated from the above report that for a 30 inch diameter plate 10,000 repetitions of a 47,000 pound load would cause a deflection of 0.5 inches. For the same 0.5 inch deflection and plate size it would require 1000 repetitions of a 51,000 pound load, or 10 repetitions of a 61,000 pound load, or 1 repetition of a 67,000 pound load. These results show the effect of a number of repetitions on stability of pavements. Therefore, both magnitude and the number of repetitions of braking stresses must be considered.

Since the graph tends to curl up at low static loads, i.e., high braking ratios at low loads, it was considered

that the braking effect caused a shock wave. At low loads the pressure due to the shock wave was large compared to the static pressure and at high loads it was small compared to the static pressure. This shock wave effect would increase the diameter of the pressure bulb and subject a larger volume of soil to the influence of higher pressures. Consequently, there was the possibility of larger deflections, and therefore, failure. The plot of the pressure bulb does not indicate a large volume within which increased stresses would occur.

The plots indicate that the large braking ratios occur at low loads, and consequently would not tend to cause damage to the pavement. At high loads the average braking ratio was 1.05, which is very small and unlikely to cause damage.

6. Discussion of Shearing Stresses

Plate 43 shows the Mohr circles for the major and minor principal stresses directly below the point of application of the load for both rigid and flexible pavements. The shearing stress at depth 20", from this figure, equals 2.08 #/□" for the flexible pavement and 0.1 #/□" for the rigid pavement.

Using the theoretical Boussinesque equations Plate 44 shows a plot of Mohr circles for stresses at various depths. From this plot, Plate 45 showing shearing strength against depth, was plotted.

Plates 46, 47, 48 and 49 show strength and moisture characteristics for several locations on Jasper Avenue. The Atterberg Limits for these locations are:

	Liquid Limit	Plastic Limit
at 109 St. and Jasper Ave.	75%	27%
119 St. and Jasper Ave.	66%	24%
120 St. and Jasper Ave.	56%	26%

The Atterberg Limits at the flexible and rigid locations are:

	Liquid Limit	Plastic Limit
at 99 St. and 66 Ave. (rigid)	56.7%	24.7%
100 St. and 82 Ave. (flexible)	60.2%	25.4%

It was then assumed that the strength characteristics would apply to both locations.

From Plate 49 it was estimated that the maximum moisture condition at the time of testing was 35%.

The compressive strength and shearing strengths of the soil at 35% moisture are tabulated below:

Plate Number	Compressive Strength	Shearing Strength
46	9.6#/ "	4.8 #/ "
47	8.3	4.1
48	12.8	6.4

The best available theory as to the failure of a loaded area is that attributed to Brandtl, which presents an expression for the ultimate bearing capacity of long loaded areas of breadth b on the ground surface. For highly cohesive soils at ground surface, the ultimate bearing capacity of a long footing reduces to

$$qu = 5.14\ C.$$

where qu = the ultimate bearing capacity per unit area, and

c = cohesion per unit area.

For a round footing on highly cohesive soils the ultimate bearing capacity becomes

$$qu = 7.4\ C.$$

The case of the round footing applies for the bus loading since the tire contact area approaches a circle.

For a saturated homogeneous clay the cohesion is equal to the shearing strength.

For the flexible pavement the theoretical shearing stress is 5 at a depth of 2 ft. If the moisture content at this depth is 35% the ultimate bearing capacity equals 37 thus indicating that the soil is safe against failure at this depth.

It is to be noted that as the depth decreases the shearing stress increases and approaches an infinite value at the ground surface. The theoretical shearing stress directly below the pavement is 24.8 . If the moisture content were 38%, the shearing strength and ultimate strength would be 3.4 and 24.8 respectively.

magnitude under the loads applied and could cause failure if the moisture content was high.

7. Discussion of Deflection

Dr. McLeod states that failure of a subgrade and bituminous surfaces will take place at a deflection of .26 and 0.225 inches respectively.

There have been no deflection measurements in this investigation. It would be very interesting, however, if a consolidation test could be run applying and releasing the load to simulate the conditions at a bus stop. This may indicate if the deflection applied by one load would remain or rebound. The test might also indicate if the deflections per loading could be added and give the order of the maximum deflection to be expected.

8. Discussion of Moisture Conditions

A critical moisture condition occurs in the early spring as the frost begins to leave the ground. This is verified by the fact that the most damage to the pavements takes place at this time. Therefore, when pavements are to be designed an investigation of the moisture conditions over several seasons would be advantageous.

It was noted during testing operations that the joint between the curbing and the concrete of the road bed proper was not very tight. It was observed during wet periods that there was a considerable increase in moisture content in the soil below the base due to leakage. This increased moisture content decreases the strength of the soil and might account for the deterioration at the stop and not between stops, since there would not be any appreciable increase in moisture throughout the road bed as a whole.

9. Discussion of Pavement Failure

When the soil below a pavement is subject to stress the direction of movement is as shown below, for both granular and plastic materials. (See reference 7 and 8.)

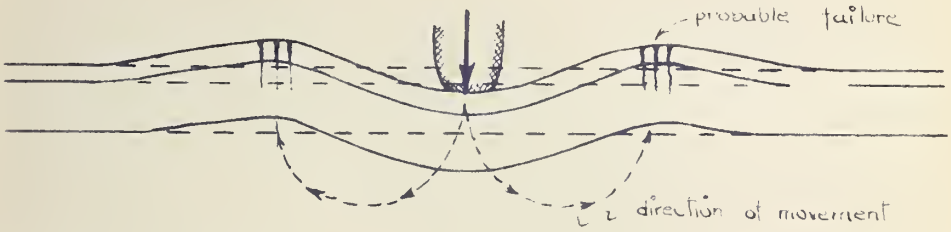

Consequently, if the movements incurred are of a magnitude such that they will cause the maximum allowable deflection, as discussed above, failure of the pavement

will take place. If the soil fails in shear the effect on the pavement will be magnified.

10. Discussion of Design

In reference 5 Dr. McLeod states "According to this series of tests, dual wheels of this size and spacing carry from 25 to 30 percent more load than a single wheel with the same contact area at any given deflection over a range of 0.2 to 0.5 inches."

The maximum load carried on the trolly buses is 31,860 pounds. The rear axle carries 65% of the weight, or 20,700 pounds, and one set of dual tires carries 10,350 pounds. Consequently, the dual tire is equivalent to a single tire of the same contact area as the dual carrying 30% less load. The load on the single tire then is 7,250 pounds. The average CBR value for the locations were 3.4 at 32% moisture. From the design chart, figure 107, reference 5, a 14 inch thickness of granular base would be required for the above load and CBR value. If the moisture content was increased, the CBR value would decrease, thus requiring an increased thickness of granular base.

An investigation of the gross weights carried by truck traffic was made. It was found that the gross weight for

the trucks of the four companies investigated was 24,000 pounds. The latest information from the Highway Traffic Board states that the gross load to be carried on a truck with number 900 dual tires is 24,000 pounds. The Highway Traffic Board also states that the rear axle carries 2/3 of the load. Therefore, the maximum load on one set of dual tires is 8,000 pounds, which is equivalent to a load of 5,600 pounds on a single tire. (See reference 5.)

Entering Dr. McLeod's chart with a CBR value of 3.4 and a maximum load of 5,600 pounds, the thickness of granular base required is 8 inches.

11. Discussion on Cell, Pocket and Cover Action

As stated under installation of the cell, the soil was packed around the cell as dense as or denser than the surrounding soil. This procedure eliminated under-registration due to cover action and gave a limited amount of over-registration due to cell and pocket action. This over-registration was not considered in any of the data. The over-registration would affect only the position of the graphs; the shapes would be similar.

12. Discussion of Installation of Cells

As was mentioned under installation of pressure cells,

there is considerable under-registration of pressure for cells placed within the soil mass and surrounding soil loosely replaced. Consequently, it is worth repeating that considerable effort and care was taken to insure that the soil around the cell was denser than the soil mass as a whole. This, according to Ref.- 5, gives a limited amount of over-registration whereas a loose pocket gives unlimited under-registration.

13. Discussion of Cell

The pressure cell used was found to work very well after the flexible membrane had been made sensitive enough. The only difficulty encountered was due to leakage resistance. The saran tubing which carried the leads from the strain gages was not stable after the exposure and slightly rough handling it received. It was found that water could enter through small cracks in the weathered saran and consequently cause a leakage resistance. Three strand rubber insulated cable would be recommended as a replacement for the saran. It is recommended that considerable care be taken to waterproof the gages and to prevent moisture from entering the cell proper.

CONCLUSIONS

1. (a) The vertical pressure below a flexible pavement follows Boussinesque theory.
   (b) The flexible pavement is equivalent to the same thickness of soil.

2. (a) The vertical pressure below a rigid pavement follows Boussinesque theory.
   (b) The rigid pavement is equivalent to 2 to 3.5 times the same thickness of soil. That is to say, the rigid pavement spreads the load such that the distribution would be the same if the point of application of the load is at a height 2 to 3.5 times the thickness of concrete.

3. The results of horizontal pressure below a flexible pavement indicate that Boussinesque theory applies.

4. The results of horizontal pressure below a rigid pavement indicate that Boussinesque theory may apply. There can be no conclusive statement made with regard to this section.

5. There does not appear to be a significant difference

between pressures due to continually moving loads and pressures due to static loads.

6. There were no large shearing stresses induced by the braking effects.

7. It was indicated that the pressures set up by braking caused a shock wave to form. The stresses due to the shock wave were insignificant.

8. The effect of braking was insignificant.

9. The actual shearing stress of 2.0 pounds per square inch at 1.67 ft. below the surface of the flexible pavement would cause a shearing failure of the soil at a moisture content of 42%. This is an increase of 7% over the actual moisture content.

The theoretical shearing stress increases with decreasing depth and approaches an infinite value at the ground surface. Directly below the pavement, 0.83 ft. from the surface, the theoretical shearing stress is 24.8 pounds per square inch, which would cause failure of the soil at a moisture content of 29%. Failure of the pavement may take place as described under discussion.

10. The deterioration occurs at the bus stop first because of the frequency of repetitions.

11. Using the results of Dr. McLeod's report, 14 inches of granular base would be required for bus loads and 8 inches for truck loads.

RECOMMENDATIONS FOR FUTURE STUDY

The stresses on pressure cells placed at angles of 45 degrees should be analyzed to see if they will follow Boussinesque relations. The horizontal pressures measured on vertical cells should be subject to a more intensive study to come to more definite conclusions.

A field set up whereby pressure cells could be installed at various depths and positions below a subgrade and then tested would be advantageous. To this subgrade could be added various sub-base materials such as gravel, concrete and asphalt. With this set up the effects of various thicknesses and combinations of the above materials could be investigated.

Another important effect to be considered is the

deflection of the pavement under loads. This is linked up with the stability of the subgrade and the effects of the two must be correctly evaluated. This study might be investigated by the use of strain gages cemented to very flexible strips of steel placed within the asphalt.

APPENDIX

Calibration of the Pressure Cell

The pressure cell with rubber mats both top and bottom was placed in a hydraulic loading machine. The cell was then connected to the Brush Strain Analyzer, grounded, and allowed to warm up for 30 minutes. Loads in 100 pound increments were then applied to the cell while the strain recorder automatically traced the pressure pattern.

Several runs were made and the data computed and plotted to give the calibration curve of figure 50.

Computation of True Radial Distance

To facilitate the computations of true radial distance and corrected radial distance for the various depths, the following formula was used:

$$R = \sqrt{x^2 + y^2 + z^2}$$

Letting z = constant and $x = 0$ we then have:

$$R = \sqrt{y^2 + z^2}$$

and $$y = \sqrt{R^2 - z^2}$$

A plot was made of this function as shown on plate 10. Using this curve, plate 11 was constructed by drawing arcs corresponding to the true radial distance with various radii of y. Thus, by entering plate 11 with the coordinates of the point of application of the load, the true radial distance, at the depth for which the chart was made, may be read off directly. These plots were made for all the depths of cells in this report.

Points cannot be averaged when the function varies as a reciprocal to a high power. The diagram

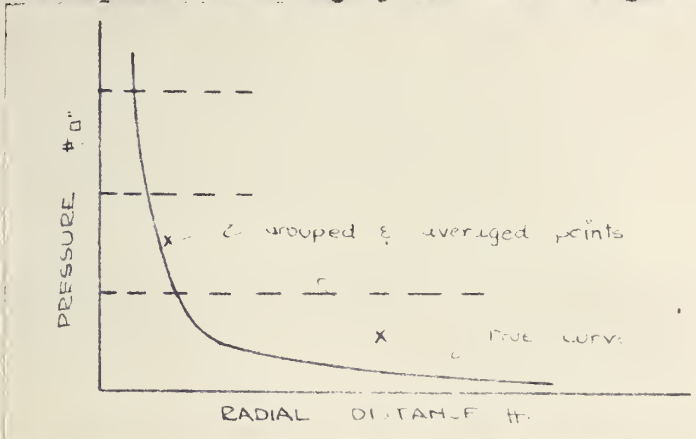

above illustrates this point. The points at low pressure have a large variation in radial distance. The radial distance

is large for these points, and consequently, the averaged radial distance will be large. Thus, the point would not fall on the true curve.

BIBLIOGRAPHY

Reference 1 - Triaxial Shear Research and Pressure Distribution Studies on Soil, under the auspices of Waterways Experiment Station.

Reference 2 - Soil Pressure Cell Investigation, Technical Memorandum No. 210-1, under the auspices of Waterways Experiment Station.

Reference 3 - Operating Instructions for Brush Strain Analyzer and Operating Information for Brush Oscillograph Equipment, the Brush Development Co., 3405 Perkins Ave., Cleveland 14, Ohio.

Reference 4 - SR-4 Portable Strain Indicator, Baldwin Southwark, Baldwin Locomotive works, Philadelphia.

Reference 5 - Airport Runway Evaluation in Canada by N. W. McLeod.

Reference 6 - Soil Mechanics by D. P. Krynine.

Reference 7 - Highway Research Board Proceedings, 1943.

Reference 8 - Highway Research Board Proceedings, 1948.

FACE PLATE

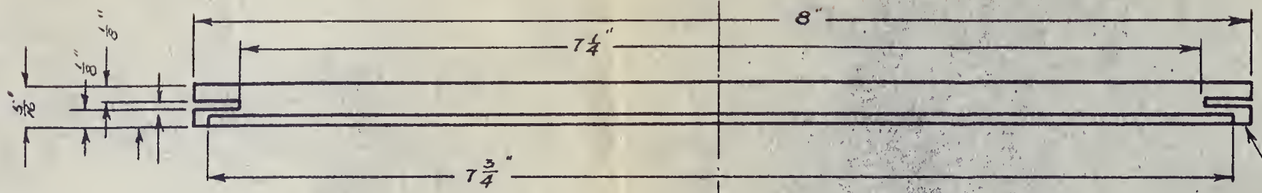

SWEAT TOGETHER

SECTION A-A
BASE PLATE

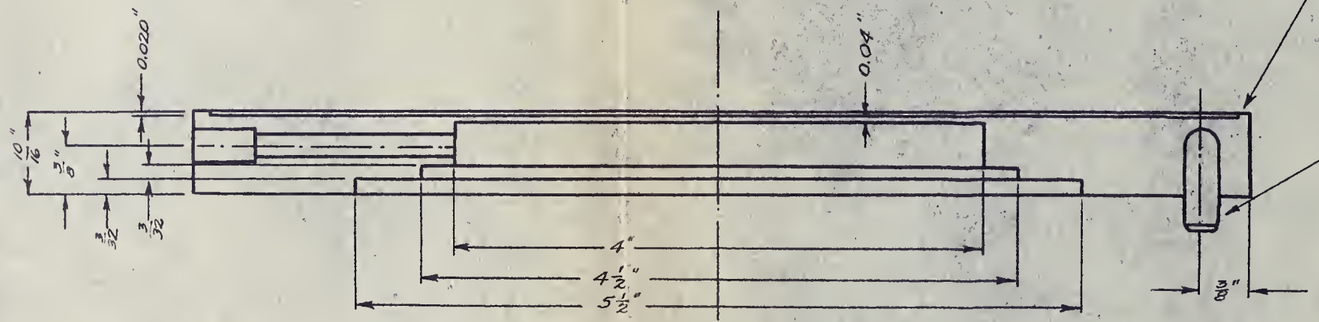

2-NO-00 TAPER PIN
drive & cut off after filling with oil

SECTION BB
COVER PLATE

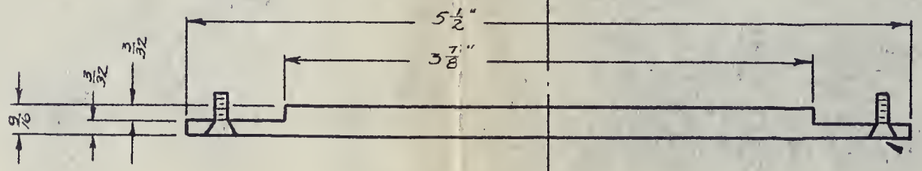

NO 6 - 32 FH
BRASS SCREWS

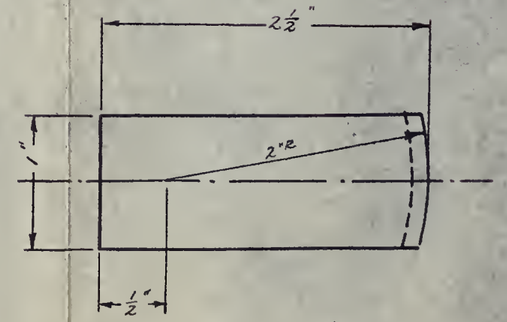

GAGE HOLDER

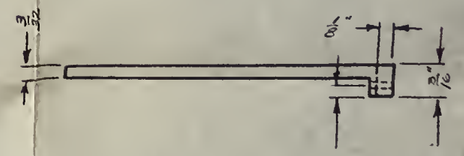

NOTE:

GAGE HOLDER

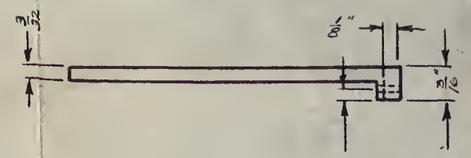

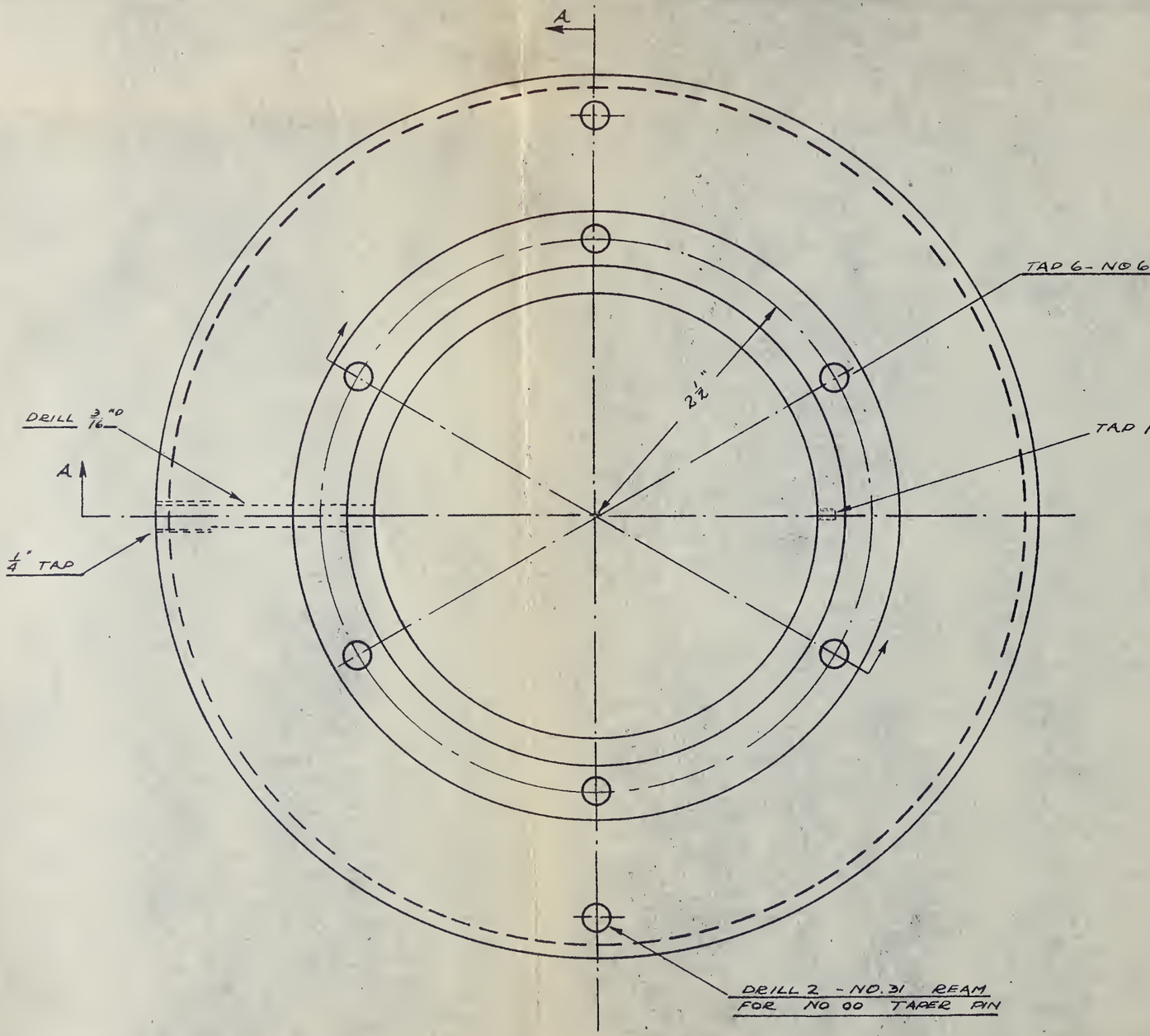

NOTE:
- all fillets 1/16" R
- all parts mild carbon hot rolled plate.

FIG 15

UNIVERSITY OF ALBERTA

DEPARTMENT OF CIVIL ENGINEERING

SOIL PRESSURE CELL

May 14. 1948 by: PJR.

Plate I

PRESSURE VS HORIZONTAL RADIAL DISTANCE

HORIZONTAL CELL - STATIONARY

WHYTE AVE & 82nd ST. OLD BUS

DEPTH 51½"

PJC.

PLATE I

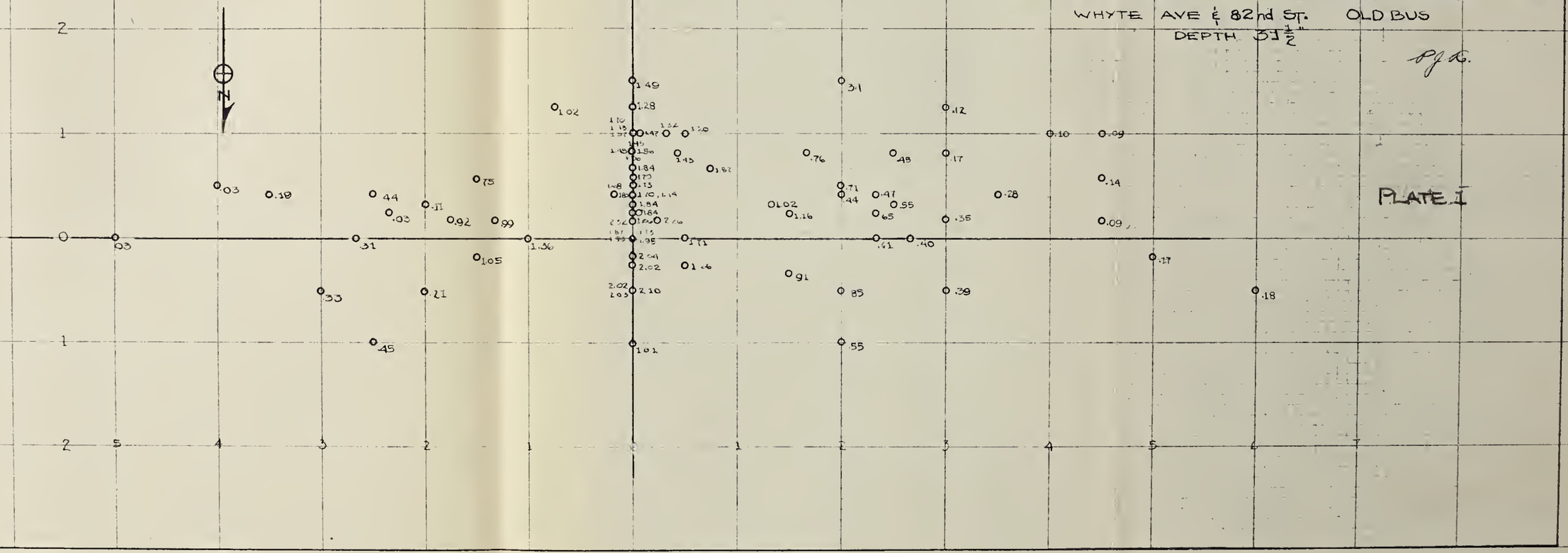

PLATE 2

GROUPED & AVERAGED PRESSURES VS. HORIZONTAL RADIAL DISTANCE

FOR FRONT WHEEL OF NEW BUSES.

STATIC BUS; HORIZONTAL CELL; DEPTH 31½"

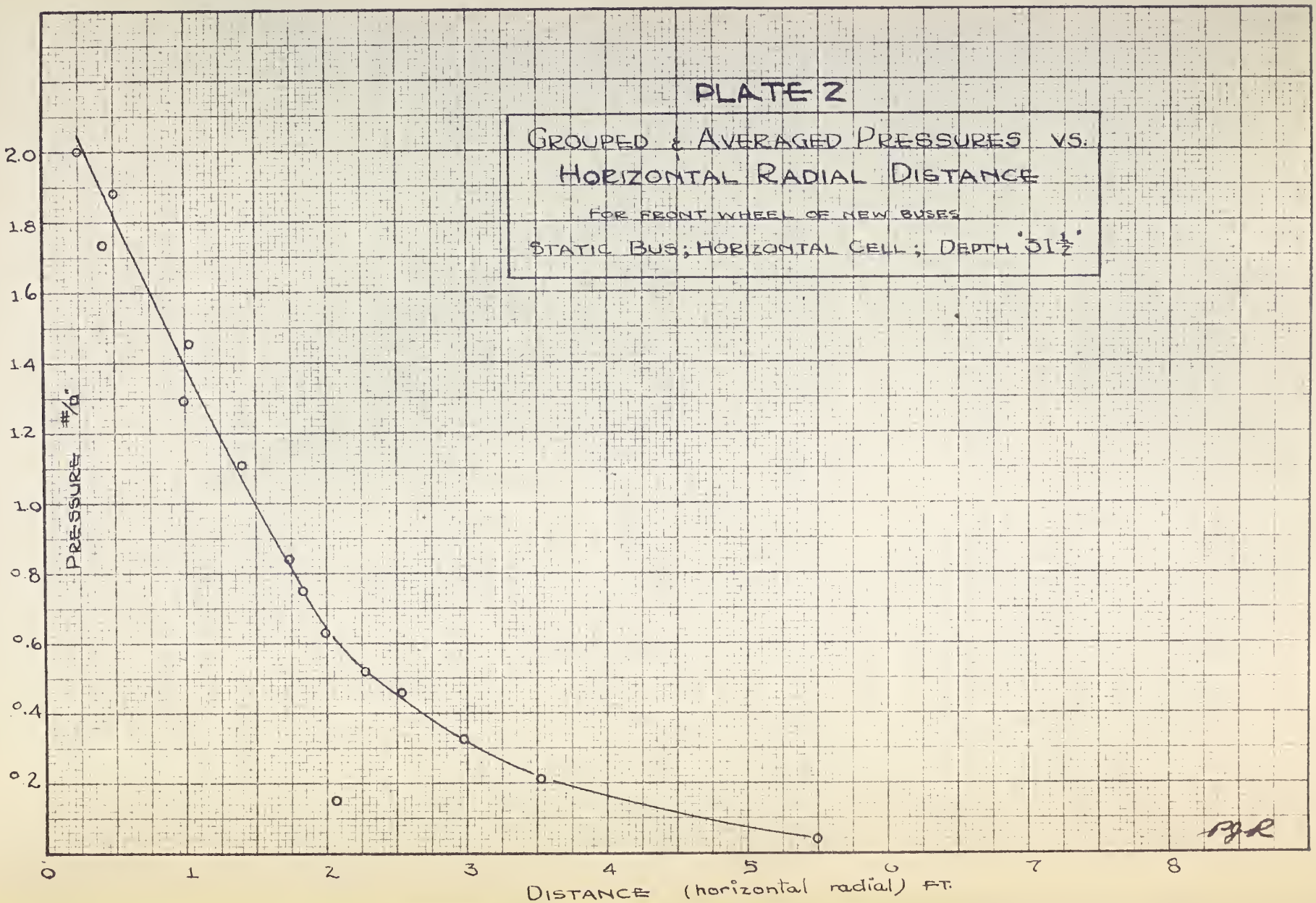

PLATE 3

GROUPED & AVERAGED PRESSURES VS. HORIZONTAL RADIAL DISTANCE

FOR FRONT WHEEL OF NEW BUSES

STATIC BUS; HORIZONTAL CELL; DEPTH 31½"

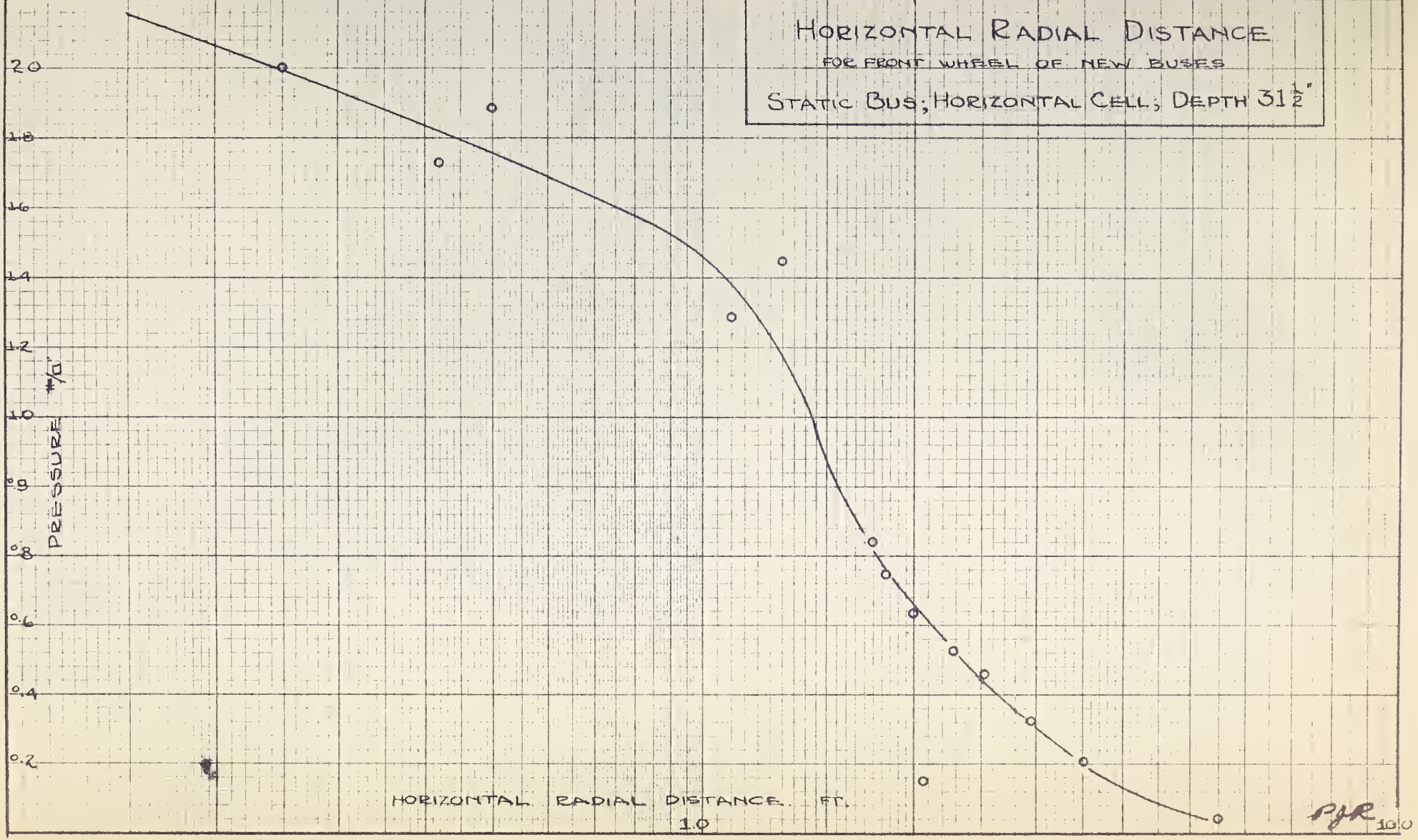

PLATE 4.

GROUPED & AVERAGED PRESSURES VS HORIZONTAL RADIAL DISTANCE

FOR FRONT WHEEL OF NEW BUSES

STATIC BUS; HORIZONTAL CELL; DEPTH $31\frac{1}{2}$"

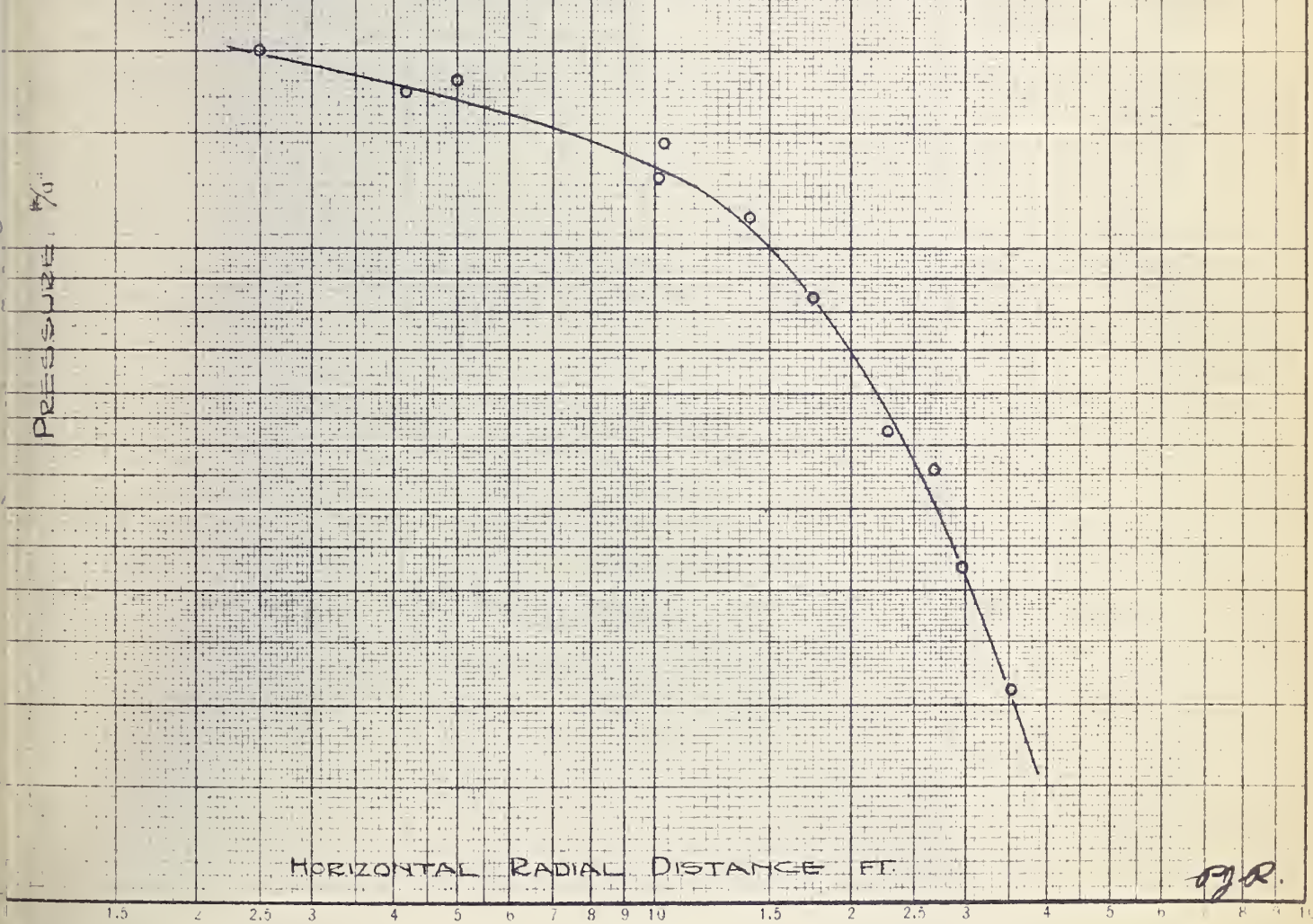

.1

10

10

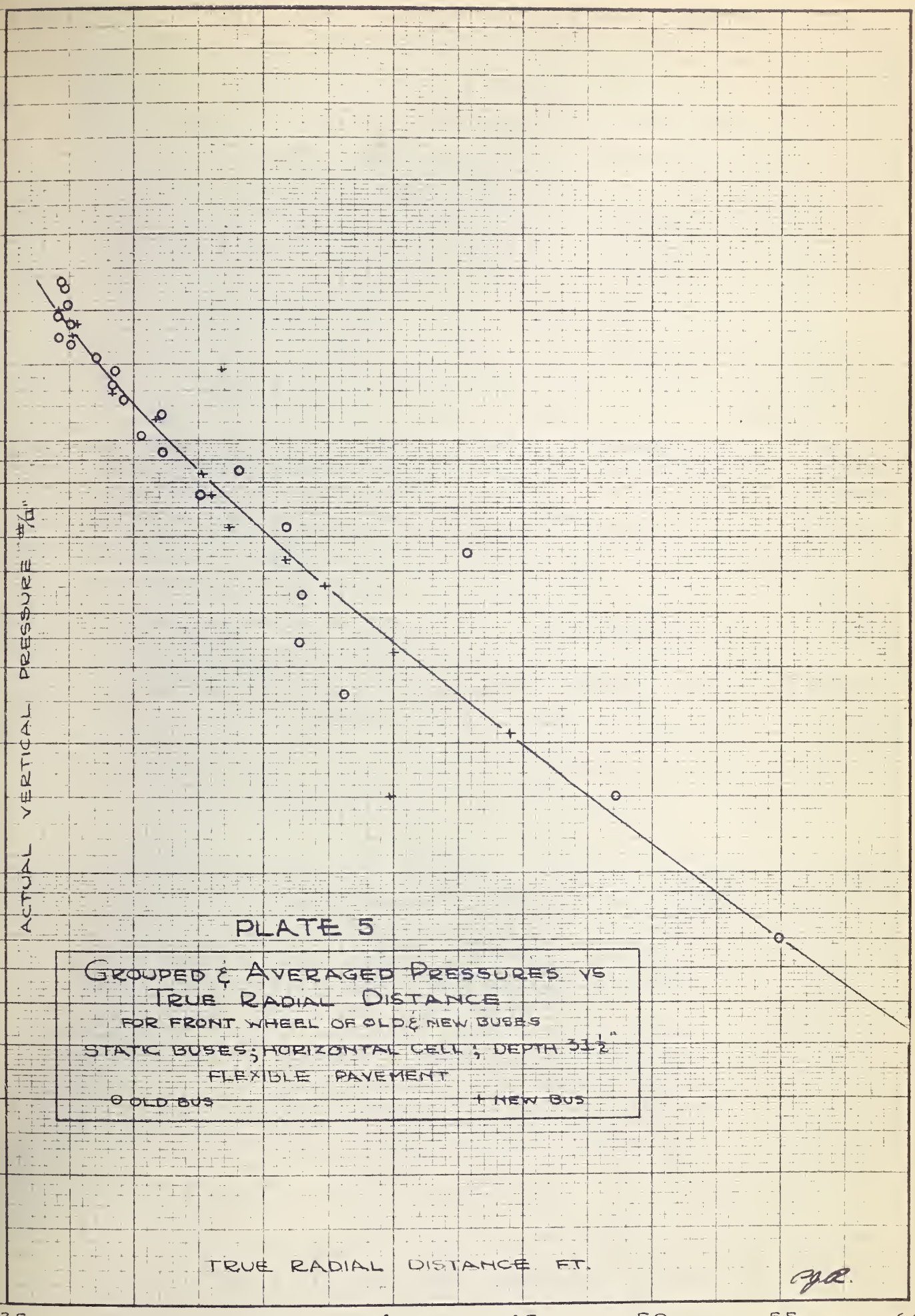

PLATE 5

GROUPED & AVERAGED PRESSURES VS TRUE RADIAL DISTANCE.
FOR FRONT WHEEL OF OLD & NEW BUSES
STATIC BUSES; HORIZONTAL CELL; DEPTH 31½"
FLEXIBLE PAVEMENT
O OLD BUS + NEW BUS

PJR.

PLATE 6

GROUPED & AVERAGED PRESSURES VS TRUE RADIAL DISTANCE

FOR FRONT WHEEL OF OLD & NEW BUSES

STATIC BUSES; HORIZONTAL CELL; DEPTH 31½"

FLEXIBLE PAVEMENT

⊙ OLD BUS + NEW BUS

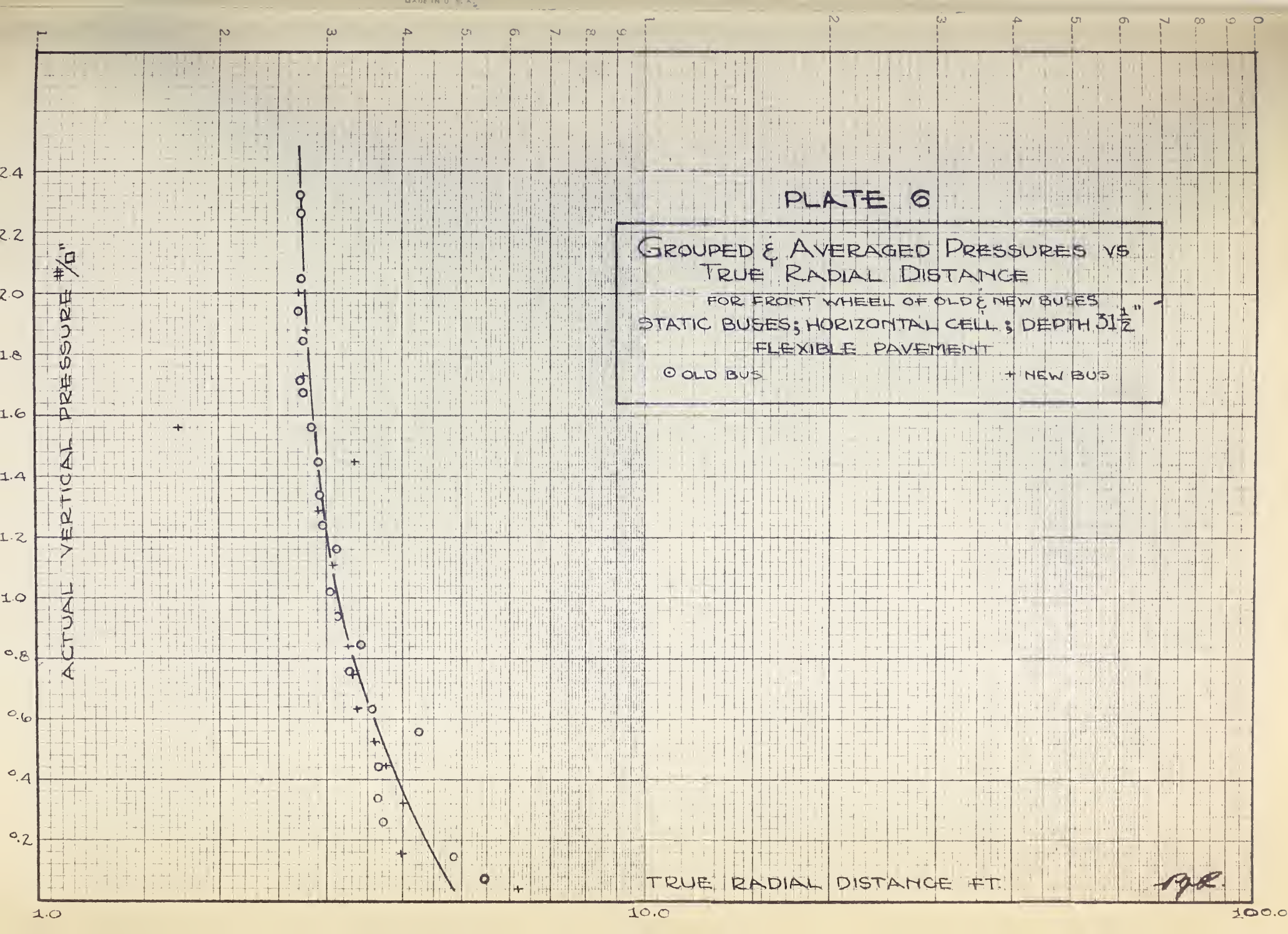

PLATE 7

GROUPED & AVERAGED PRESSURES VS TRUE RADIAL DISTANCE

FOR FRONT WHEEL OF OLD & NEW BUSES

STATIC BUSES; HORIZONTAL CELL; DEPTH 31½"

FLEXIBLE PAVEMENT

o OLD BUS + NEW BUS

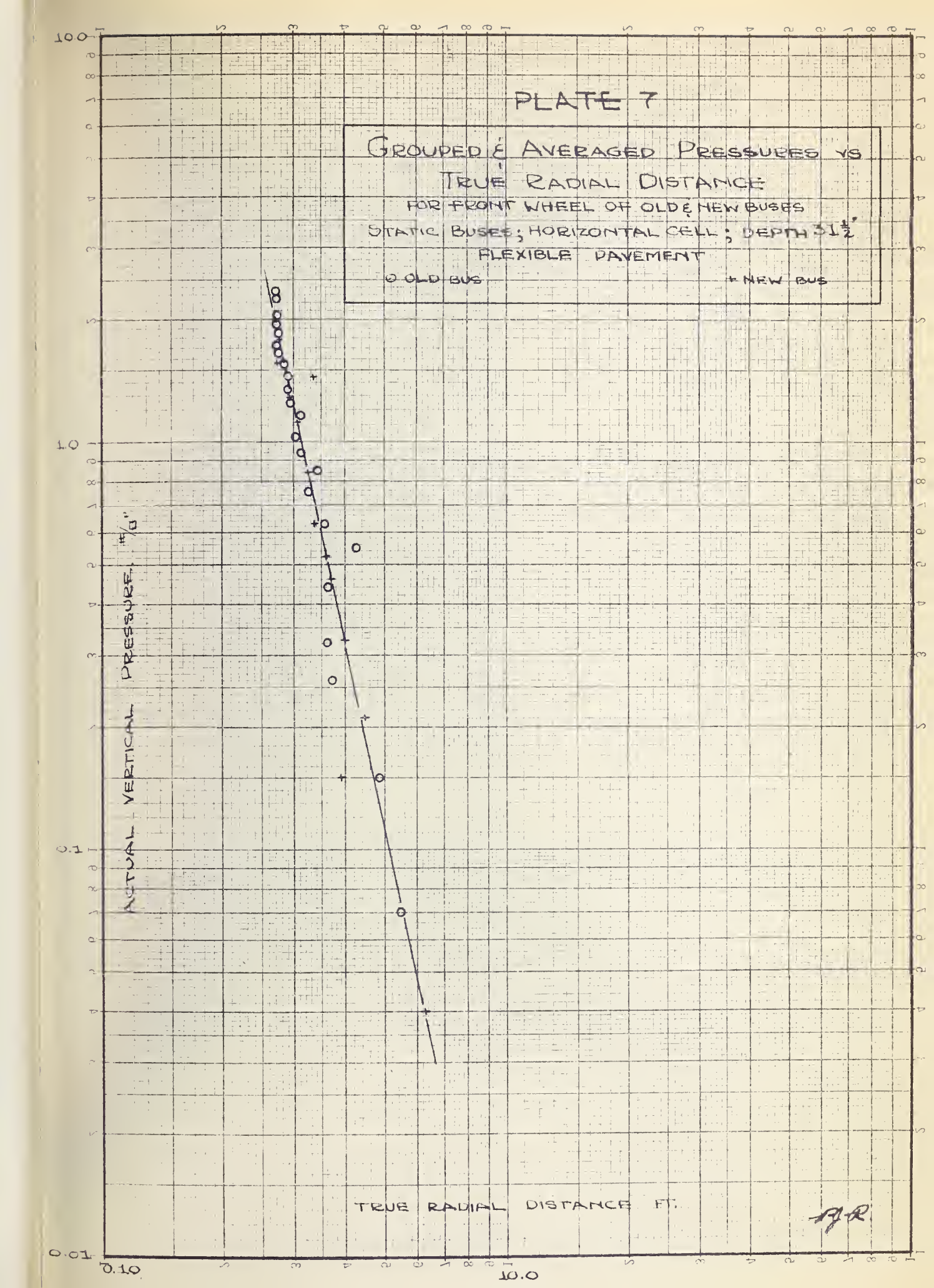

PLATE 8

GROUPED & AVERAGED PRESSURES VS TRUE RADIAL DISTANCE

FOR FRONT WHEEL OF NEW & OLD BUSES
STATIC BUSES; HORIZONTAL CELL; DEPTH 20"
FLEXIBLE PAVEMENT

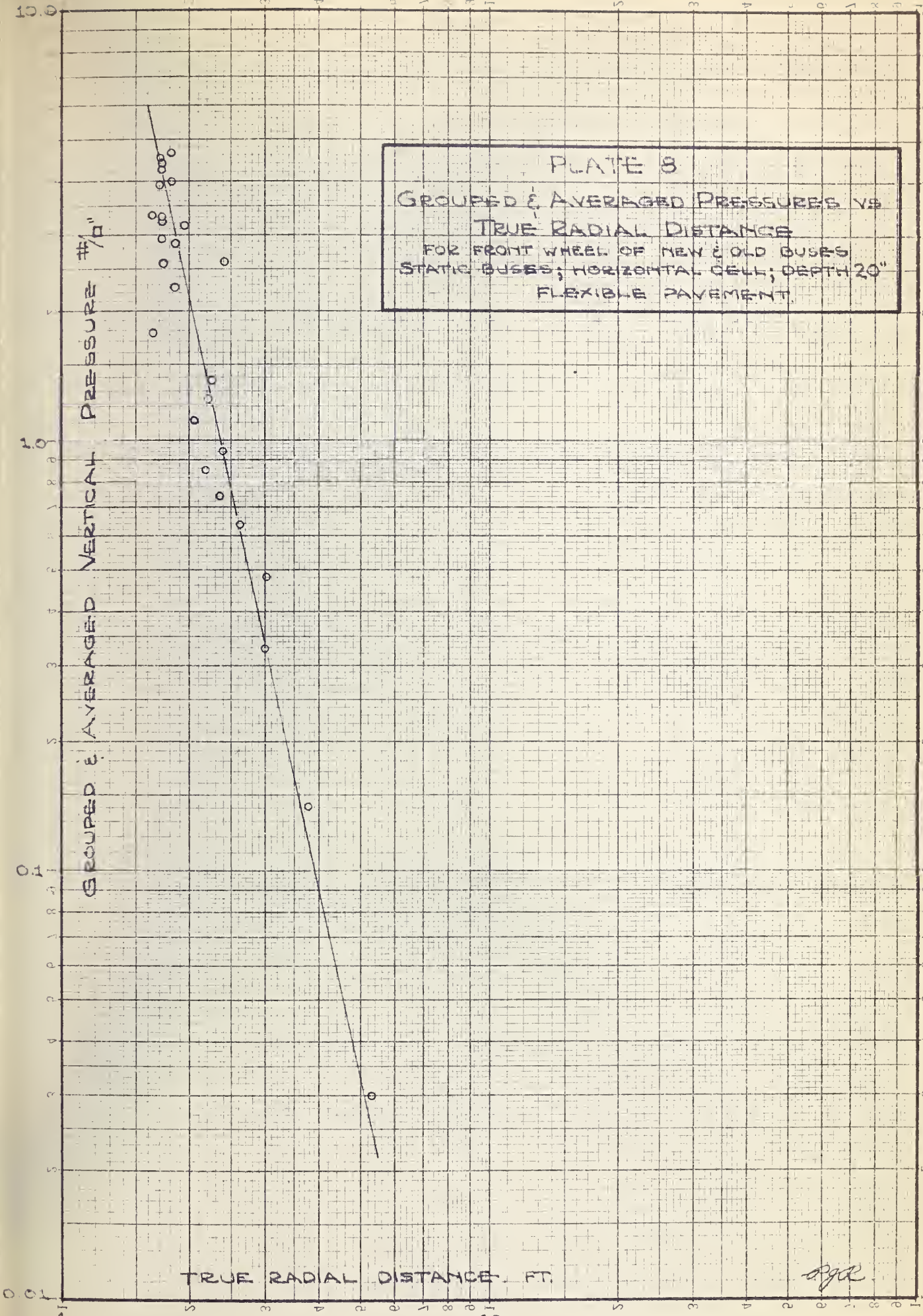

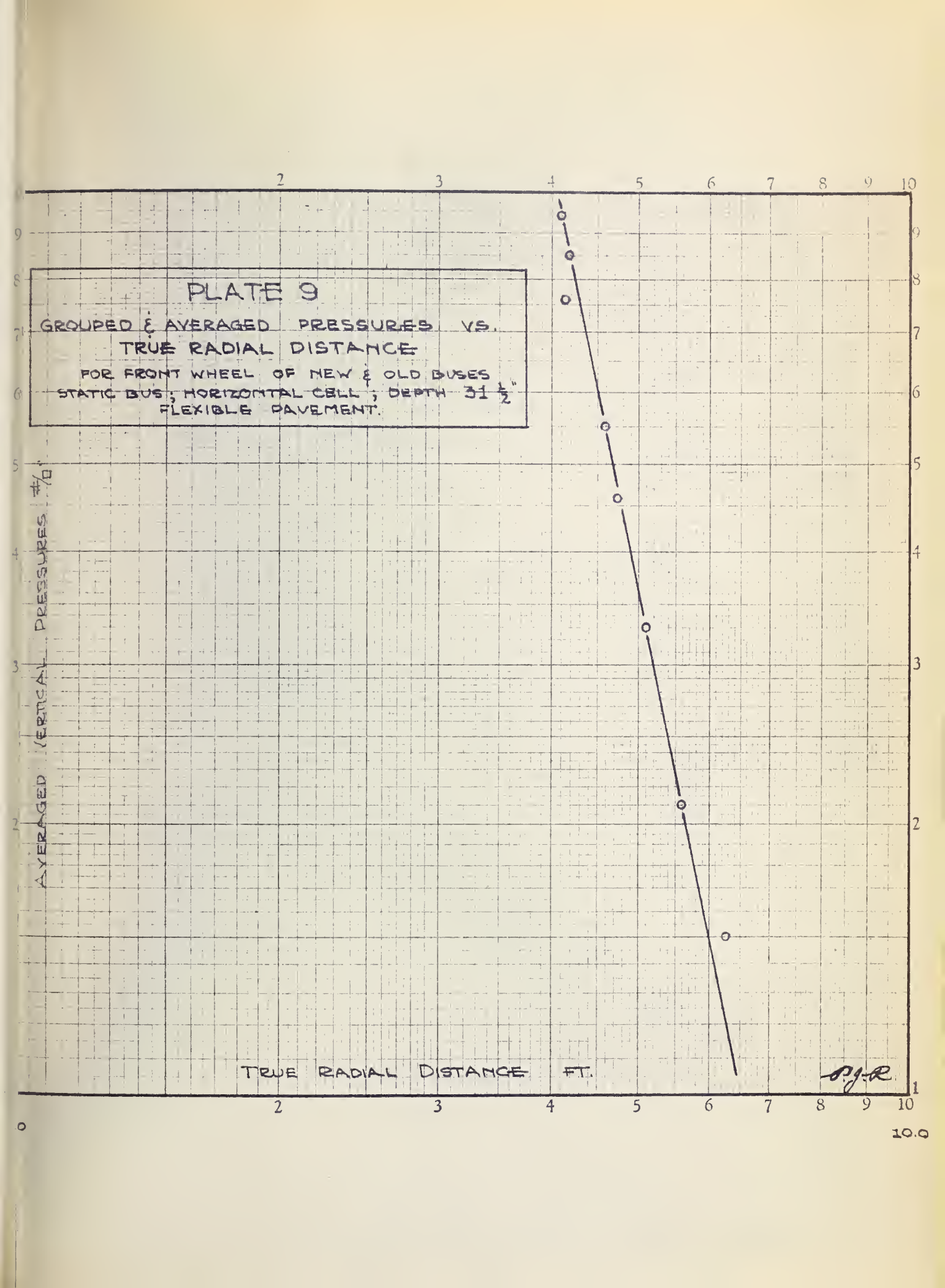
PLATE 9
GROUPED & AVERAGED PRESSURES VS. TRUE RADIAL DISTANCE
FOR FRONT WHEEL OF NEW & OLD BUSES
STATIC BUS; HORIZONTAL CELL; DEPTH 31 ½"
FLEXIBLE PAVEMENT.
AVERAGED VERTICAL PRESSURES #/□"
TRUE RADIAL DISTANCE FT.
P.J.R
10.0

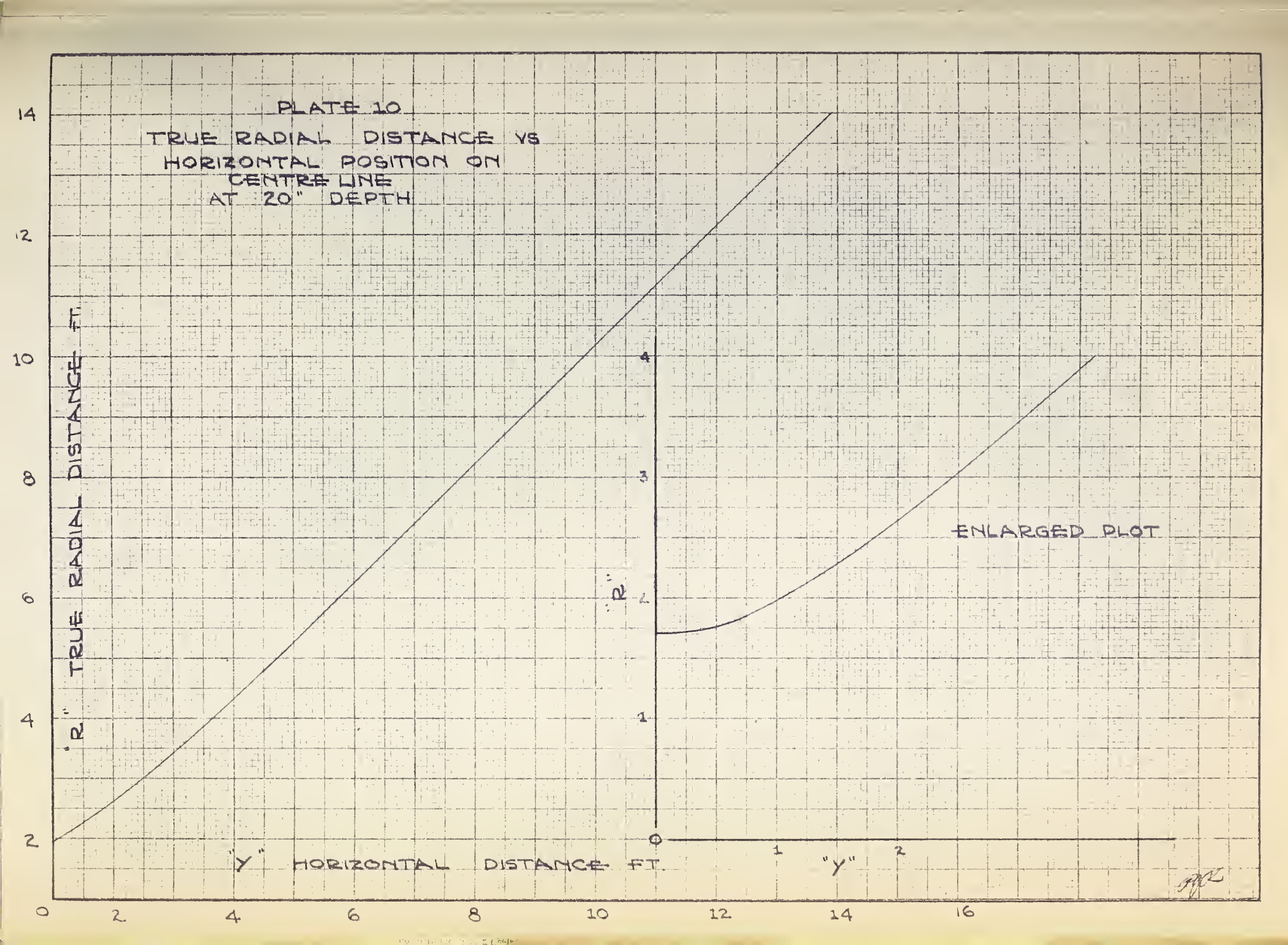
PLATE 10
TRUE RADIAL DISTANCE VS
HORIZONTAL POSITION ON
CENTRE LINE
AT 20" DEPTH
"R" TRUE RADIAL DISTANCE FT.
"Y" HORIZONTAL DISTANCE FT.
ENLARGED PLOT
"R"
"Y"
0
2
4
6
8
10
12
14
16
1
2
3
4

PLATE 11

FOR COMPUTATION OF TRUE RADIAL DISTANCE AT DEPTH 15"

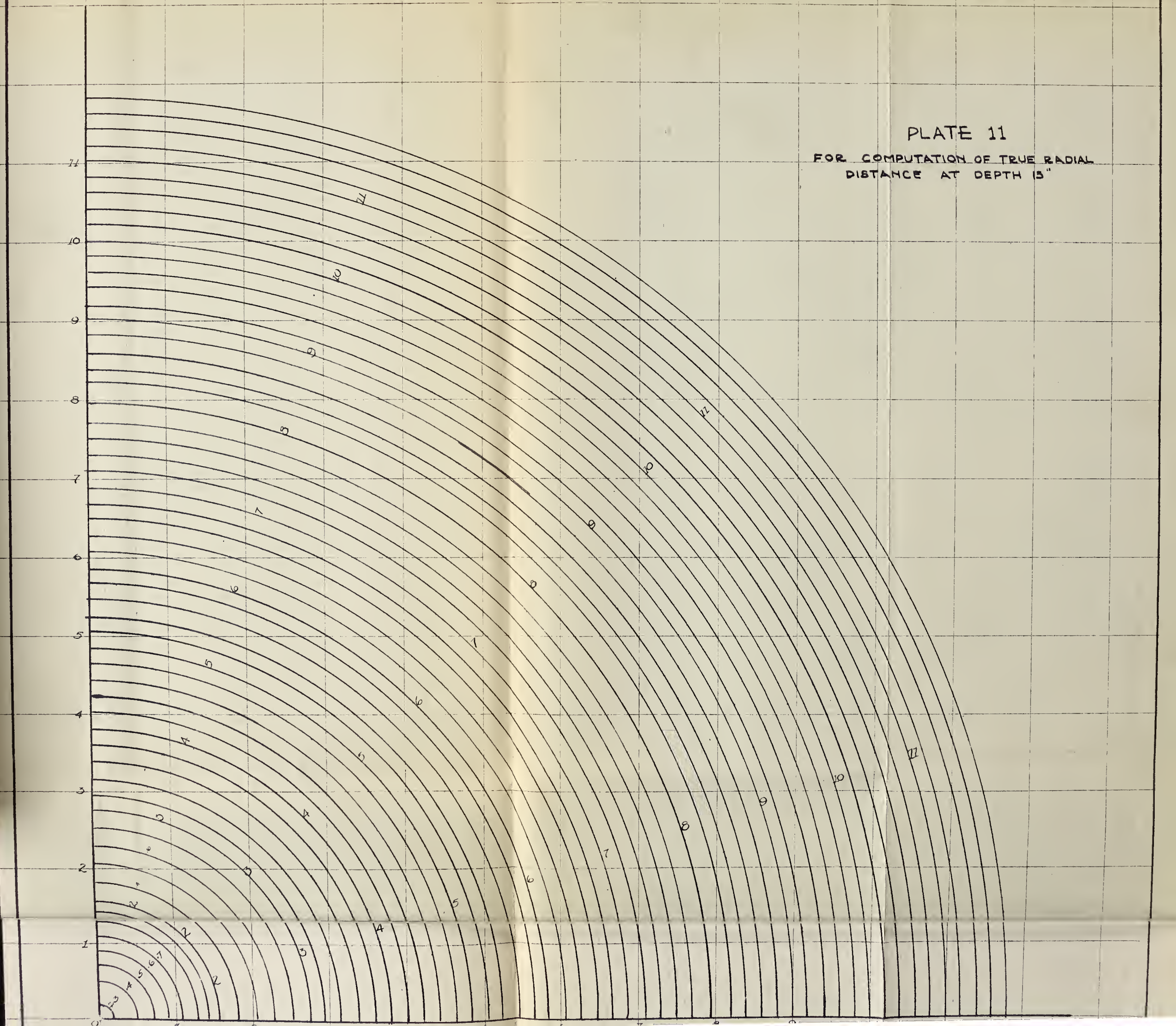

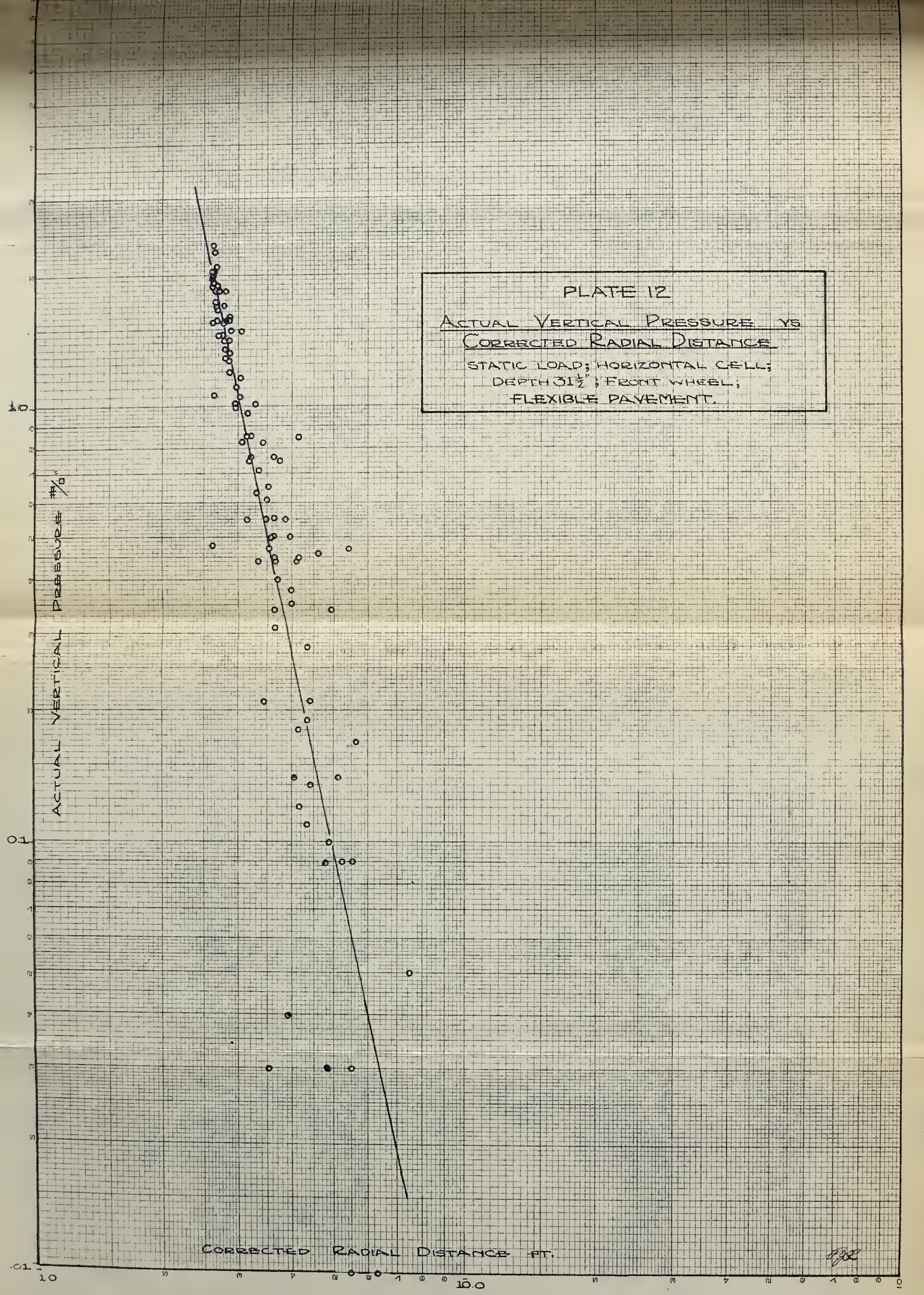

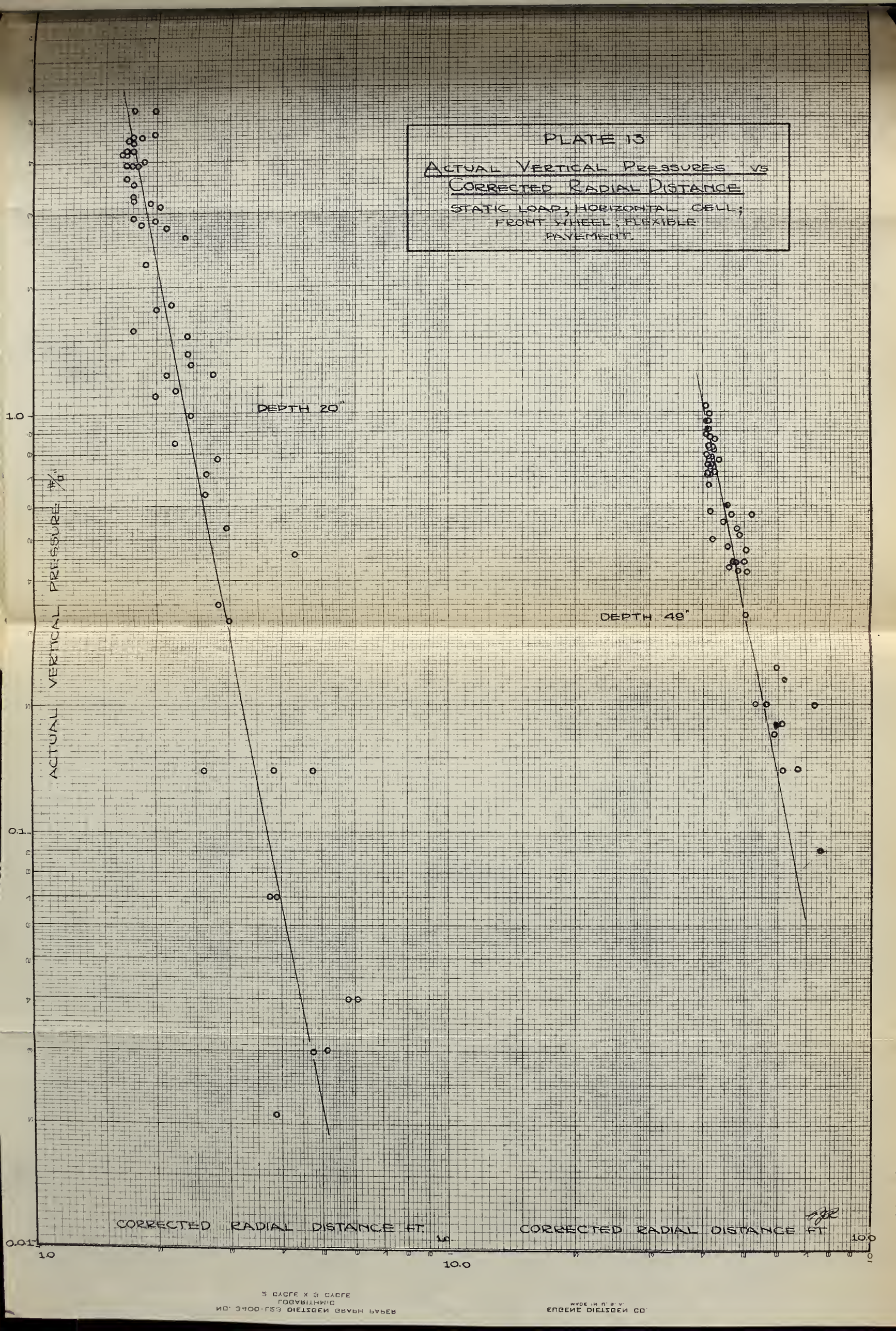
PLATE 13
ACTUAL VERTICAL PRESSURES VS CORRECTED RADIAL DISTANCE
STATIC LOAD; HORIZONTAL CELL; FRONT WHEEL; FLEXIBLE PAVEMENT.
DEPTH 20"
DEPTH 48"
ACTUAL VERTICAL PRESSURE #/□"
1.0
0.1
0.01
CORRECTED RADIAL DISTANCE FT.
1.0
10.0
CORRECTED RADIAL DISTANCE FT.
10.0

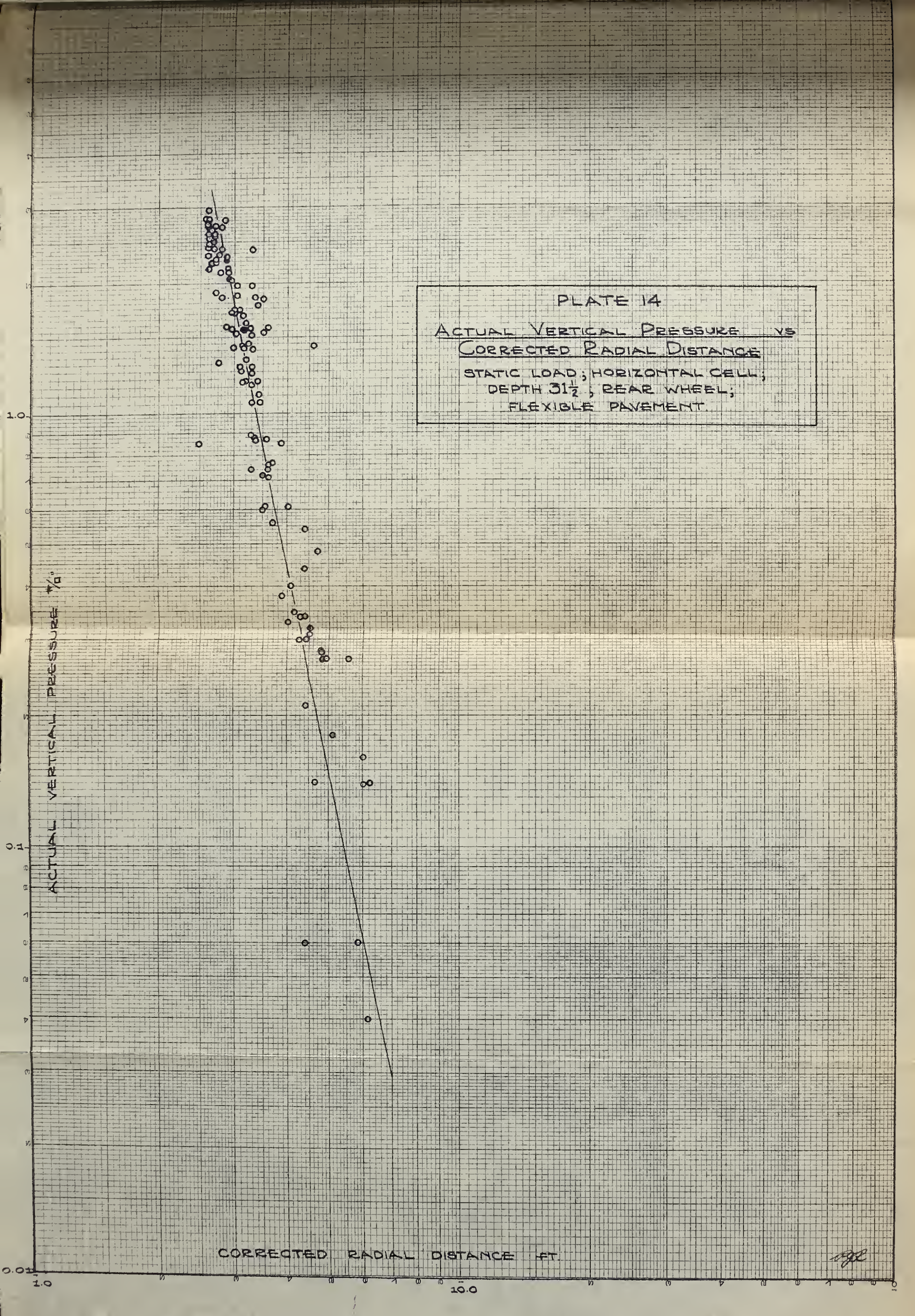
PLATE 14
ACTUAL VERTICAL PRESSURE VS
CORRECTED RADIAL DISTANCE
STATIC LOAD; HORIZONTAL CELL;
DEPTH 31½; REAR WHEEL;
FLEXIBLE PAVEMENT
ACTUAL VERTICAL PRESSURE #/□"
CORRECTED RADIAL DISTANCE FT.
1.0
0.1
0.01
10.0

PLATE 15

ACTUAL VERTICAL PRESSURE VS CORRECTED RADIAL DISTANCE

STATIC LOAD; HORIZONTAL CELL; REAR WHEEL; FLEXIBLE PAVEMENT.

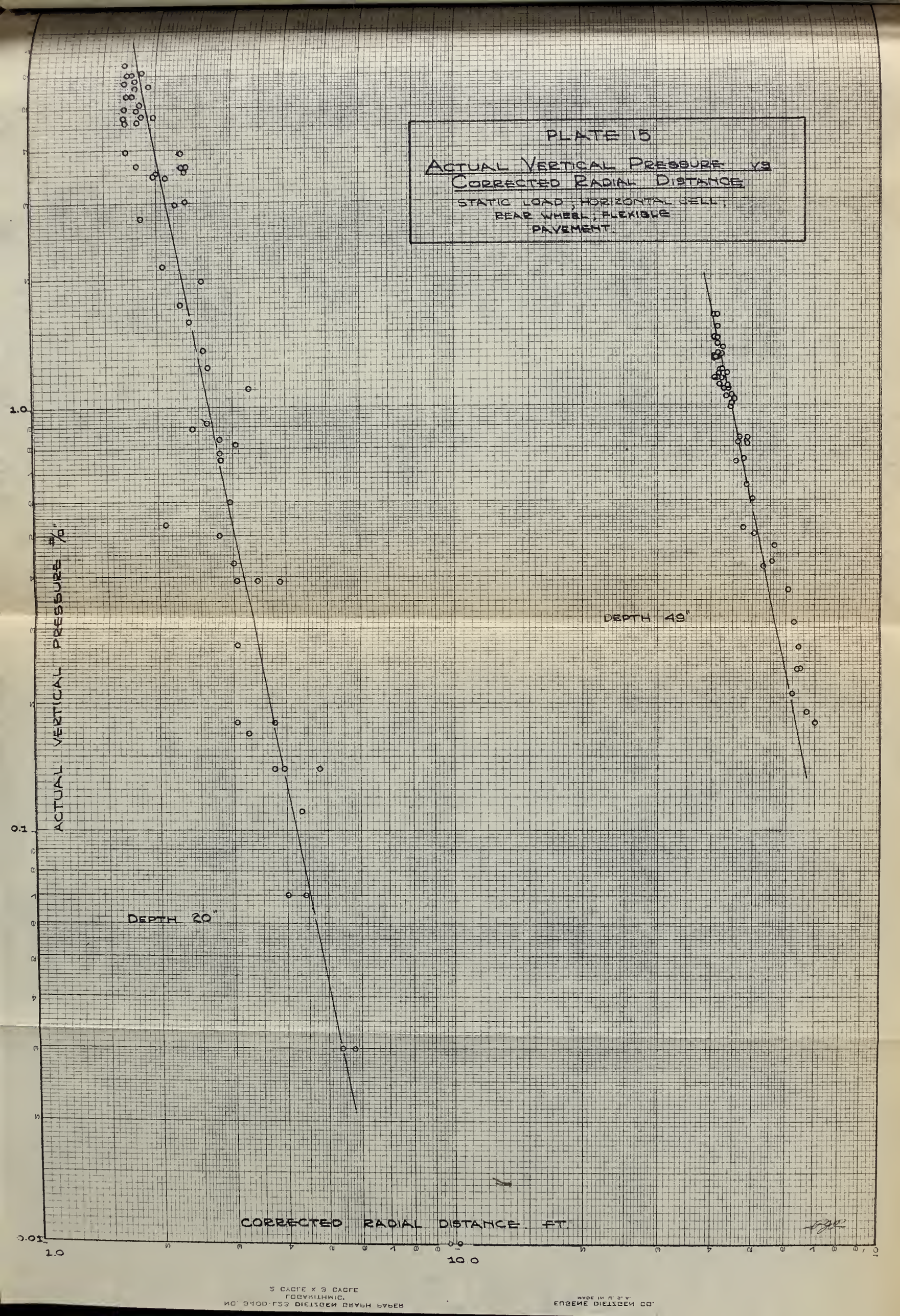

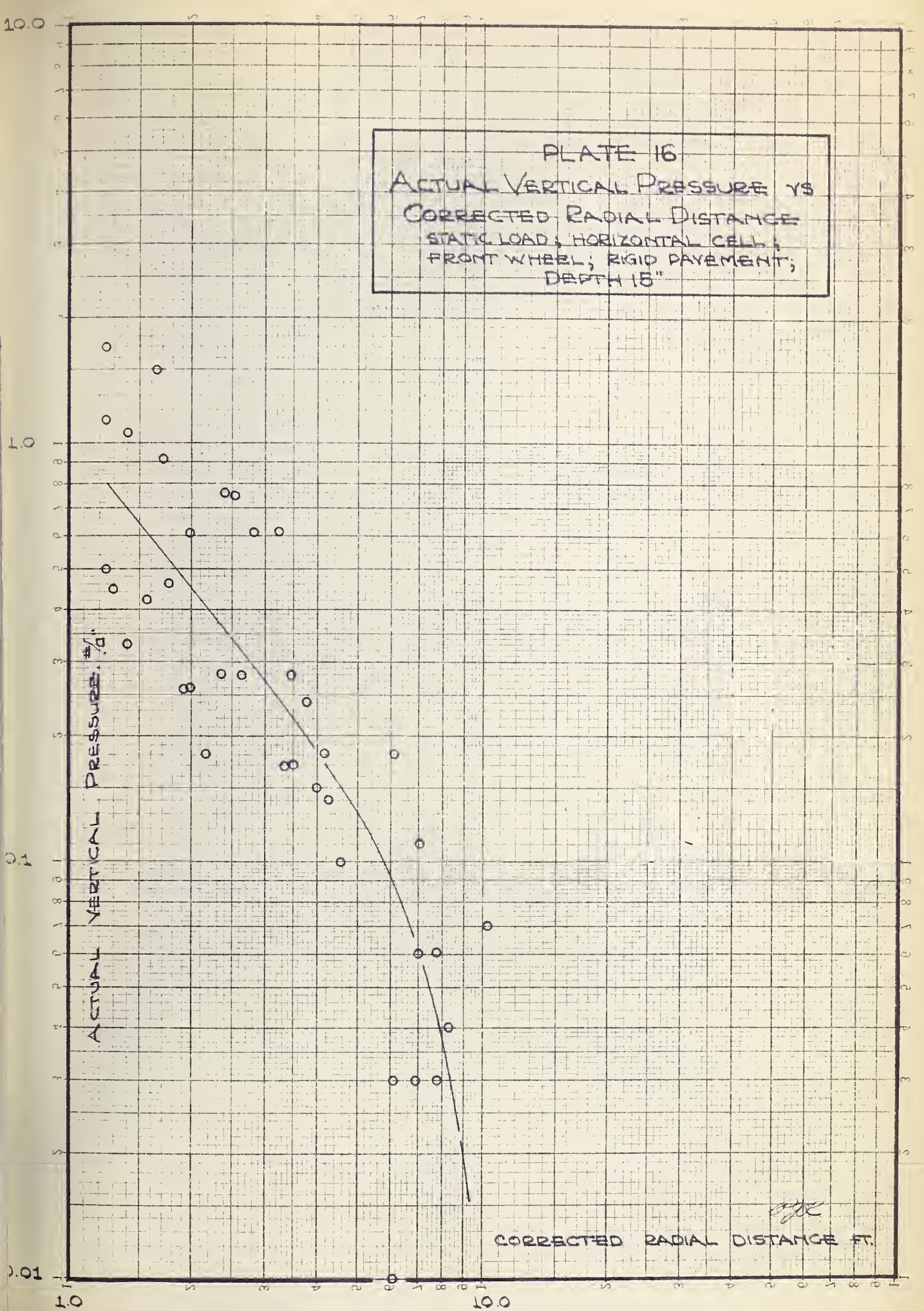
PLATE 16
ACTUAL VERTICAL PRESSURE VS
CORRECTED RADIAL DISTANCE
STATIC LOAD; HORIZONTAL CELL;
FRONT WHEEL; RIGID PAVEMENT;
DEPTH 15"
ACTUAL VERTICAL PRESSURE #/□"
CORRECTED RADIAL DISTANCE FT.
10.0
1.0
0.1
0.01
1.0
10.0

PLATE 17

ACTUAL VERTICAL PRESSURE VS CORRECTED RADIAL DISTANCE

STATIC LOAD; HORIZONTAL CELL; FRONT WHEEL; RIGID PAVEMENT; DEPTH 19"

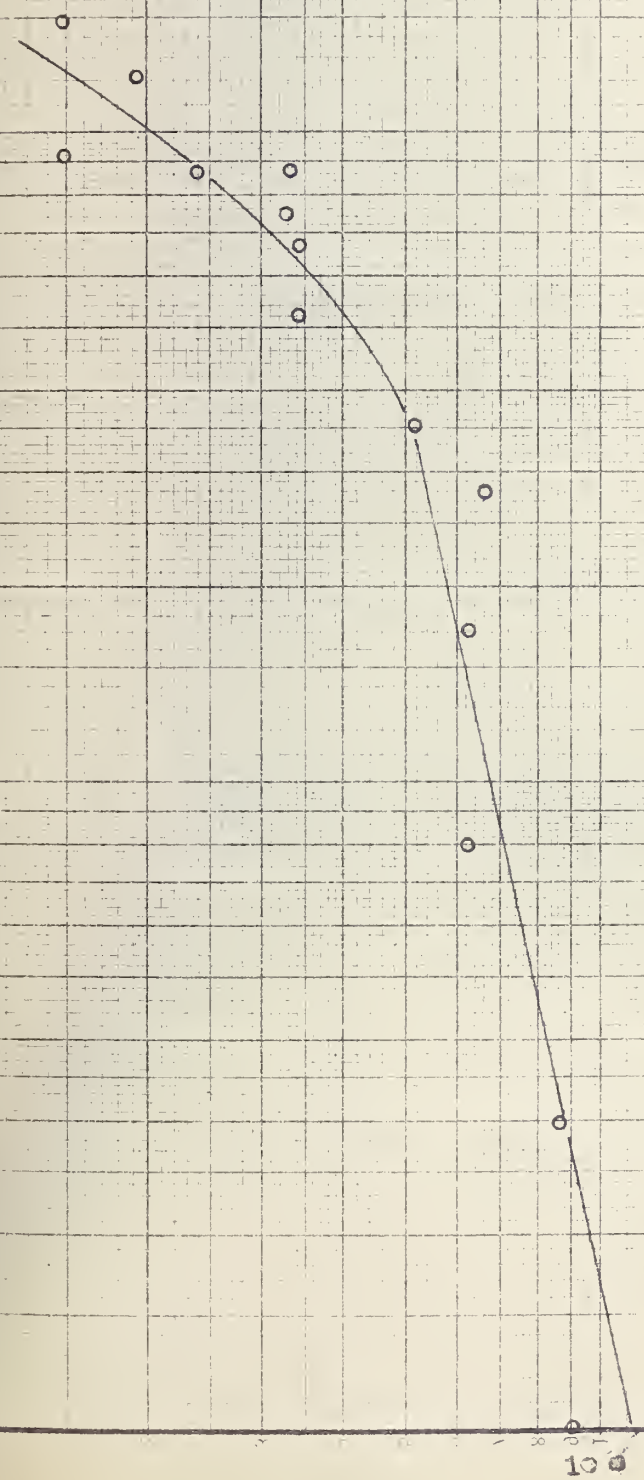

CORRECTED RADIAL DISTANCE FT.

1.0

10.0

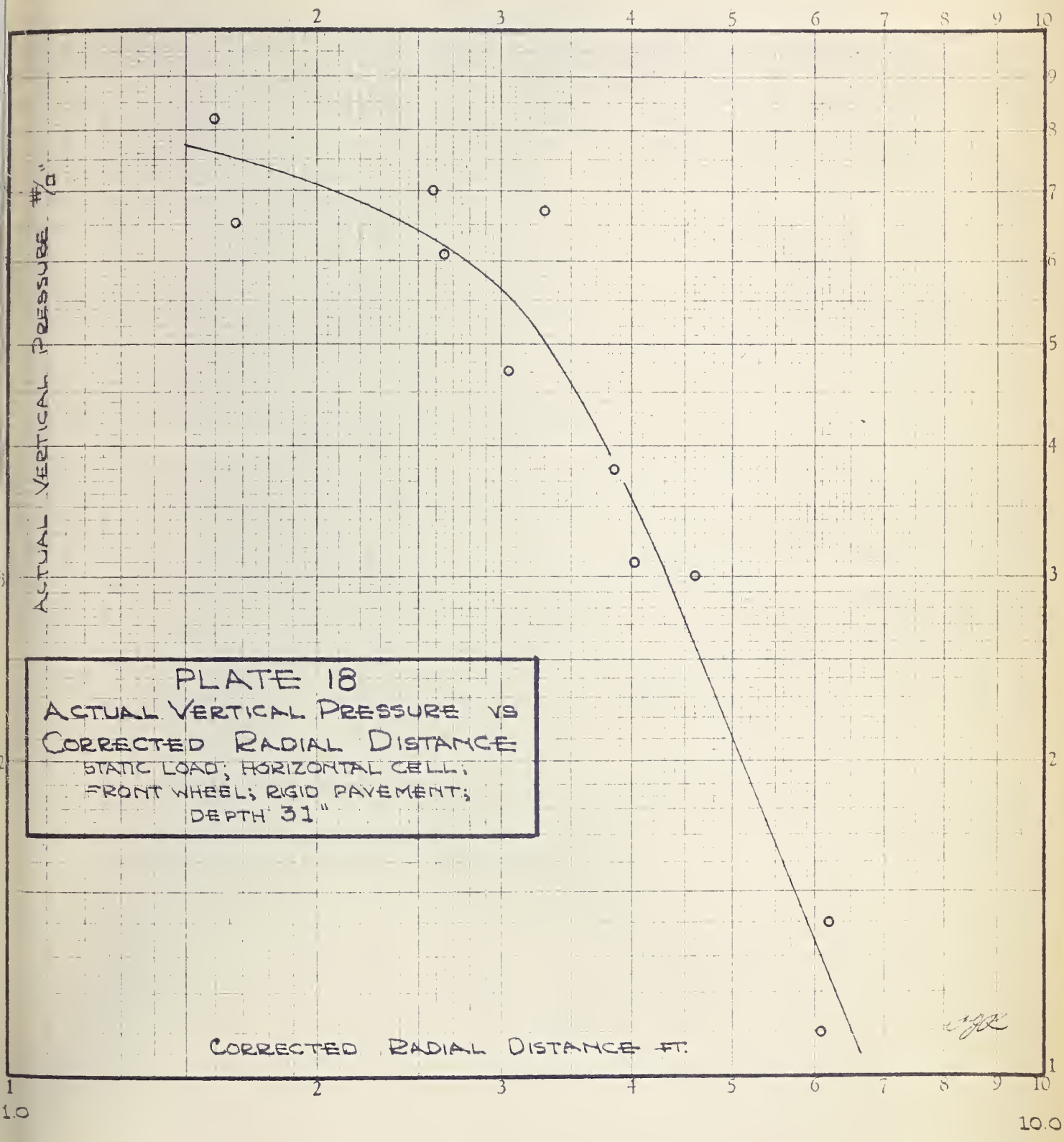

PLATE 18

ACTUAL VERTICAL PRESSURE VS CORRECTED RADIAL DISTANCE

STATIC LOAD; HORIZONTAL CELL; FRONT WHEEL; RIGID PAVEMENT; DEPTH 31"

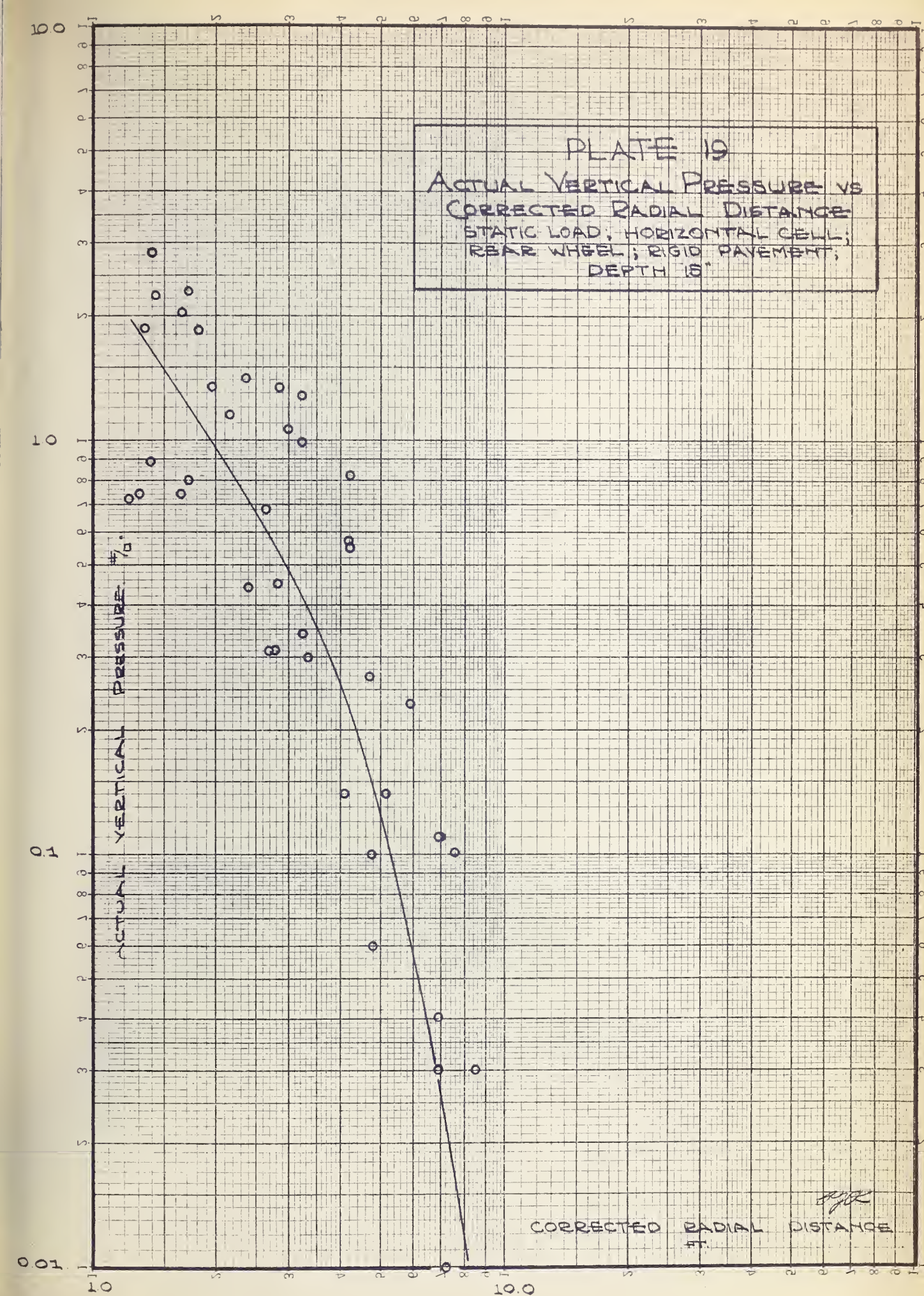
PLATE 19
ACTUAL VERTICAL PRESSURE VS CORRECTED RADIAL DISTANCE
STATIC LOAD; HORIZONTAL CELL; REAR WHEEL; RIGID PAVEMENT; DEPTH 18"
ACTUAL VERTICAL PRESSURE #/□"
CORRECTED RADIAL DISTANCE FT.
10.0
1.0
0.1
0.01
1.0
10.0

PLATE 20

ACTUAL VERTICAL PRESSURE VS CORRECTED RADIAL DISTANCE

STATIC LOAD; HORIZONTAL CELL; REAR WHEEL; RIGID PAVEMENT DEPTH 31

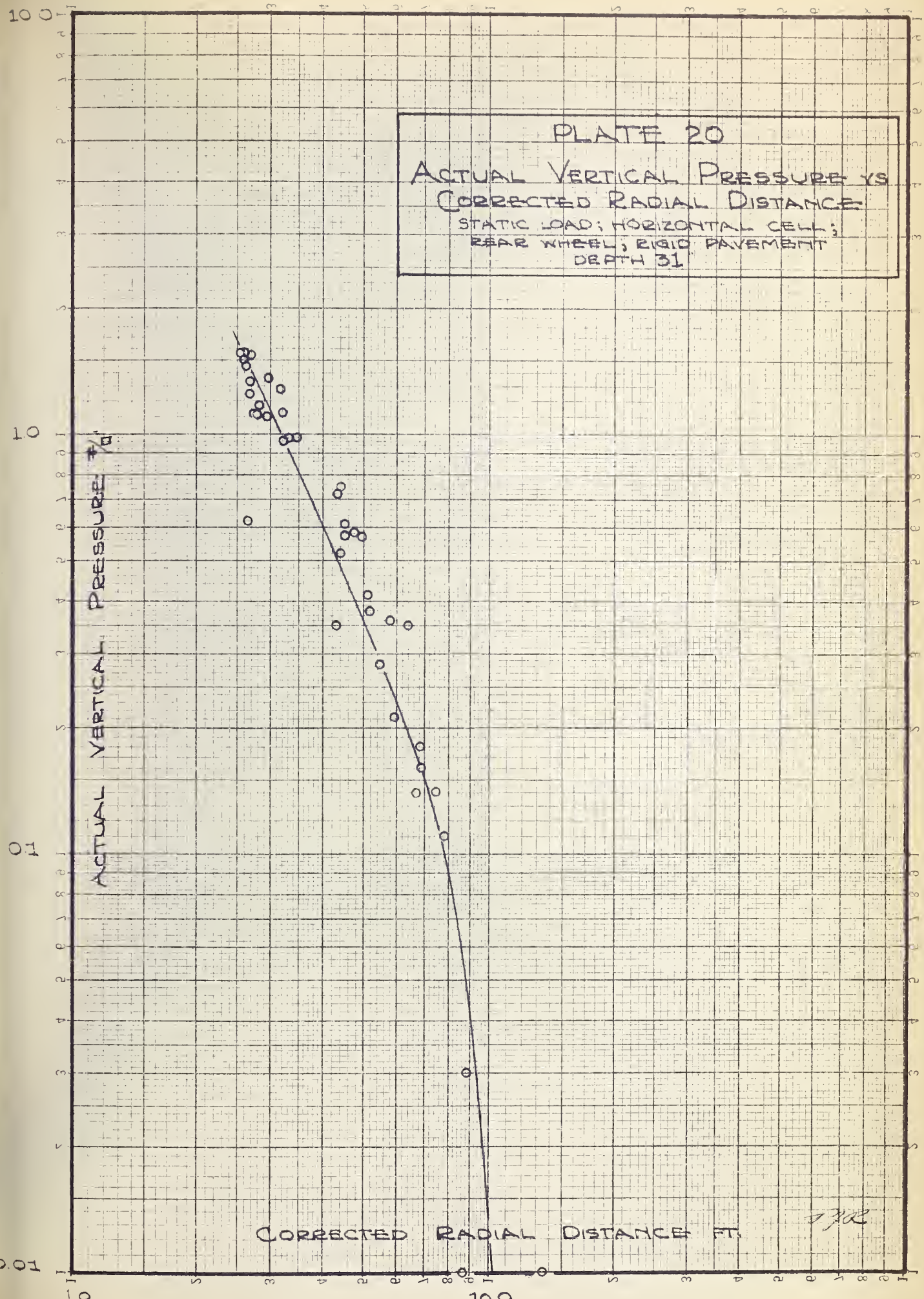

PLATE 21

ACTUAL VERTICAL PRESSURE VS EQUIVALENT RADIAL DISTANCE

STATIC LOAD; HORIZONTAL CELL; FRONT WHEEL; RIGID PAVEMENT; DEPTH 15"

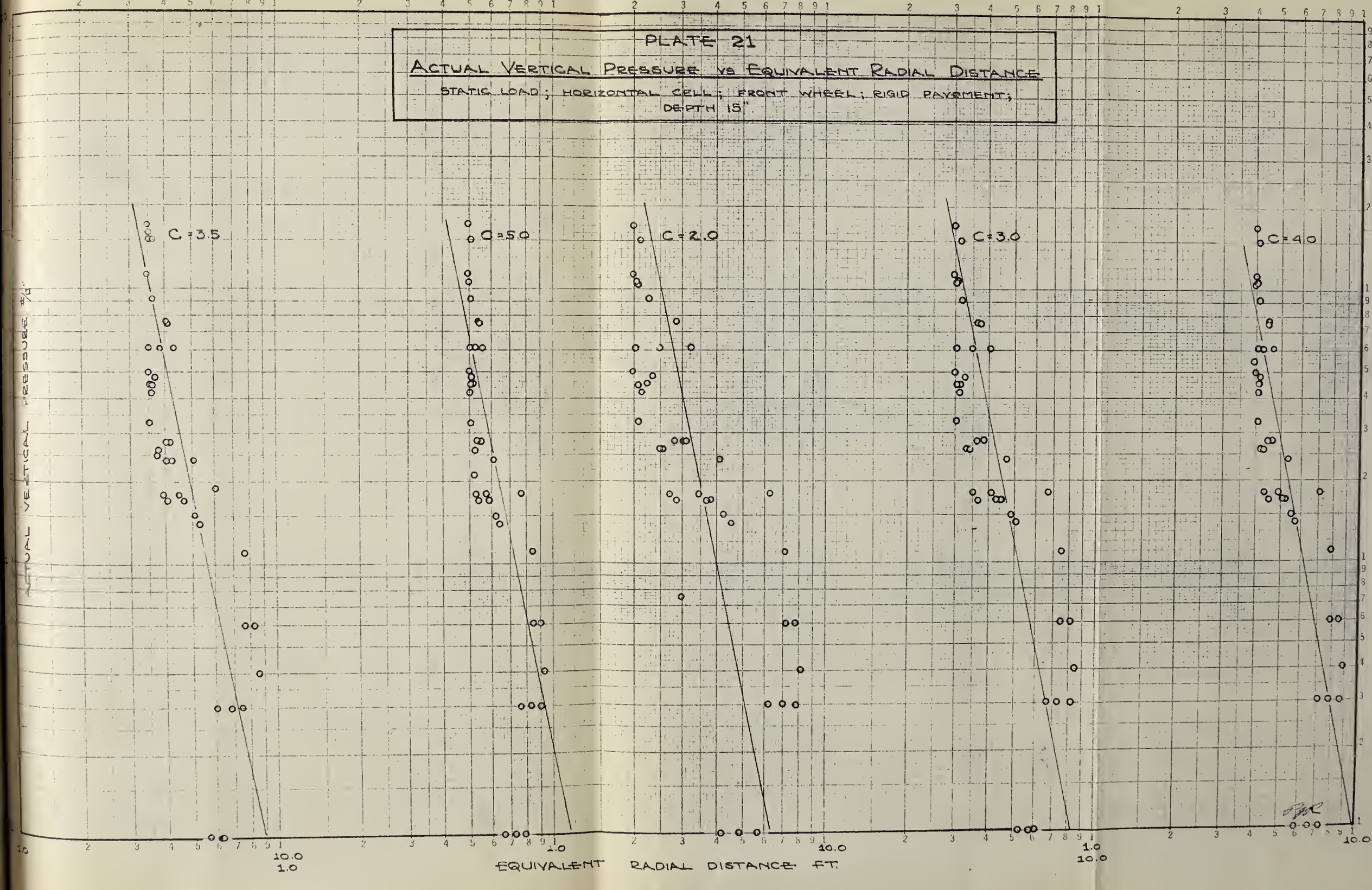

PLATE 22

ACTUAL VERTICAL PRESSURE VS EQUIVALENT RADIAL DISTANCE

STATIC LOAD; HORIZONTAL CELL; FRONT WHEEL; RIGID PAVEMENT; DEPTH 19"

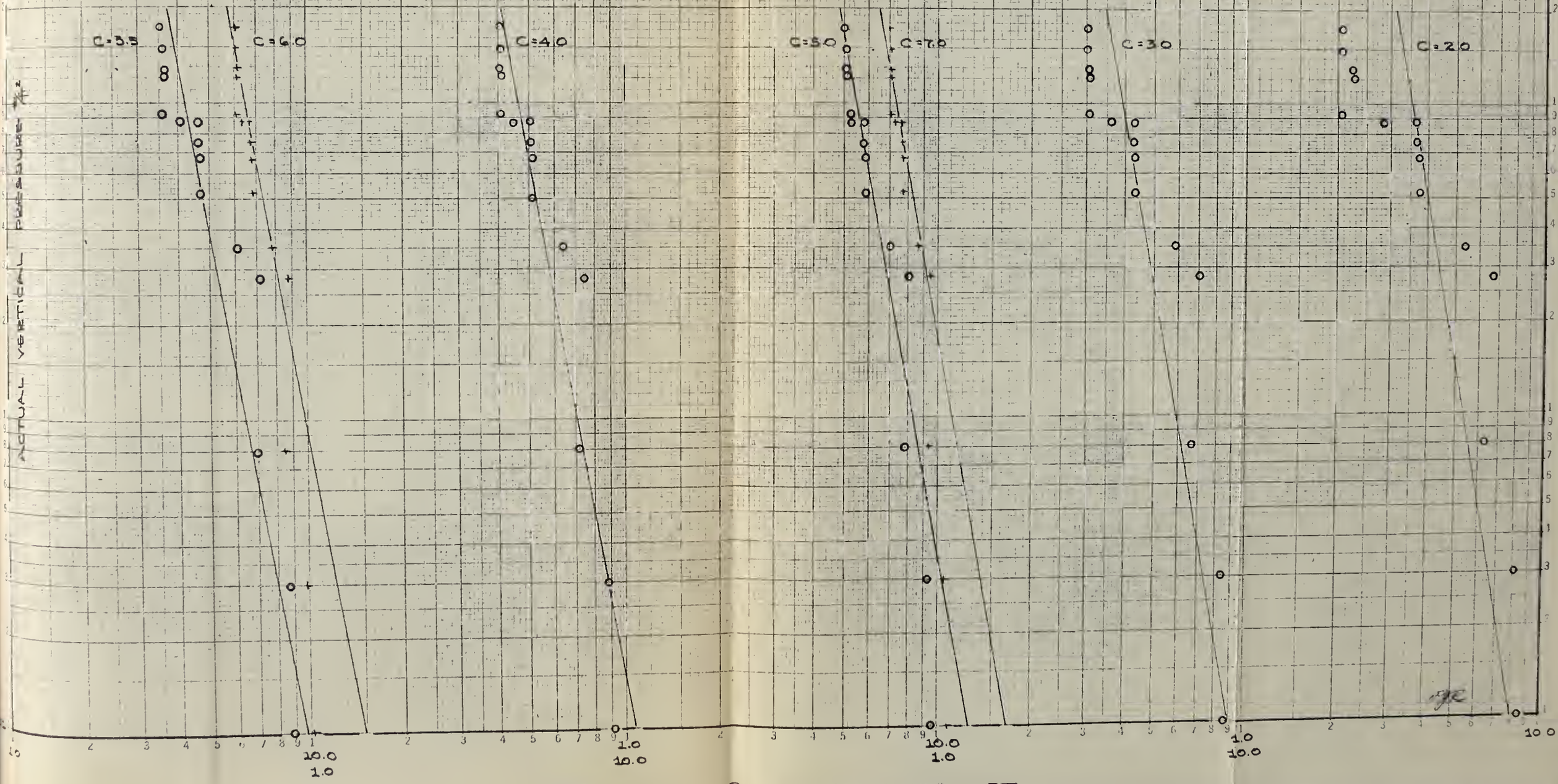

EQUIVALENT RADIAL DISTANCE FT.

PLATE 23

ACTUAL VERTICAL PRESSURE VS EQUIVALENT RADIAL DISTANCE

STATIC LOAD; HORIZONTAL CELL; REAR WHEEL; RIGID PAVEMENT; DEPTH 19"

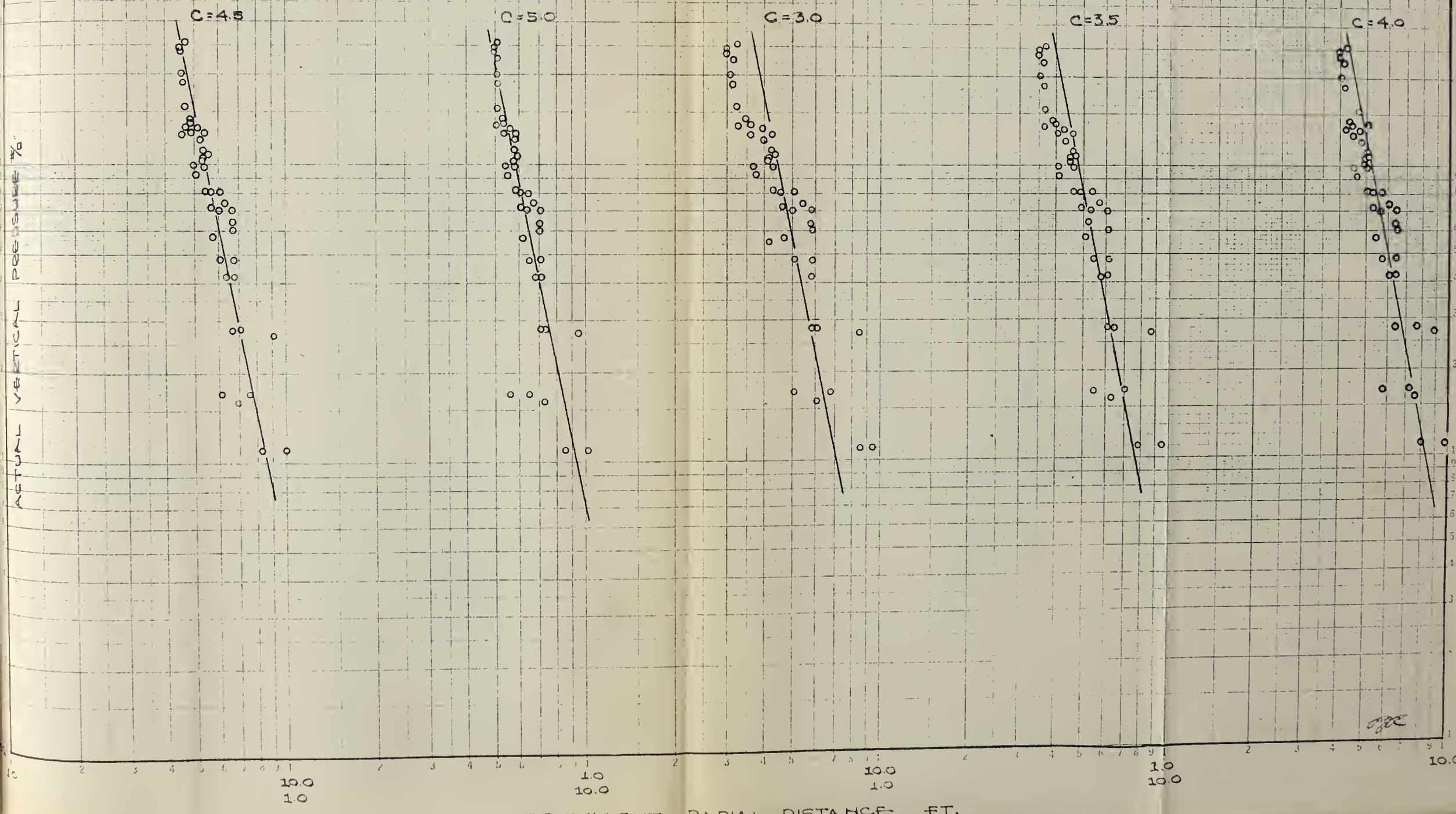

PLATE 24

ACTUAL VERTICAL PRESSURE VS EQUIVALENT RADIAL DISTANCE

STATIC LOAD; HORIZONTAL CELL ; REAR WHEEL ; RIGID PAVEMENT; DEPTH 15"

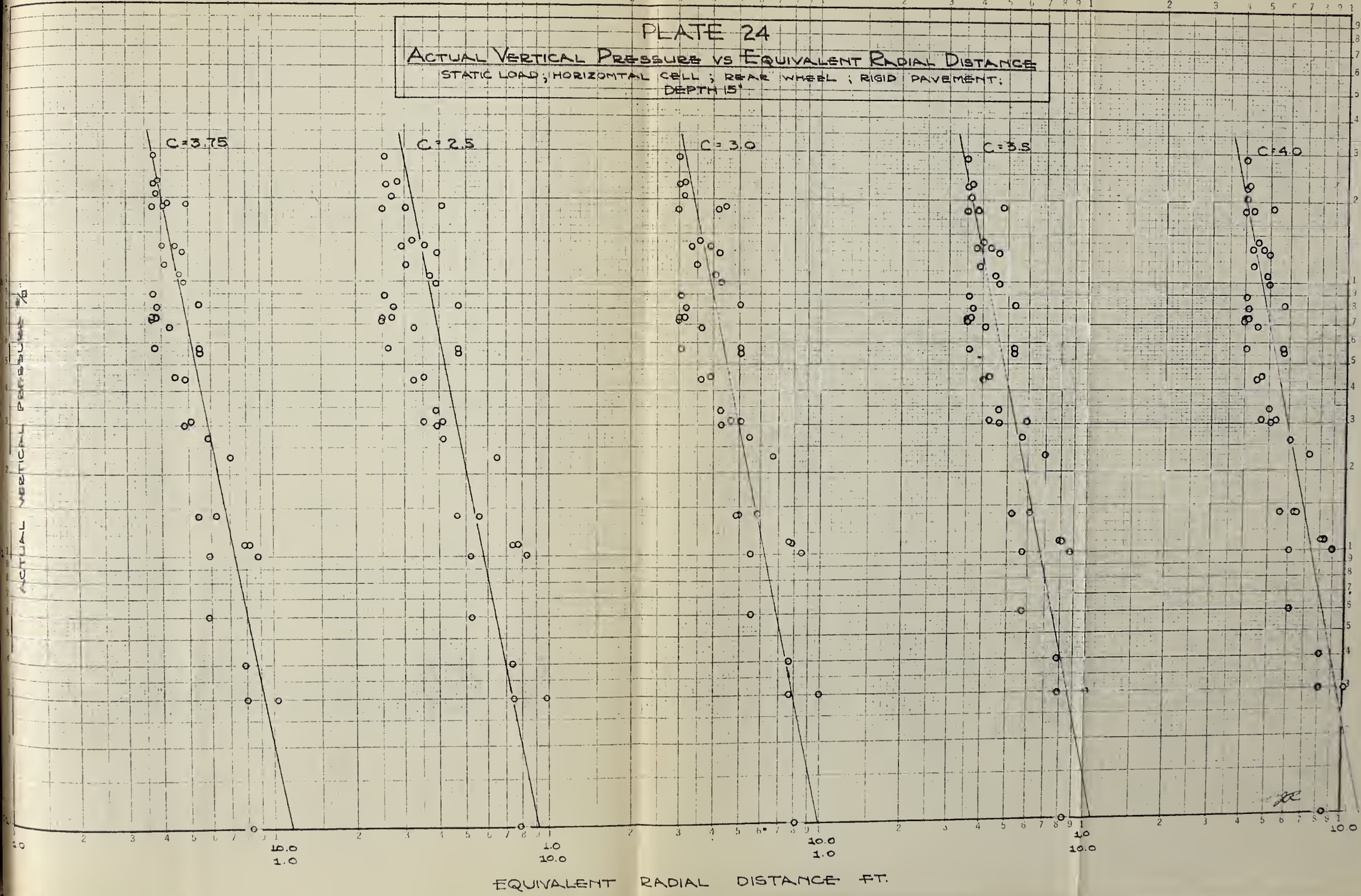

PLATE 25

ACTUAL VERTICAL PRESSURE VS EQUIVALENT RADIAL DISTANCE

STATIC LOAD; HORIZONTAL CELL; REAR WHEEL; RIGID PAVEMENT; DEPTH 31".

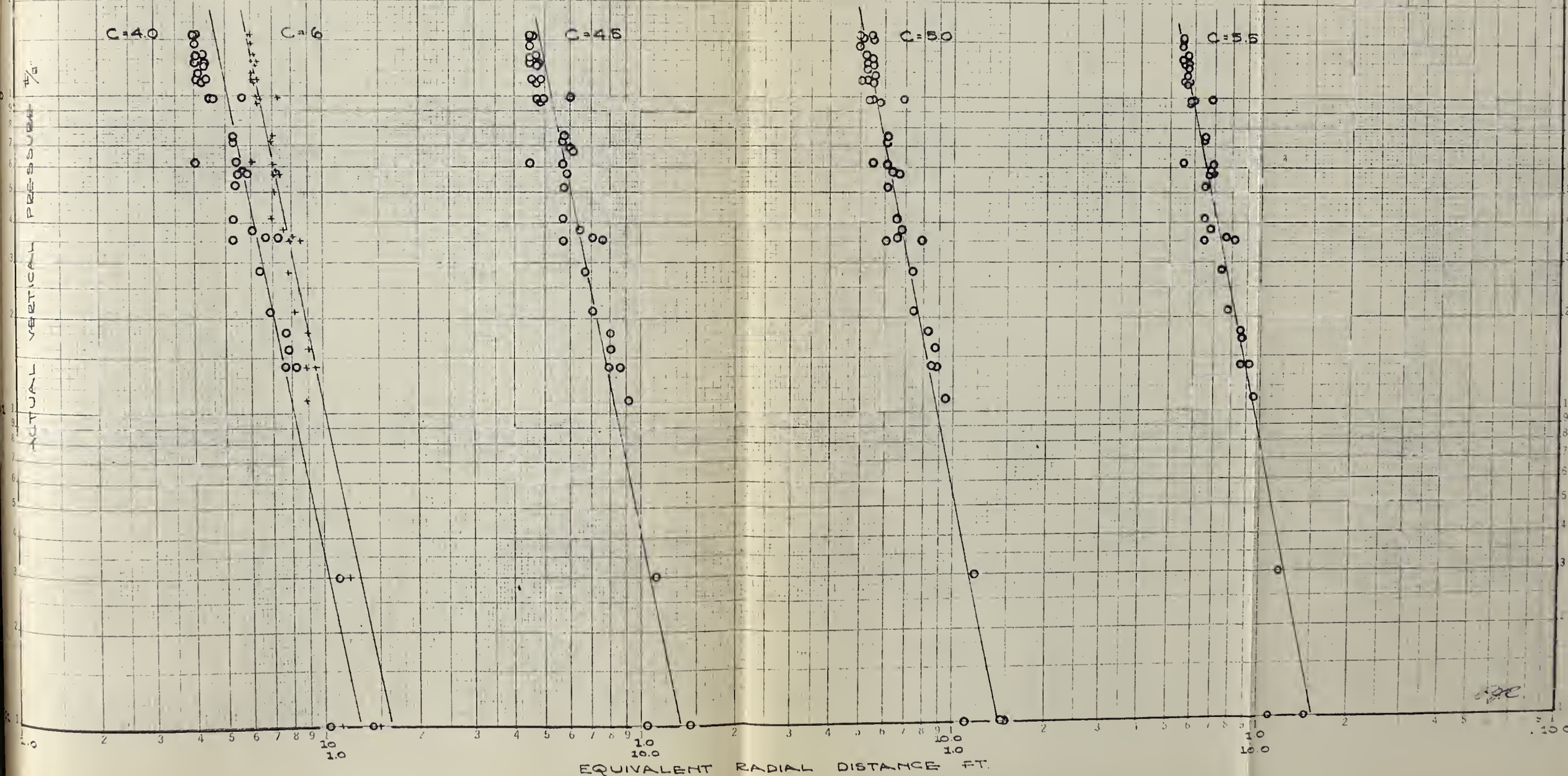

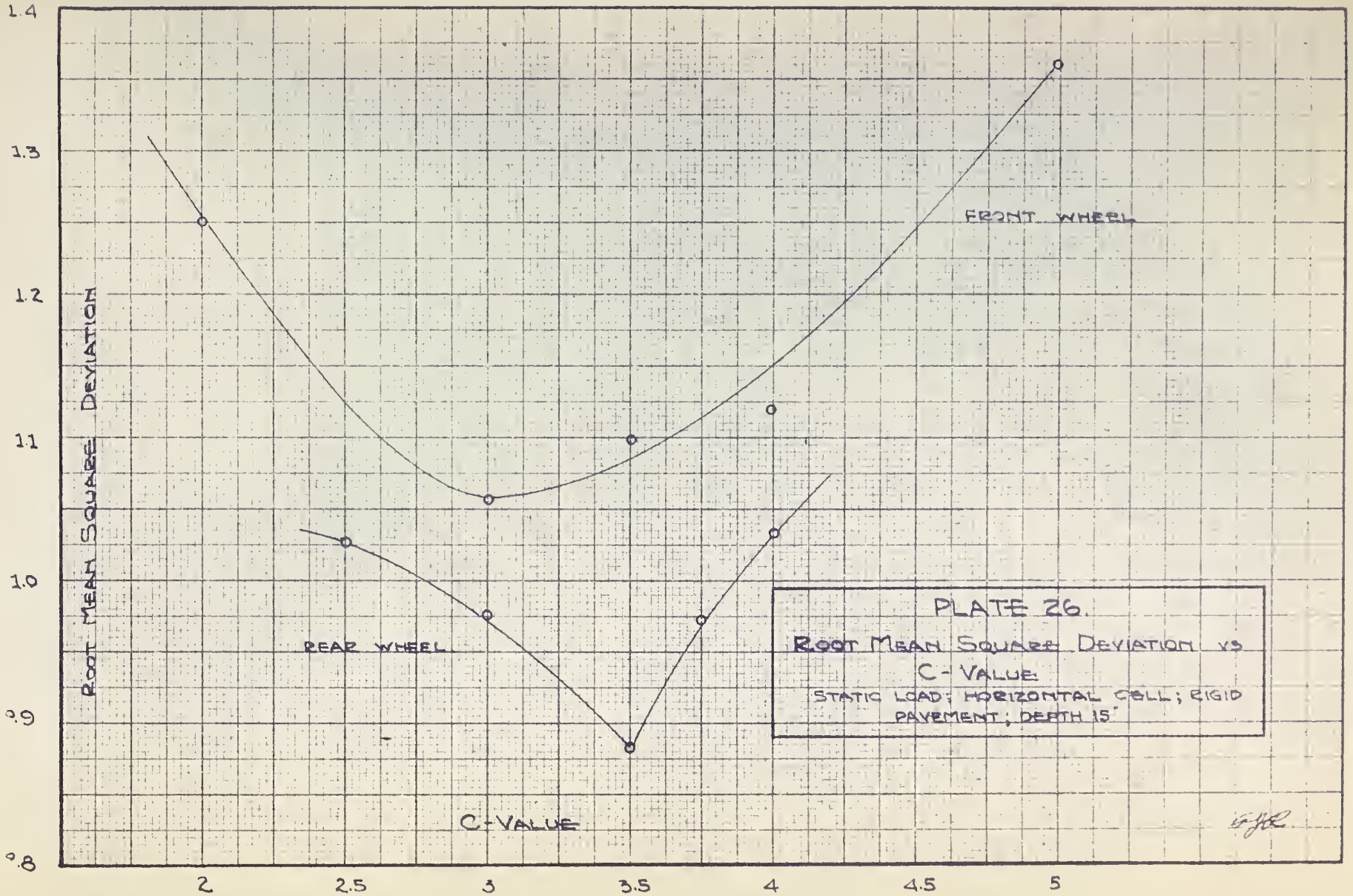

PLATE 26.

ROOT MEAN SQUARE DEVIATION VS C-VALUE.

STATIC LOAD; HORIZONTAL CELL; RIGID PAVEMENT; DEPTH 15"

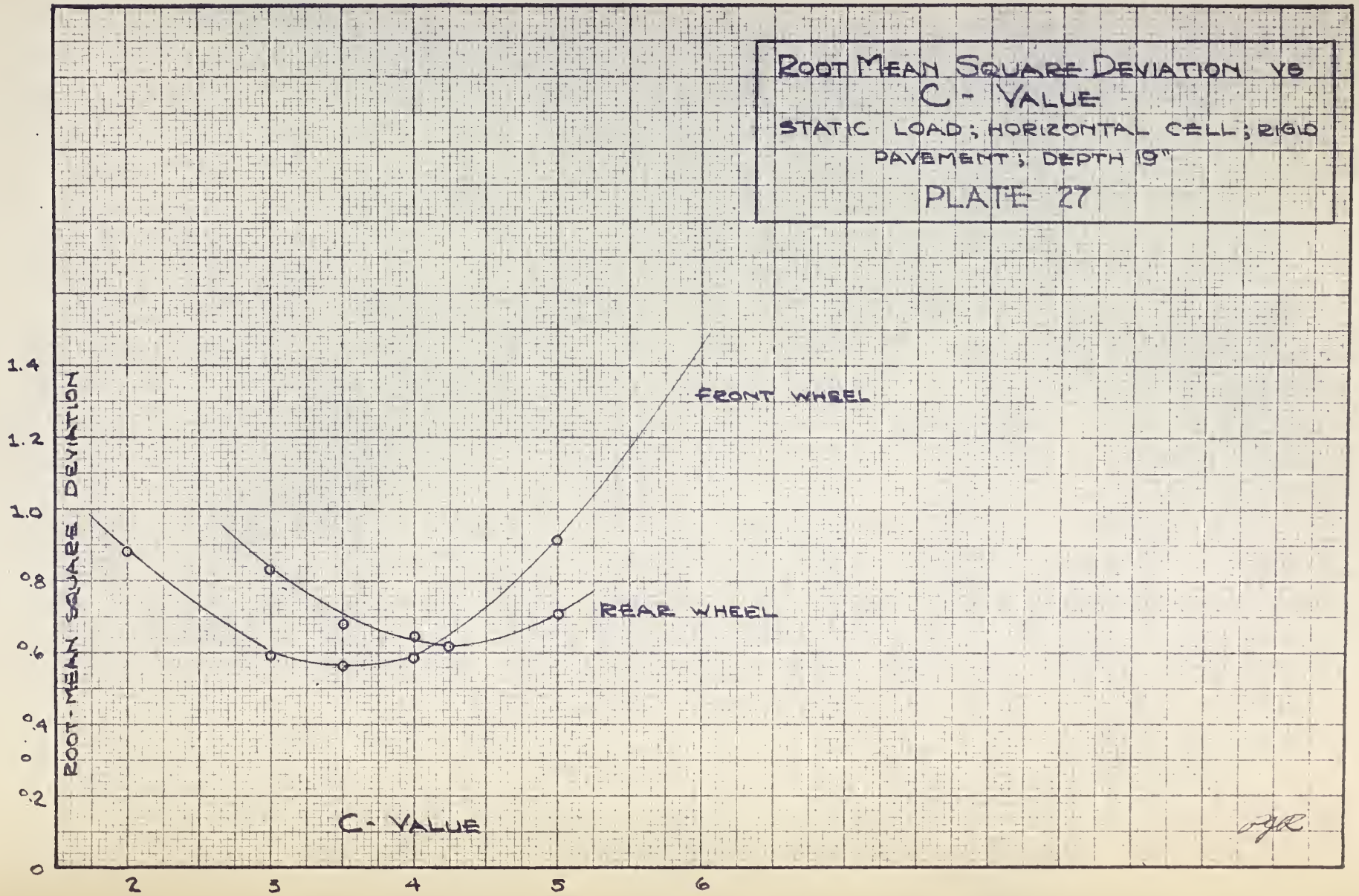
ROOT MEAN SQUARE DEVIATION VS
C - VALUE
STATIC LOAD; HORIZONTAL CELL; RIGID
PAVEMENT; DEPTH 19"
PLATE 27
ROOT-MEAN SQUARE DEVIATION
0
.2
.4
.6
.8
1.0
1.2
1.4
2
3
4
5
6
C - VALUE
FRONT WHEEL
REAR WHEEL

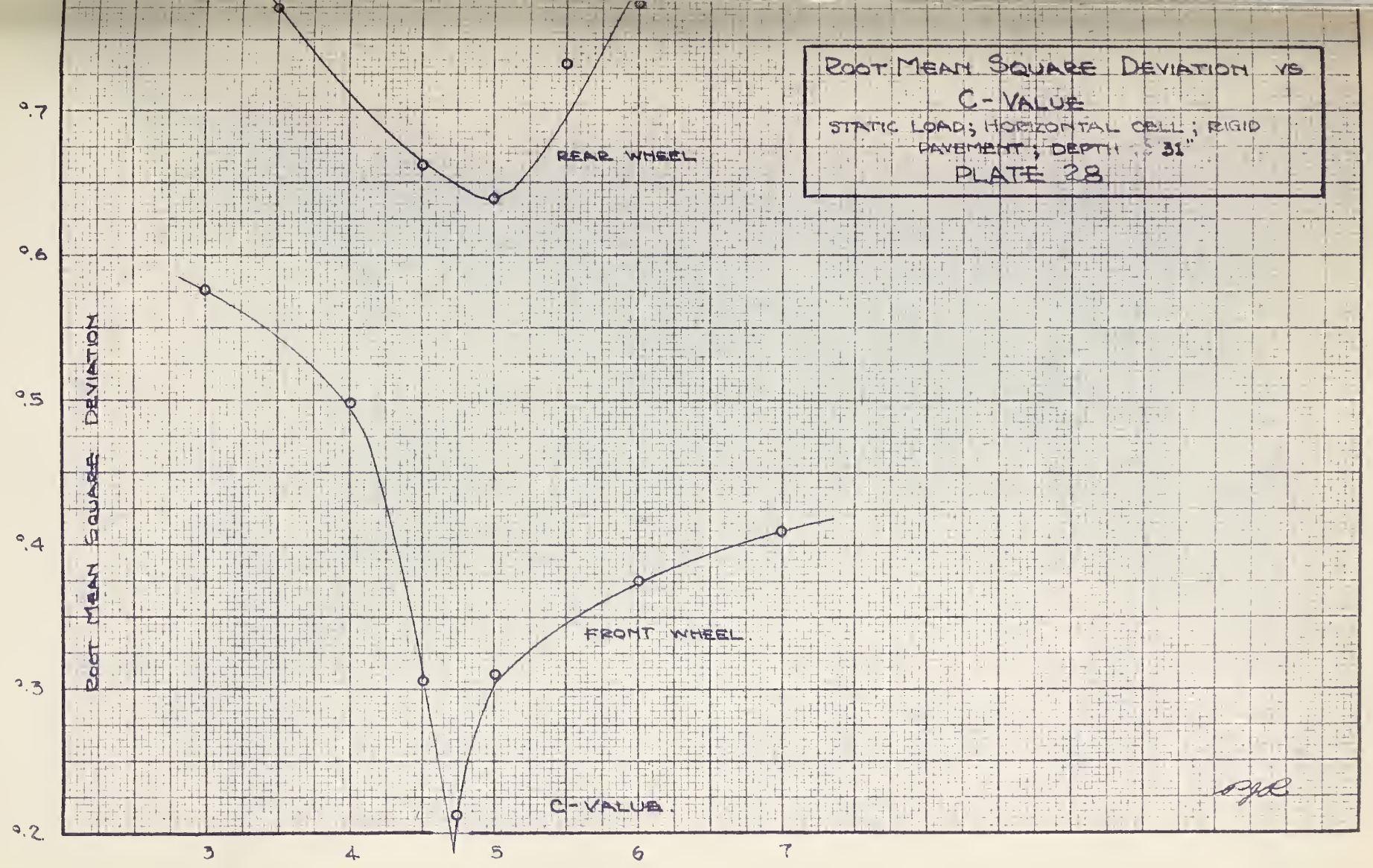
ROOT MEAN SQUARE DEVIATION VS
C-VALUE
STATIC LOAD; HORIZONTAL CELL; RIGID PAVEMENT; DEPTH = 31"
PLATE 28
ROOT MEAN SQUARE DEVIATION
.7
.6
.5
.4
.3
.2
3
4
5
6
7
REAR WHEEL
FRONT WHEEL
C-VALUE

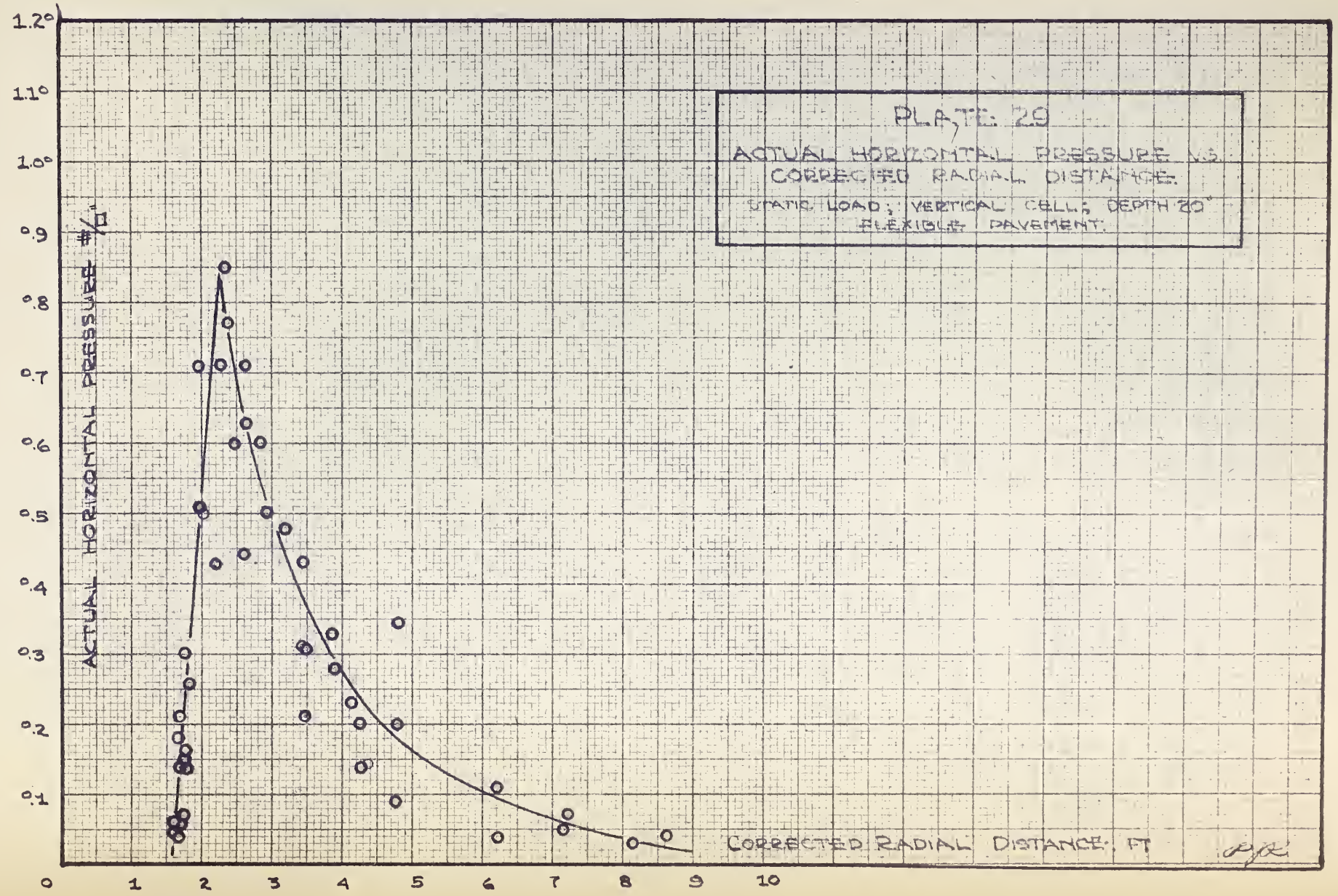
PLATE: 29
ACTUAL HORIZONTAL PRESSURE VS. CORRECTED RADIAL DISTANCE.
STATIC LOAD; VERTICAL CELL; DEPTH 20"
FLEXIBLE PAVEMENT.
ACTUAL HORIZONTAL PRESSURE #/□"
1.2
1.1
1.0
0.9
0.8
0.7
0.6
0.5
0.4
0.3
0.2
0.1
0
1
2
3
4
5
6
7
8
9
10
CORRECTED RADIAL DISTANCE. FT

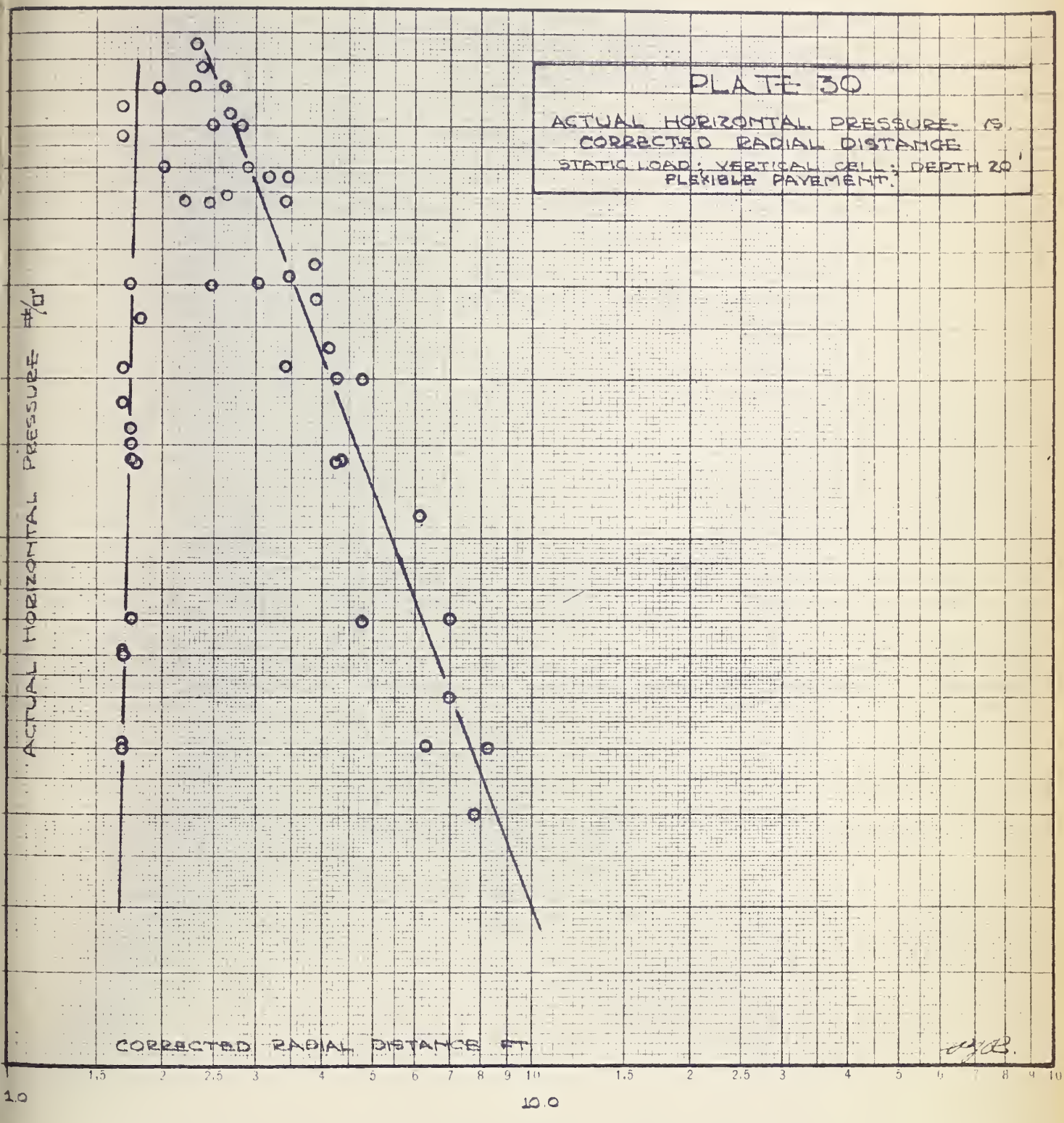
PLATE 30
ACTUAL HORIZONTAL PRESSURE VS. CORRECTED RADIAL DISTANCE
STATIC LOAD; VERTICAL CELL; DEPTH 20'
FLEXIBLE PAVEMENT.
ACTUAL HORIZONTAL PRESSURE #/□"
CORRECTED RADIAL DISTANCE FT
1.0
1.5
2
2.5
3
4
5
6
7
8
9
10
10.0

PLATE 31

INFLUENCE DIAGRAM FOR THEORETICAL PRESSURE AND HORIZONTAL DISTANCE

DEPTH 20'

ASSUMING $\nu = 0.4$; $\frac{Q}{2\pi} = 1.0$.

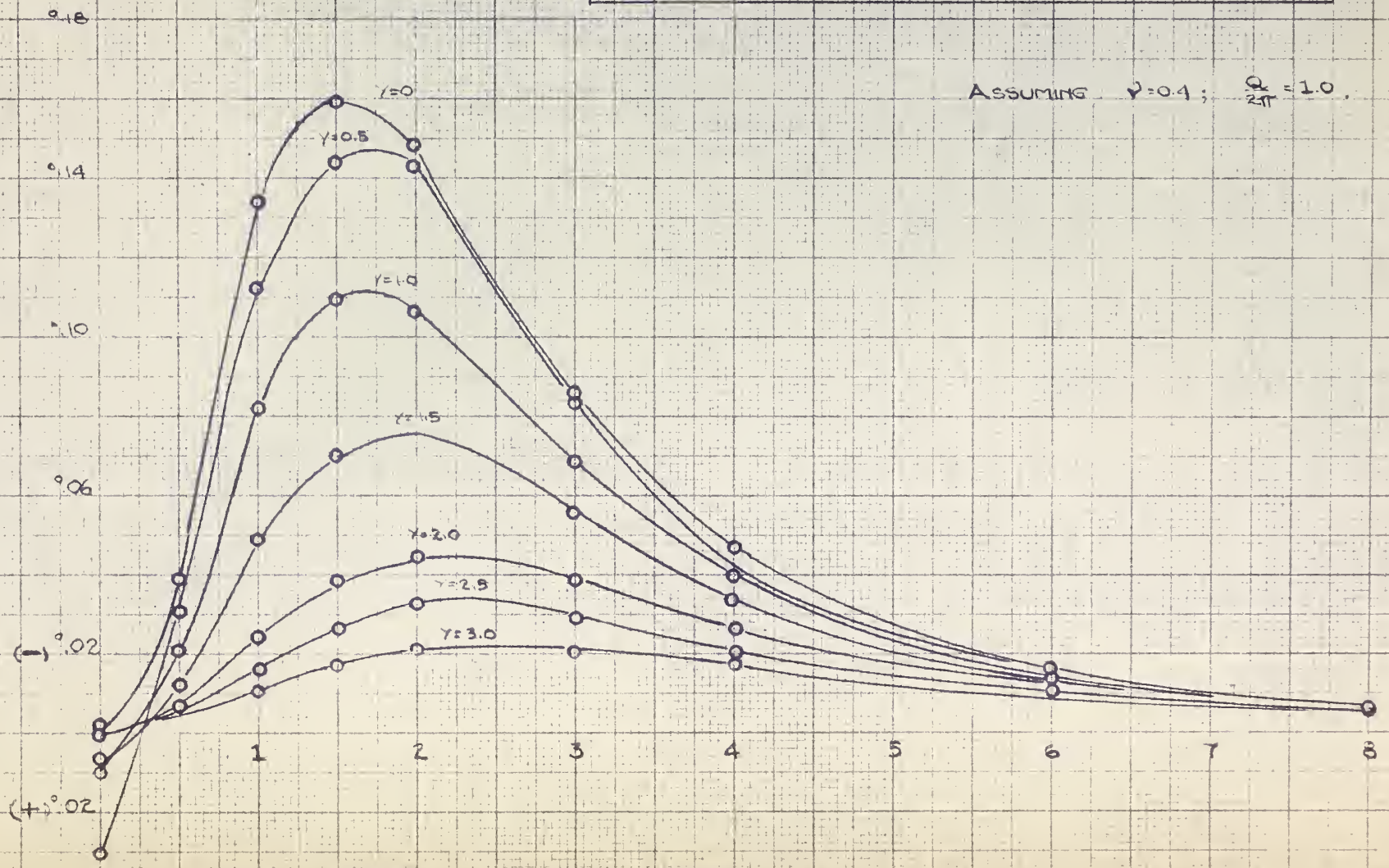

PLATE 32.

CONTOUR DIAGRAM OF THEORETICAL PRESSURE

DEPTH 20"

THEORETICAL PRESSURE

HORIZONTAL POSITION FT.

HORIZONTAL POSITION FT.

.01 .02 .03 .04 .05 .06 .07 .08 .09 .10 .11 .12 .13 .14 .15 .16

0 0.5 1.0 1.5 2.0 2.5 3.0

0 1 2 3 4 5 6 7

.01 .02 .03 .04 .05 .06 .07 .08 .09 .10 .11 .12 .13 .14 .15 .16

pjk

PLATE 33

THEORETICAL HORIZONTAL PRESSURE VS. ACTUAL HORIZONTAL PRESSURE

STATIC LOAD ; VERTICAL CELL ; FLEXIBLE PAVEMENT DEPTH 20"

FRONT WHEELS

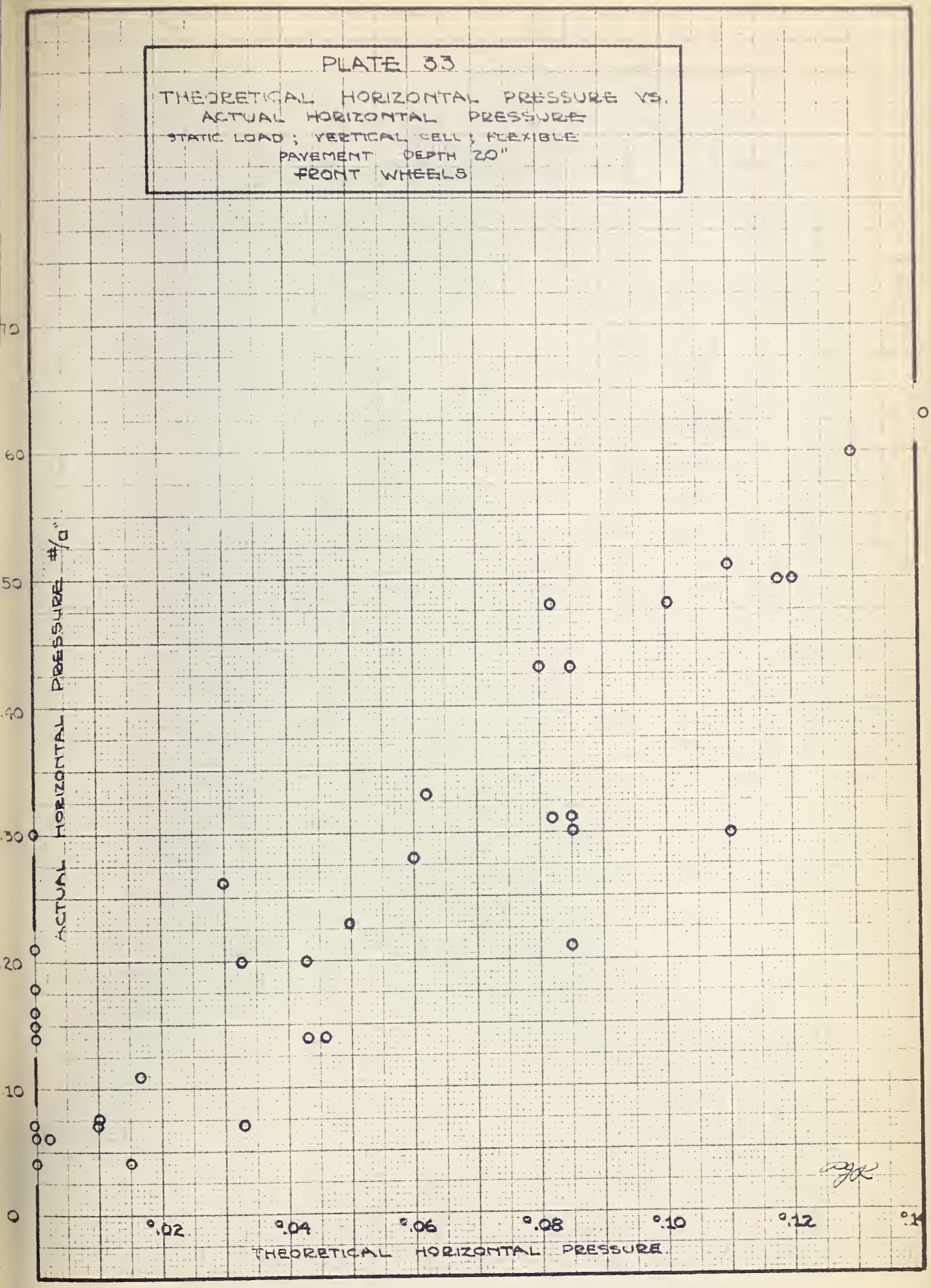

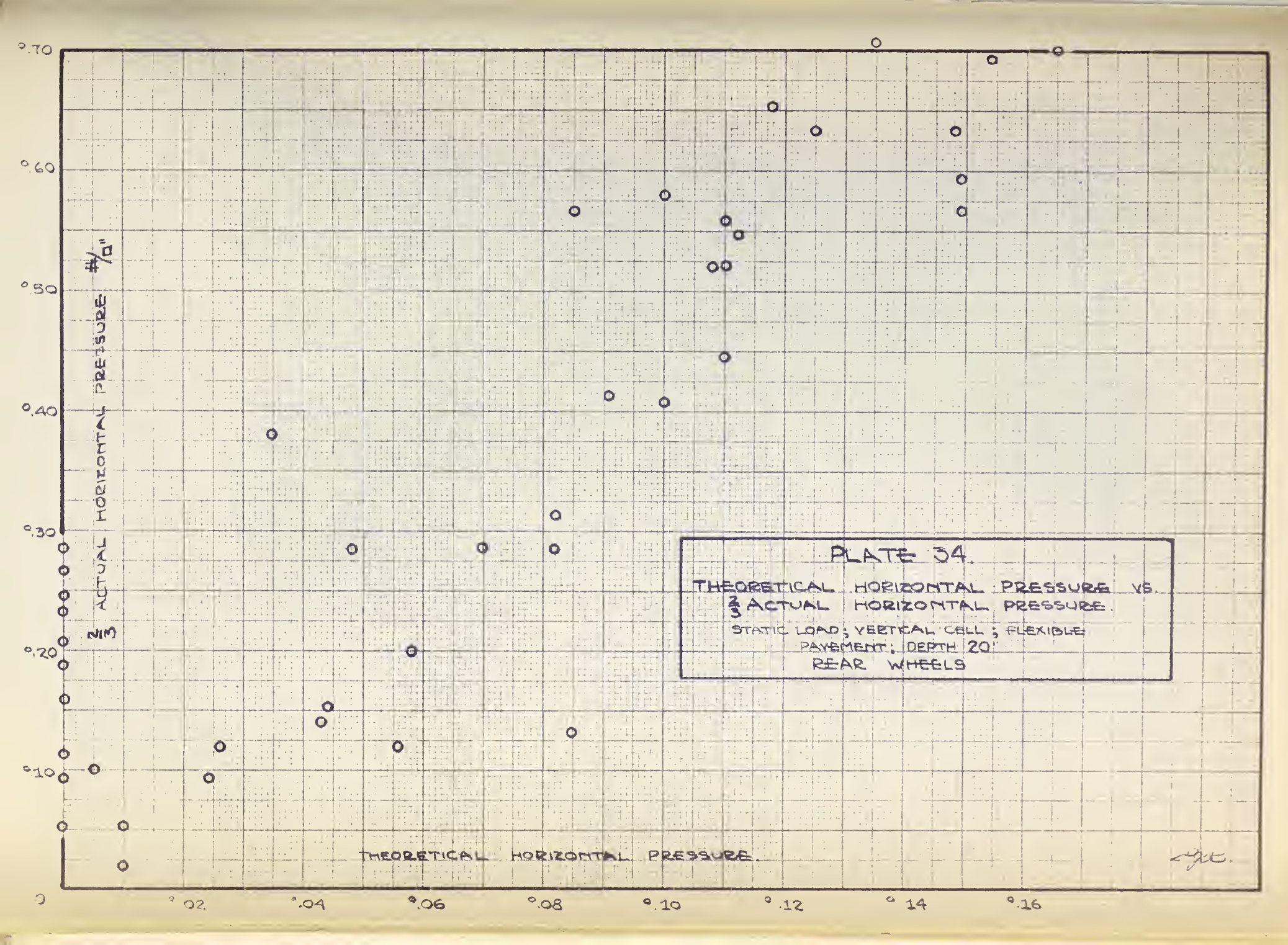
.70
.60
.50
.40
.30
.20
.10
0
.02
.04
.06
.08
.10
.12
.14
.16
2/3 ACTUAL HORIZONTAL PRESSURE #/□"
THEORETICAL HORIZONTAL PRESSURE.
PLATE 34.
THEORETICAL HORIZONTAL PRESSURE VS.
2/3 ACTUAL HORIZONTAL PRESSURE.
STATIC LOAD; VERTICAL CELL; FLEXIBLE
PAVEMENT; DEPTH 20"
REAR WHEELS

PLATE 35.

ACTUAL HORIZONTAL PRESSURE VS. x^2/R^5

STATIC LOAD, VERTICAL CELL, FLEXIBLE PAVEMENT, DEPTH - 20"

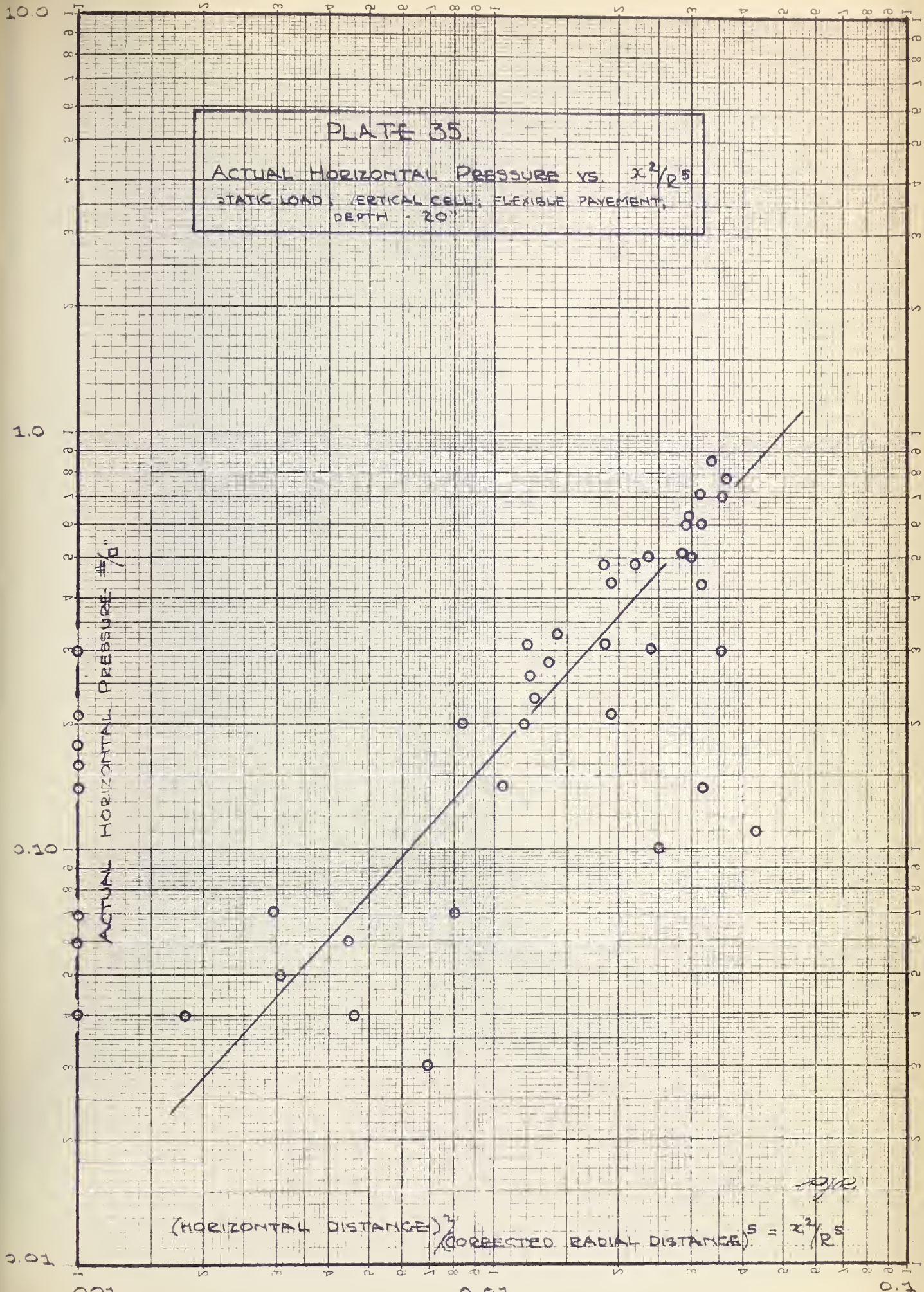

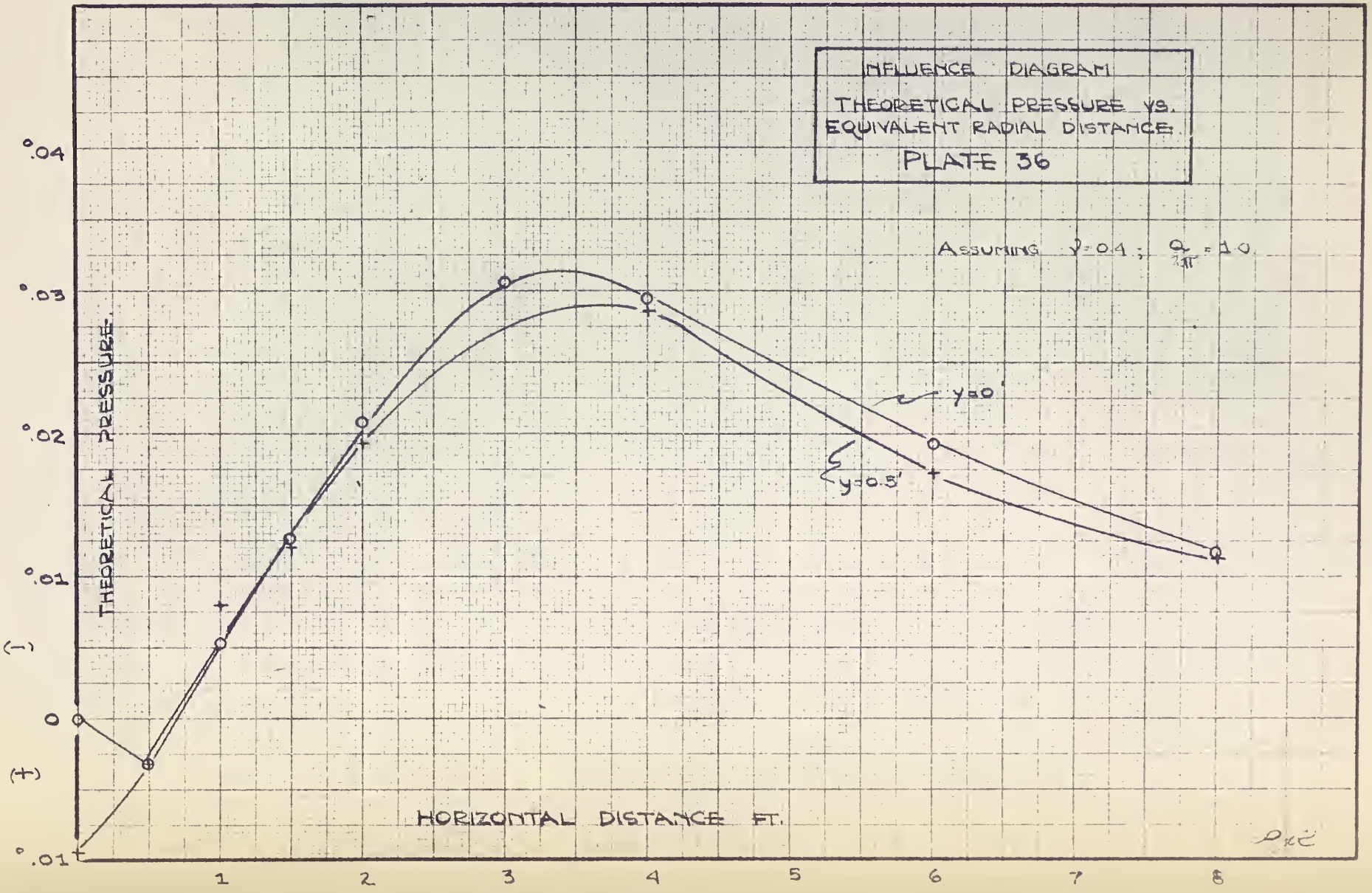
INFLUENCE DIAGRAM
THEORETICAL PRESSURE VS.
EQUIVALENT RADIAL DISTANCE.
PLATE 36
ASSUMING $\nu = 0.4$; $\frac{Q}{2\pi} = 1.0$
y=0
y=0.5'
THEORETICAL PRESSURE.
(-)
0
(+)
.01
.02
.03
.04
1
2
3
4
5
6
7
8
HORIZONTAL DISTANCE FT.

PLATE 37

INFLUENCE DIAGRAM FOR THEORETICAL PRESSURE AND HORIZONTAL DISTANCE

DEPTH $8\frac{1}{2}$"

Assuming: $\nu = 0.4$; $\frac{q}{2\pi} = 1.0$

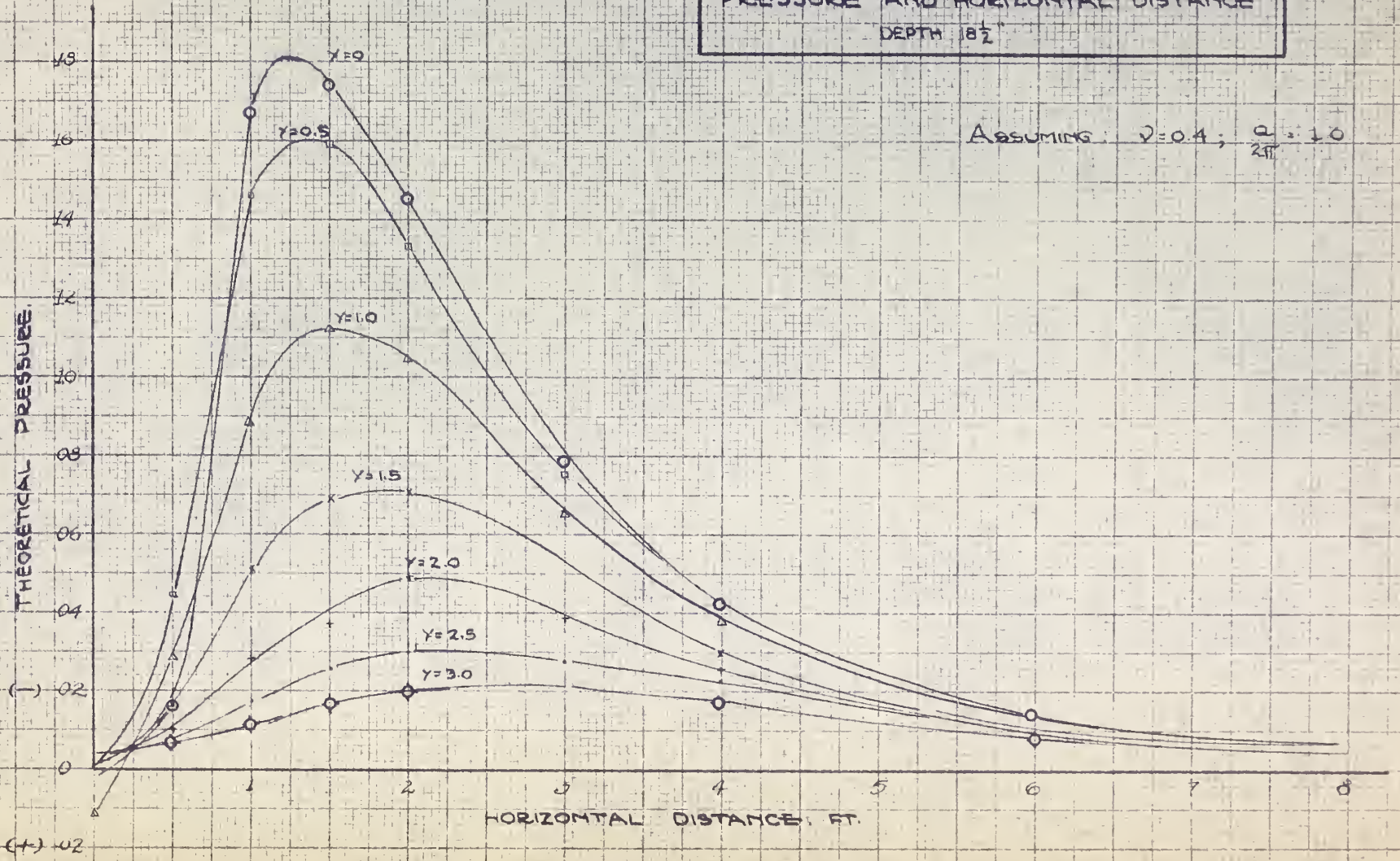

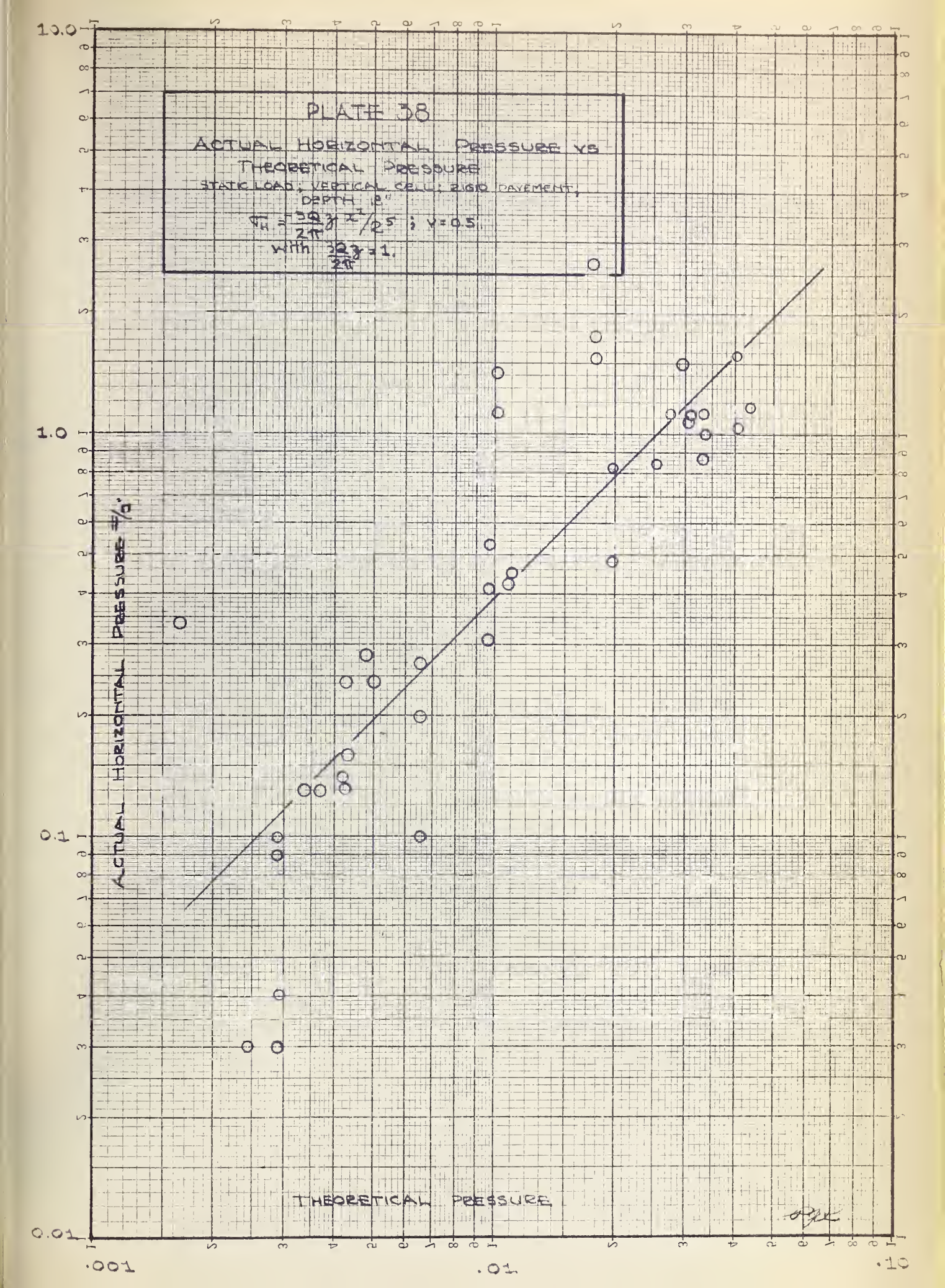
PLATE 38
ACTUAL HORIZONTAL PRESSURE VS THEORETICAL PRESSURE
STATIC LOAD; VERTICAL CELL; 2100 PAVEMENT, DEPTH 12"
$\sigma_H = \frac{3Q}{2\pi} \gamma \frac{x^2}{z^5}$; $\nu = 0.5$,
with $\frac{3Q}{2\pi}\gamma = 1$.
ACTUAL HORIZONTAL PRESSURE #/□"
THEORETICAL PRESSURE
10.0
1.0
0.1
0.01
.001
.01
.10

PLATE 39

ACTUAL PRESSURE VS HORIZONTAL DISTANCE
FOR DYNAMIC AND STATIC PRESSURE
FLEXIBLE PAVEMENT; HORIZONTAL CELL
DEPTH 31½"

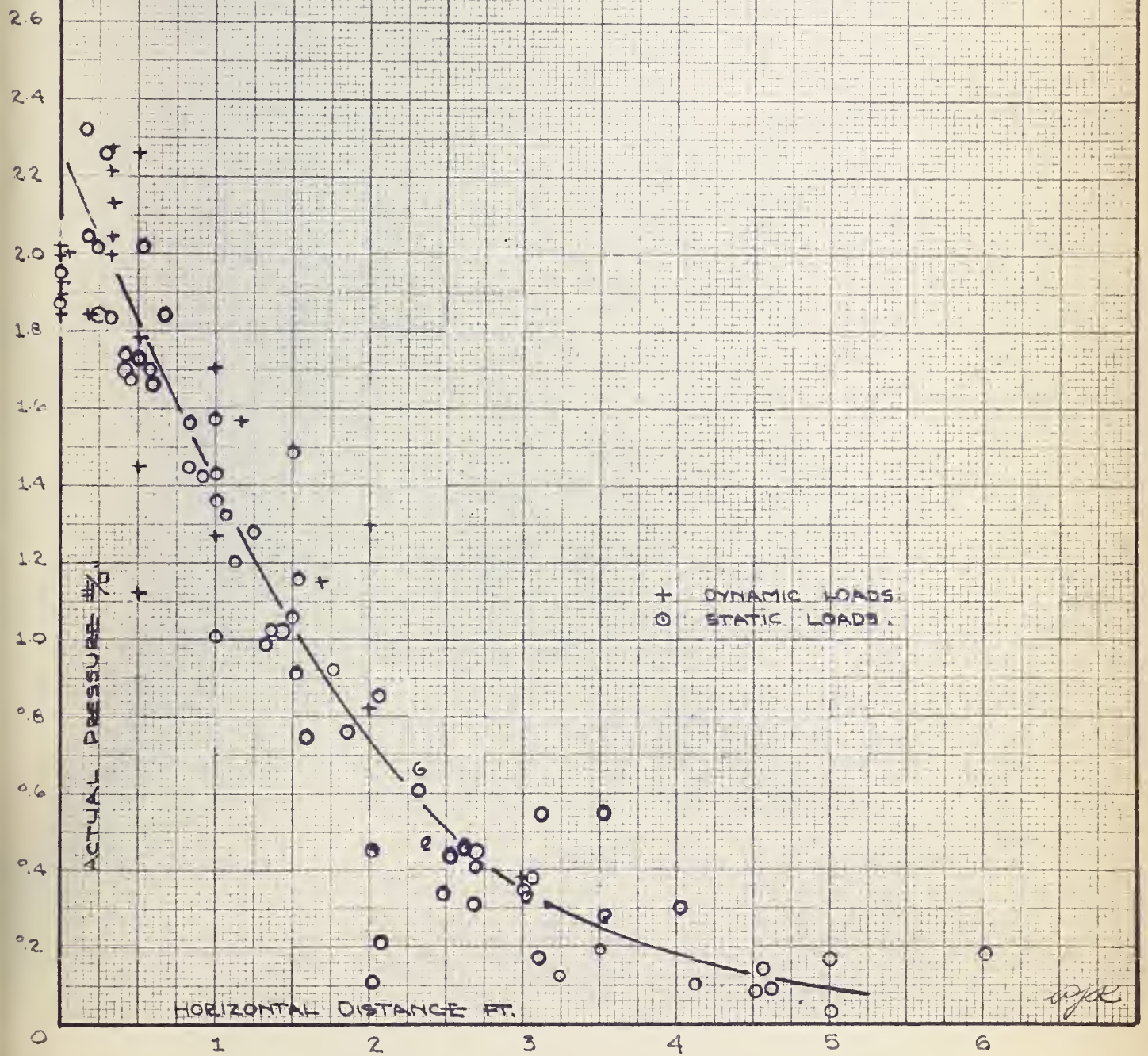

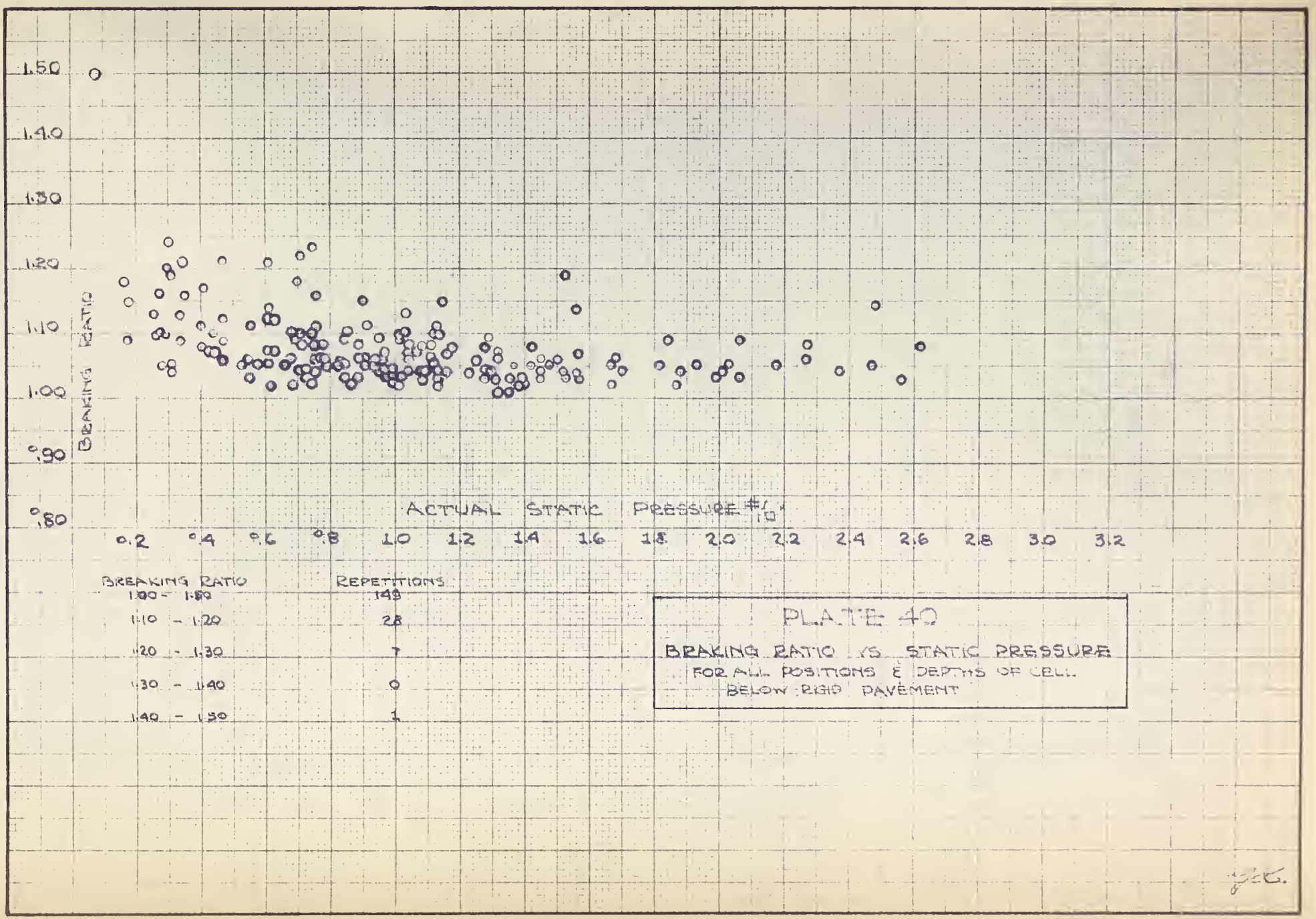

BREAKING RATIO	REPETITIONS
1.00 - 1.10	149
1.10 - 1.20	28
1.20 - 1.30	7
1.30 - 1.40	0
1.40 - 1.50	1

PLATE 40

BRAKING RATIO VS STATIC PRESSURE
FOR ALL POSITIONS & DEPTHS OF CELL
BELOW RIGID PAVEMENT

WES.

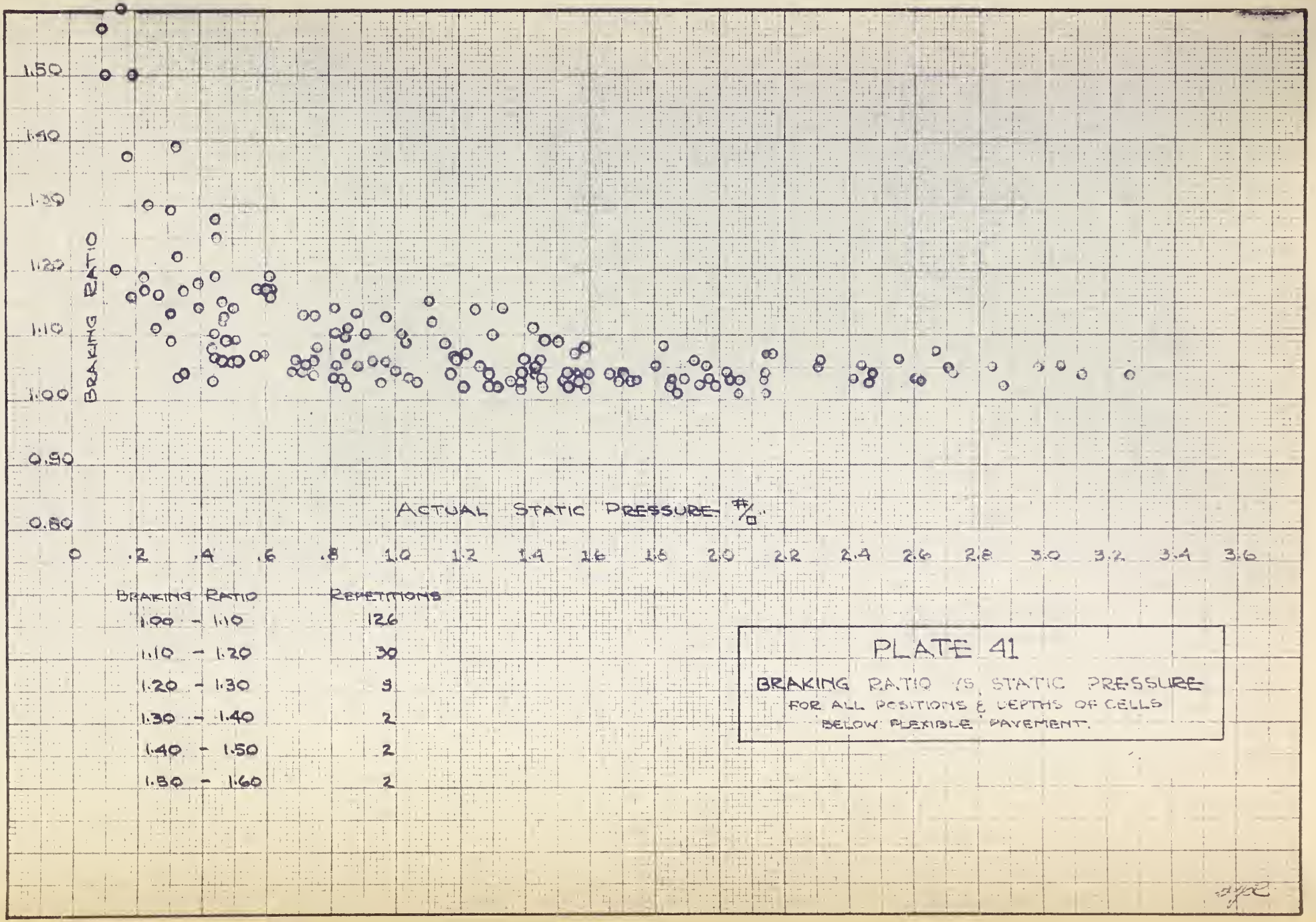

Braking Ratio	Repetitions
1.00 - 1.10	126
1.10 - 1.20	30
1.20 - 1.30	9
1.30 - 1.40	2
1.40 - 1.50	2
1.50 - 1.60	2

PLATE 41

BRAKING RATIO VS STATIC PRESSURE
FOR ALL POSITIONS & DEPTHS OF CELLS
BELOW FLEXIBLE PAVEMENT.

6 5 4 3 2 1 0 1 2 3 4 5 6

HORIZONTAL DISTANCE FT.

HORIZONTAL DISTANCE FT.

Increase in stress due to braking

Limit of plotted points

Increase in stress due to braking

2.00 #/a²

1.50

1.00

0.90

0.80

0.70

0.60

0.50

0.40

0.30

0.20

0.1 #/a²

PLATE 42.

PRESSURE BULB SHOWING INCREASE STRESS DUE TO BRAKING FOR FLEXIBLE PAVEMENT

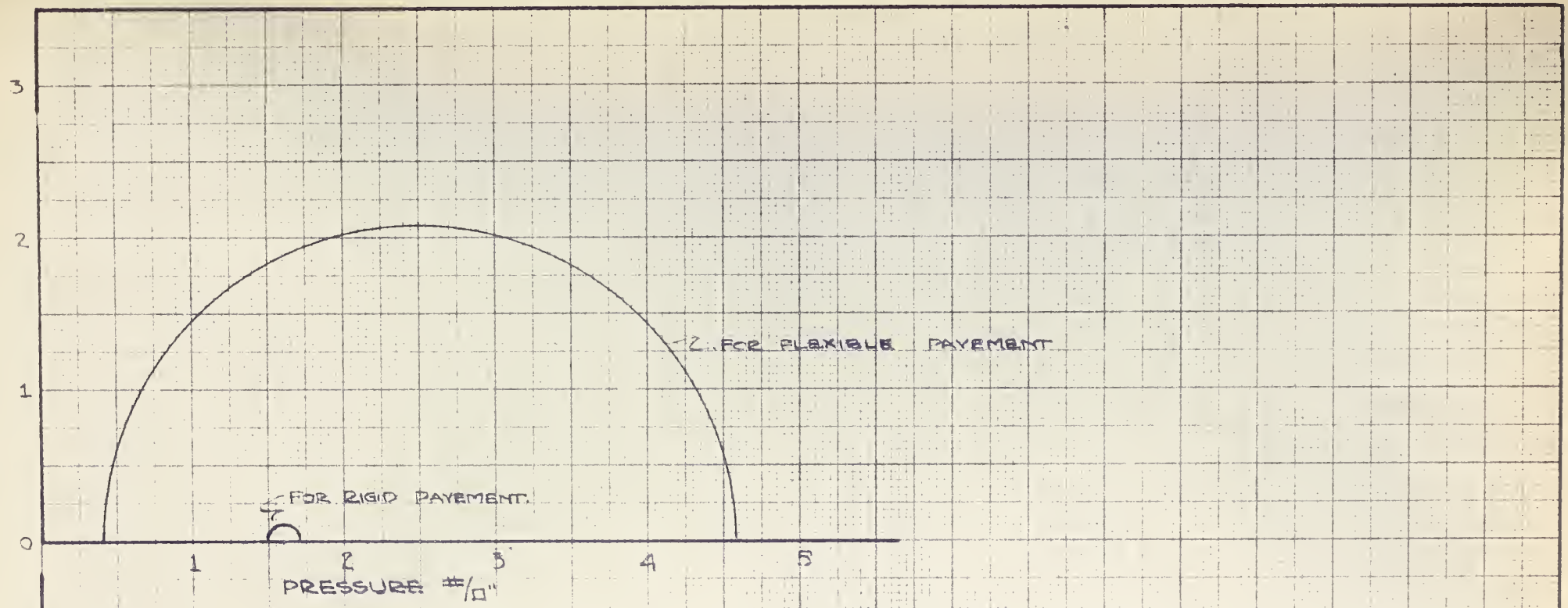

MOHR CIRCLE FOR ACTUAL HORIZONTAL AND VERTICAL PRESSURE AT DEPTH 20"; FOR FLEXIBLE AND RIGID PAYEMENT

PLATE 43

PLATE 44

MOHR CIRCLE FOR THEORETICAL HORIZONTAL AND VERTICAL PRESSURE FOR VARIOUS DEPTHS

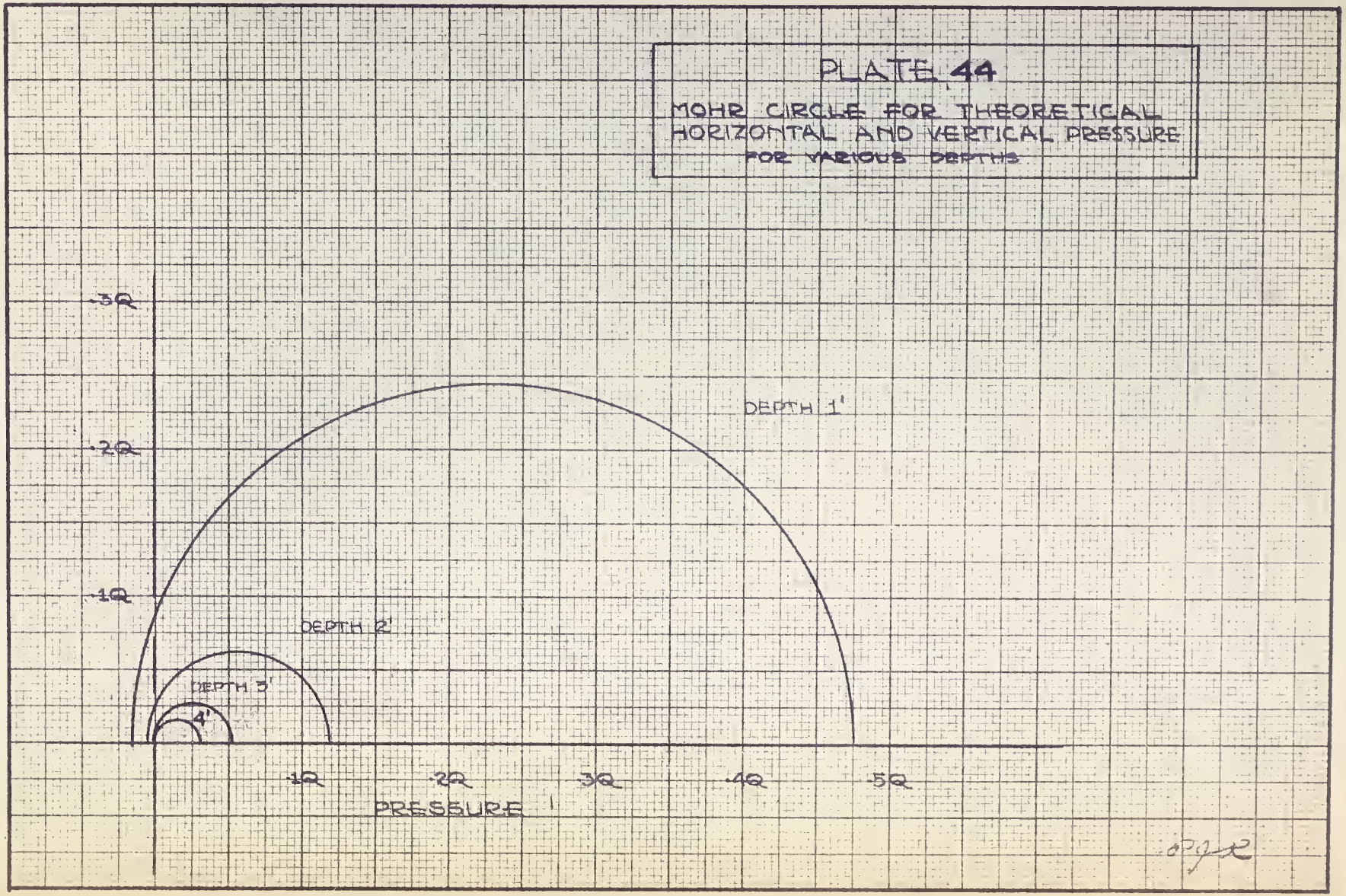

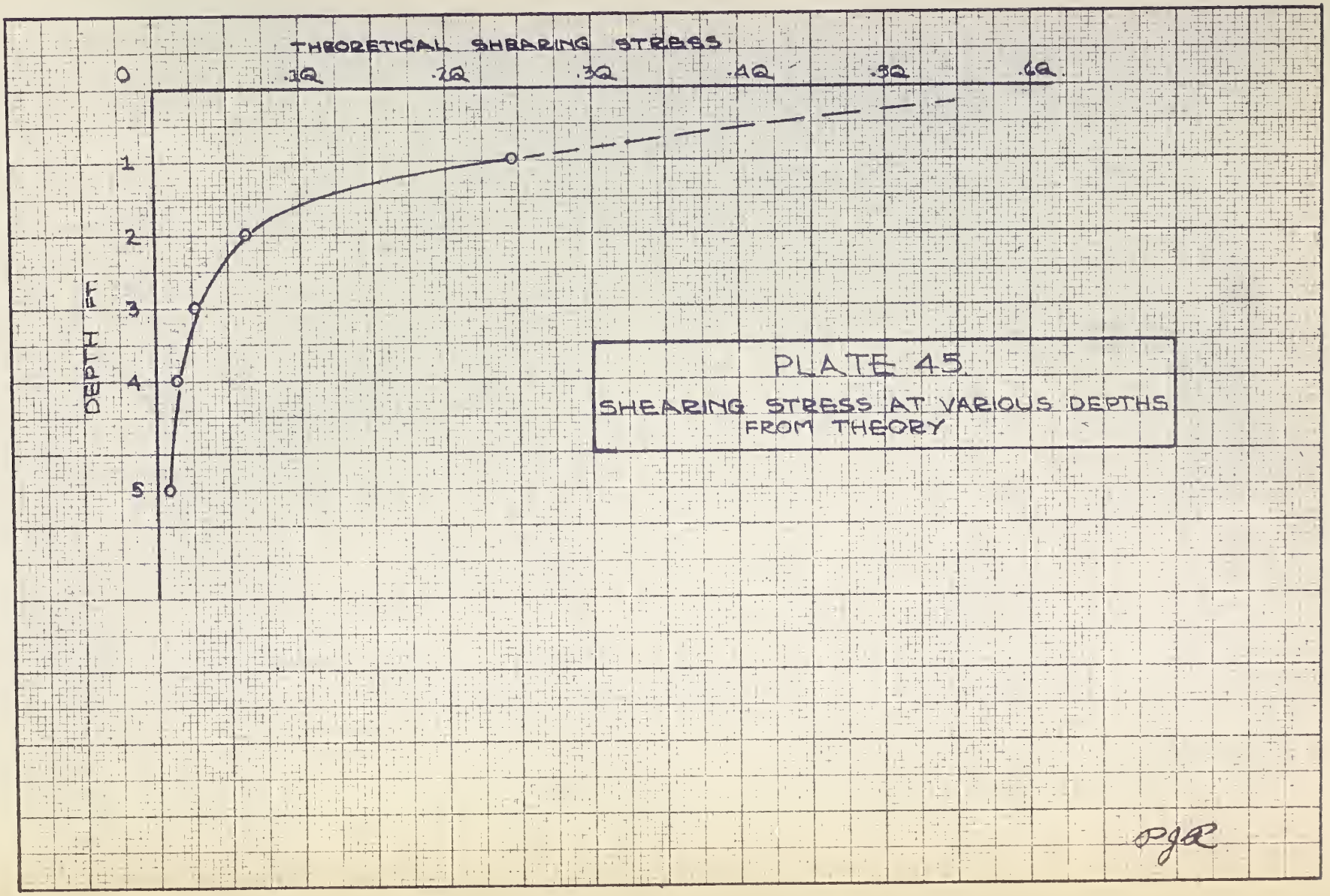

PLATE 45

SHEARING STRESS AT VARIOUS DEPTHS FROM THEORY

PJR

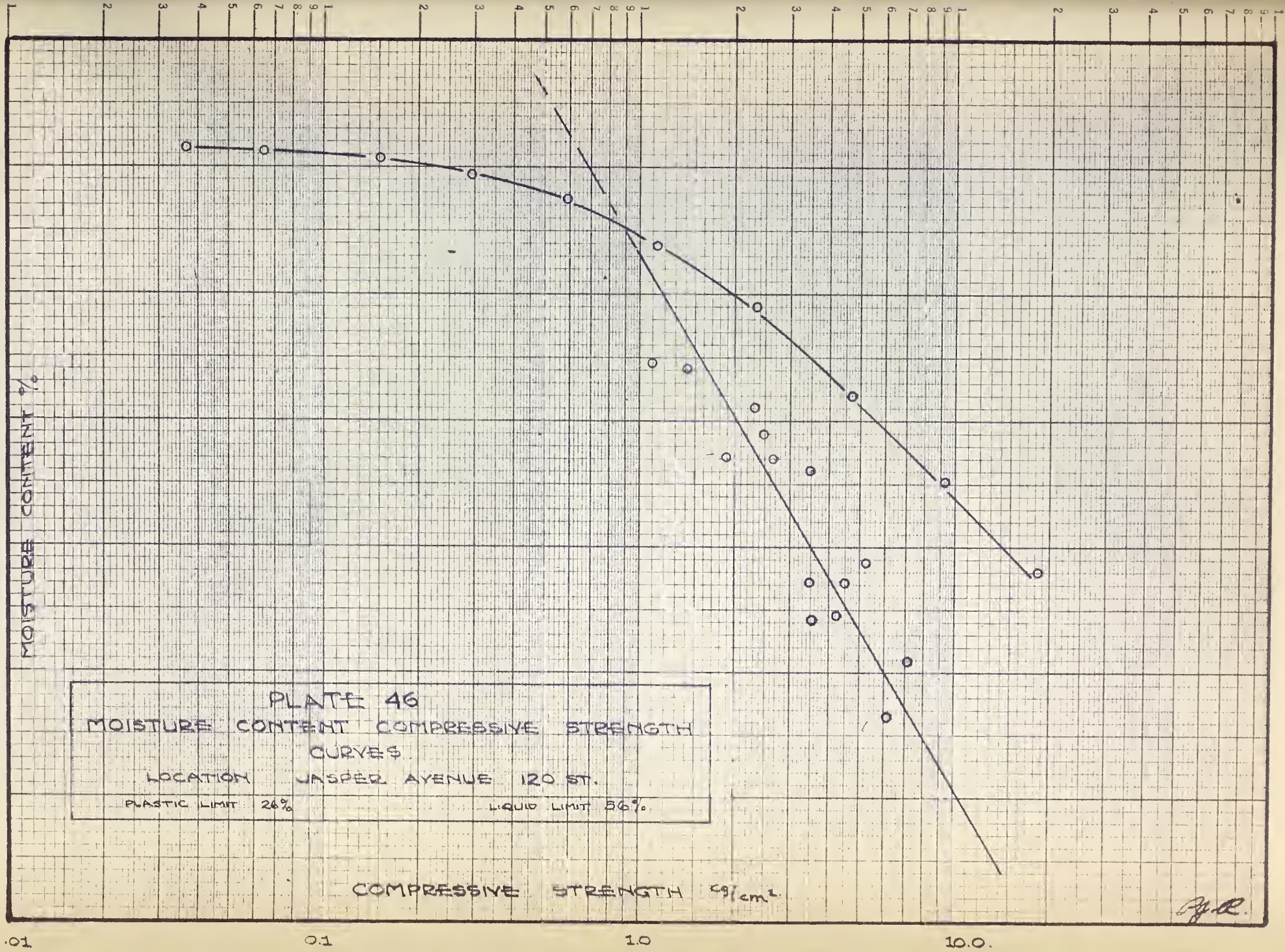
38
34
30
26
22
18
14
MOISTURE CONTENT %
PLATE 46
MOISTURE CONTENT COMPRESSIVE STRENGTH CURVES
LOCATION JASPER AYENUE 120 ST.
PLASTIC LIMIT 26%
LIQUID LIMIT 56%
COMPRESSIVE STRENGTH kg/cm²
.01
0.1
1.0
10.0.

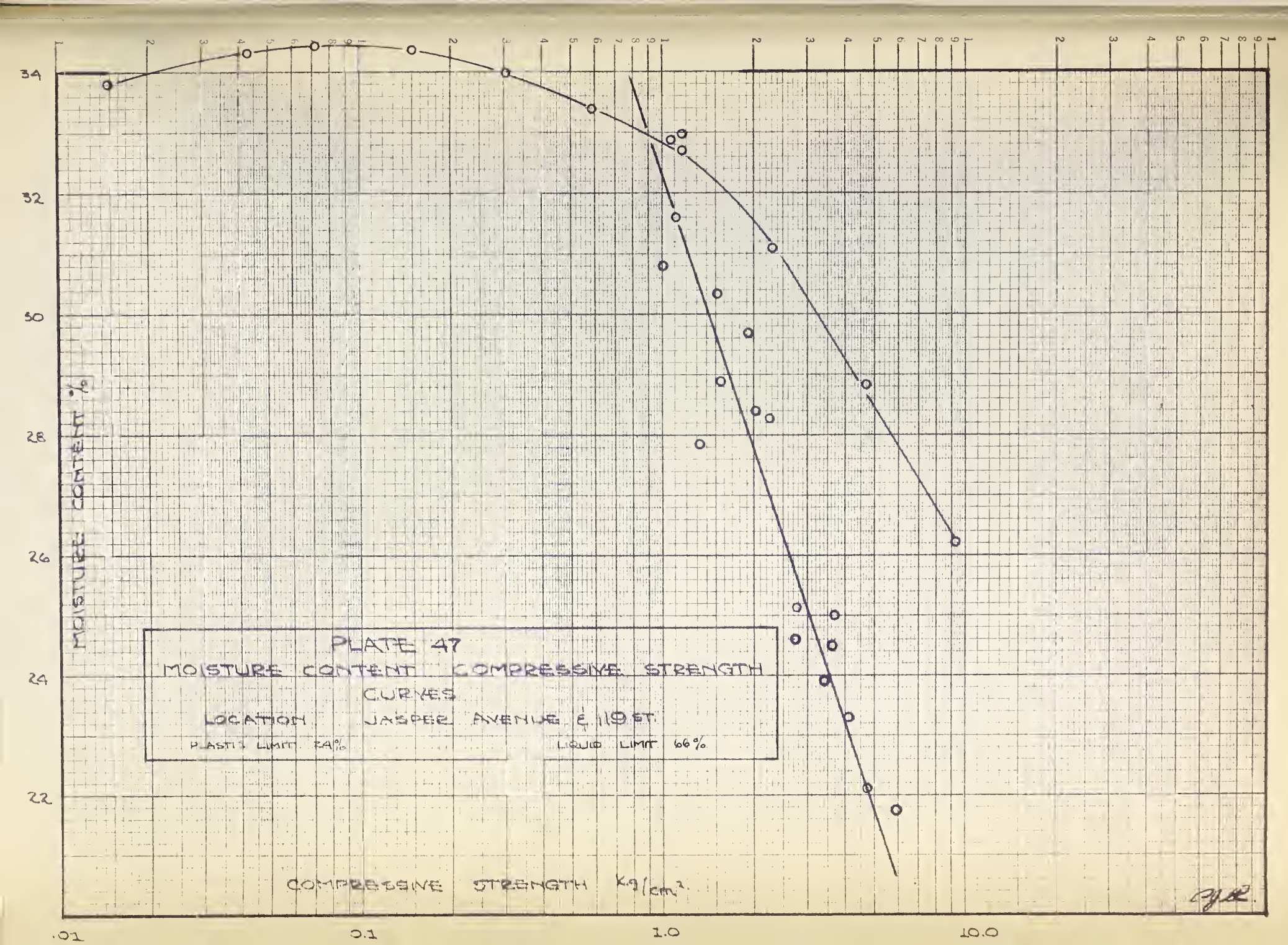
34
32
30
28
26
24
22
MOISTURE CONTENT %
.01
0.1
1.0
10.0
COMPRESSIVE STRENGTH Kg/cm²
PLATE 47
MOISTURE CONTENT COMPRESSIVE STRENGTH CURVES
LOCATION JASPER AVENUE & 119 ST.
PLASTIC LIMIT 24%
LIQUID LIMIT 66%

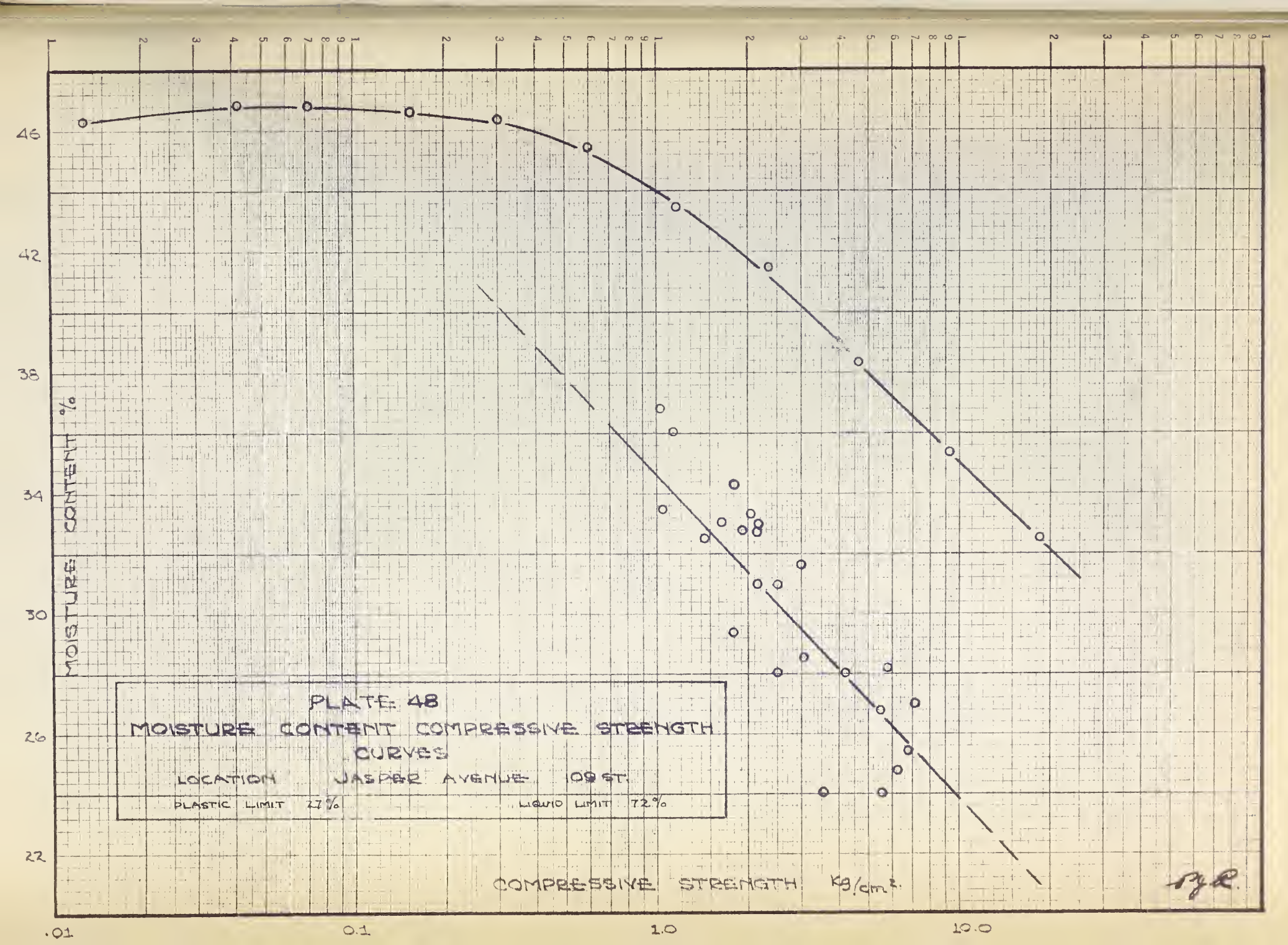
46
42
38
34
30
26
22
MOISTURE CONTENT %
.01
0.1
1.0
10.0
COMPRESSIVE STRENGTH Kg/cm².
PLATE 48
MOISTURE CONTENT COMPRESSIVE STRENGTH CURVES
LOCATION JASPER AVENUE 109 ST.
PLASTIC LIMIT 27%
LIQUID LIMIT 72%

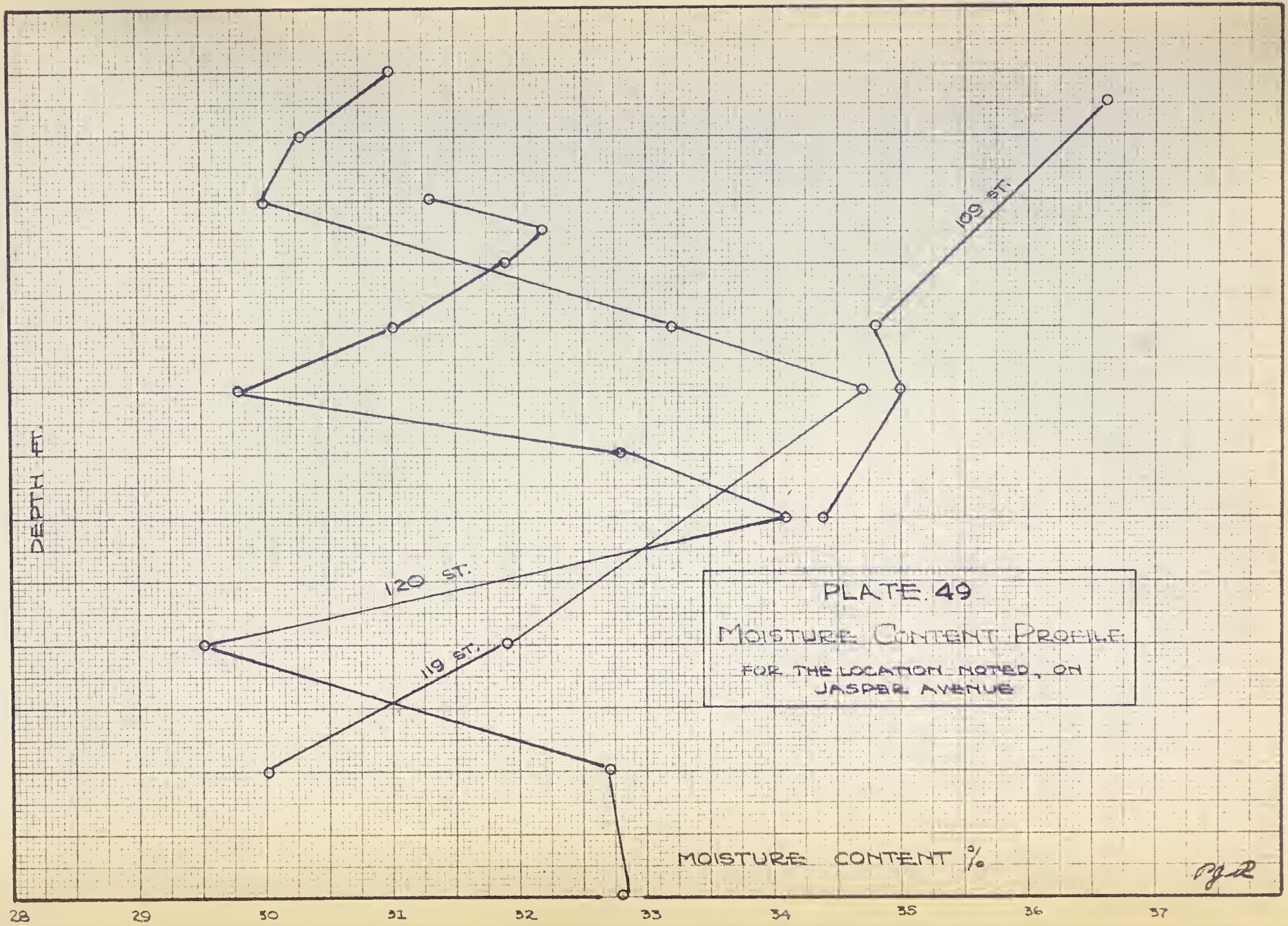
0
1
2
3
4
5
6
7
DEPTH FT.
28
29
30
31
32
33
34
35
36
37
MOISTURE CONTENT %
109 ST.
120 ST.
119 ST.
PLATE. 49
MOISTURE CONTENT PROFILE
FOR THE LOCATION NOTED, ON JASPER AVENUE

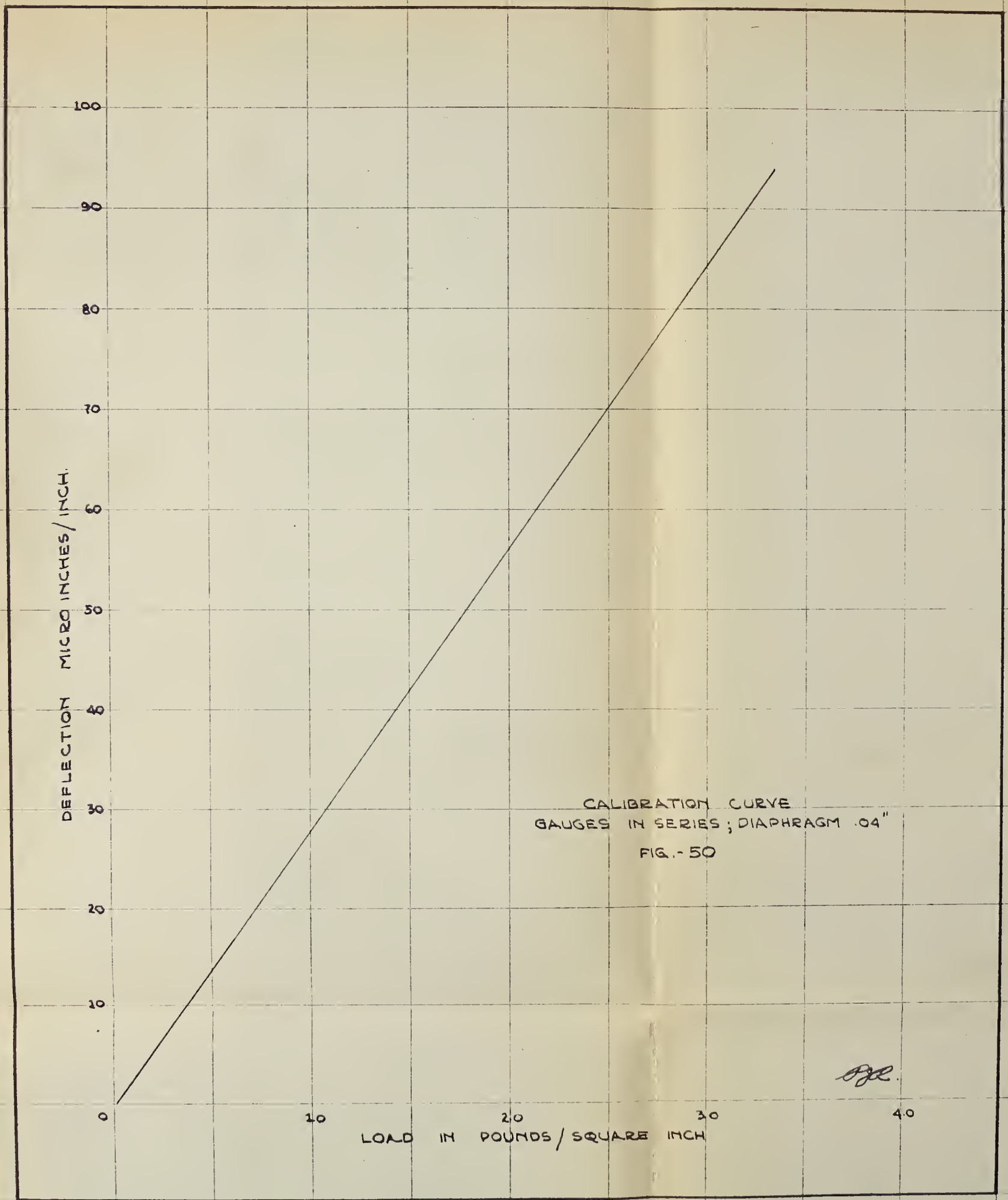

CALIBRATION CURVE
GAUGES IN SERIES ; DIAPHRAGM .04"

FIG. - 50